Improved grid interaction of photovoltaics using smart micro-inverters

Improved grid interaction of photovoltaics using smart micro-inverters

PROEFSCHRIFT

ter verkrijging van de graad van doctor aan de Technische Universiteit Eindhoven, op gezag van de rector magnificus prof.dr.ir. F.P.T. Baaijens, voor een commissie aangewezen door het College voor Promoties, in het openbaar te verdedigen op donderdag 3 februari 2021 om 11:00 uur

door

Ognjen Gagrica

geboren te Novi Sad, Servië

Dit proefschrift is goedgekeurd door de promotoren en de samenstelling van de promotiecommissie is als volgt:

voorzitter:	prof.dr.ir. S.M. Heemstra de Groot
1e promotor:	prof.dr.ir. J.F.G. Cobben
2e promotor:	prof.dr. T. Uhl (AGH UST)
copromotor(en):	dr. H.P. Nguyen
leden:	prof.dr.ing. A.J.M. Pemen
	prof.dr. M. Gibescu (UU)
	prof.ir. W. Zeiler
adviseur(s):	dr. V. Cuk

Het onderzoek of ontwerp dat in dit proefschrift wordt beschreven is uitgevoerd in overeenstemming met de TU/e Gedragscode Wetenschapsbeoefening.

SUMMARY

Small-scale solar photovoltaic (PV) generators are a popular choice for renewable energy supply in residential and small commercial applications, because of good possibility of roof utilization. Solar PV is also one of the least controllable RES due to intermittency of prime mover. A major industry driver is improving energy harvest efficiency through better maximum power point tracking (MPPT). In grid-connected applications an inverter is required as a conversion and grid synchronization interface. The module-integrated inverters or micro-inverters (aka AC solar panels) are becoming a preferred choice over string inverters in residential installations due to several reasons: greater MPPT efficiency under partial shading conditions (yield gain 10%-19.5%); easier installation in the absence of DC wiring; and easier maintenance and troubleshooting due to panel-level monitoring capability.

Attractive incentives and relatively quick return on investment (5-6 years) are promoting fast expansion of PV capacities in residential low voltage (LV) grids. The LV grids are generally not designed for high PV penetration scenarios. This creates suboptimal inverter-grid interaction and power quality deterioration. The overvoltage due to exceeded grid hosting capacity is one of the most immediate problems in large-scale integration of PV. The random process of single-phase PV deployment to three-phase LV grid creates voltage unbalance, which, combined with limited hosting capacity, increases chances for overvoltage. The overvoltage can cause significant feed-in losses due to inverter being frequently disconnected by its overvoltage protection system. A 6 kW PV system can experience 0-12.5% annual feed-in loss, while for a 30 kW system this loss can go even up to 70% of energy yield. The rise of feed-in loss prolongs the system payback time up to 18%.

Most PV inverters deployed to date only have basic functionalities such as power output maximization and protective disconnection in case of grid disturbance. The term "smart micro-inverter" signifies the introduction of new control functionalities that can optimally balance between grid operational requirements and feed-in power maximization. Reactive power support and active power curtailment (APC) are inverter functionalities considered for mitigating the overvoltage problem. To make the transition towards smart inverters, the old inverters either have to be replaced or retrofitted. Large-scale software retrofits are already a reality: retrofit in Germany, 315,000 PV plants over 4 year period; retrofit of 800,000 micro-inverters in Hawaii in a single day. Software retrofit can be challenging from the design-for-reliability aspect, especially for micro-inverters, due to their outdoor application and direct exposure to the environment. The capability of accessing the inverter remotely is essential for a cost-efficient software retrofit.

In this thesis, being oriented on inverter-based solutions for integrating PV into the grid, the title phrase "improved grid interaction" signifies the transition from the "old", grid-interactive inverters to the new, smart inverters as means of expanding grid-connected PV capacities in a seamless, sustainable manner. The thesis reveals how the micro-inverters coupled with standard ICT support can be pushed beyond their current use, in order to deliver high PV penetration neighborhoods, while keeping the grid safe and supporting the inverter reliability. The APC is recognized as a retrofit-friendly voltage control method for micro-inverters in LV grids. It is implemented as the *Sequential Module-level Tripping* (SMT), a modified overvoltage protection scheme that achieves curtailment on a system level, without modifying the functionality of an individual micro-inverter unit. The SMT algorithm and controller are applied in a typical Dutch LV residential feeder and simulated for effects on voltage and feed-in losses. Both local and wide-area control schemes are tested, allowing the distribution system operators to optimize between various priorities such as voltage levels vs.

total feeder output, economic equality between connected parties, voltage unbalance level, and curtailment execution time. A successful PV penetration increase from 5A to 8A per house was achieved without changing the grid infrastructure.

Simulations are followed by a techno-economic analysis with emphasis on annual feed-in loss study and the reliability prediction study. The feed-in loss study compares the conventional overvoltage protection and SMT. On the entire feeder over 550 kWh was saved by SMT, accounting for 78% of energy that would have been lost to conventional protection. The reliability prediction confirms the proposed reliability advantages of SMT over droop control APC. The reliability study projects beneficial reduction in failure rates for MOSFETs (up to 20%) and electrolytic capacitors (up to 54%). The thesis concludes with a hardware-in-the-loop comparison study of three different voltage control strategies: SMT, reactive power control and droop APC for their applicability in a software retrofit scenario. These voltage control strategies are compared with respect to internal effects on micro-inverter like electrical stress and thermal behavior, as well as effects on the grid voltage magnitude and harmonic contribution. The SMT implementation provides the highest grid voltage reduction of 0.9V, and the highest inverter internal temperature reduction of up to 11°C. Furthermore, it does not clash with constant power factor control mode, unlike droop APC and, especially, reactive power control. The effectiveness of voltage control along with compatibility with existing inverter functionality make it the most likely choice for practical implementation of software retrofit.

TABLE OF CONTENTS

LIST OF FIGURES

LIST OF TABLES

DEDICATION

I dedicate this thesis to my parents.

ACKNOWLEDGEMENTS

My deep gratitude goes to late Prof. Wil L. Kling who welcomed and mentored me as a supervisor during my stay at TU/e. Sadly, he passed away without the chance to follow through the end of my research. I owe a big thanks to Prof. Sjef Cobben who selflessly accepted to replace Prof. Kling's role as a first supervisor and who made sure that my research continues without interruption. I am thankful to dr. Phuong Nguyen for co-supervising me. His expertise and guidance were crucial for producing the core of this research. Also he encouraged me to aim high when it comes to publishing papers and it was very well worth it.

I would also like to thank my second supervisor, prof. Tadeusz Uhl, for his guidance, and contributions to the content of my research project during my stay at AGH University of Science and Technology.

Special thanks goes to my industrial supervisor, dr. Michał Lubieniecki. Without his contribution in patent registration, spinoff company setup, promotion of research, attracting funding, etc., the progress of industrial application of my research would not be the same.

I gratefully acknowledge the support of Erasmus Mundus Joint Doctoral Programme SELECT+ for providing the funding for this research.

My final and greatest thanks goes to my family who supported me all the way.

CHAPTER 1

Introduction

The decentralization has demonstrated productivity gains in many industries and aspects of human life. The same is taking place in the electricity production sector. What does the expansion of decentralized generation and its integration into built environment mean for the electricity grid? Figuratively speaking, these developments are almost turning the power system operation upside down. To understand this figure of speech a traditional operation of electricity grids needs to be reviewed and put in the context of changes introduced by the increase in energy demand, expansion of distributed generation and renewable energy sources.

1.1 Future of energy consumption and demand

The energy demand is a mirror of the industrial, residential and services development level of each country [1]. Increased electricity consumption is positively correlated with an increase in human development (income, education) [2]. The European energy demand will grow mainly in residential and service sectors (Figure 1.1) with the highest annual growth of consumption of 2.1% in the residential sector. These major consumption sectors are characterized by higher number of spatially dispersed points of consumption compared to the industry sector. This implies that the future energy demand will be more spatially dispersed and will require supply from distributed energy resources, in order to cut down the costs of electricity distribution.

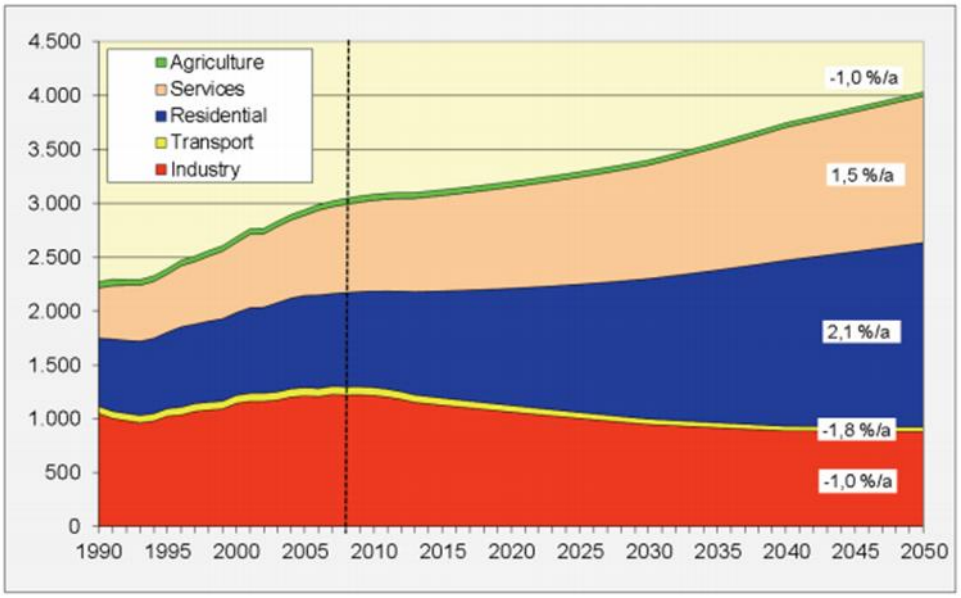

Figure 1.1: Power consumption in TWh in EU27+ until 2050

For the industry and transport a long term decline in consumption is forecasted. This means these sectors will become more high-tech and energy efficient. This development comes with new grid loading profiles. The electrification of transport brings with it the occurrences of massive charging and discharging of electric cars. Due to inflow of intermittent renewable energy sources (RES) like wind and especially PV in the residential sector new grid loading profiles are expected.

1.2 Expansion of distributed generation

The fossil fuel and nuclear power plants have very low efficiencies due to the second law of thermodynamics. This means that they produce more heat than electricity. The heat must be disposed either by cooling systems or used for district heating. However, heating networks are expensive to build and not practical for power plants that are very remote from populated areas or facilities that could use heat in an industrial process.

The non-renewable energy sources have much higher energy density (W/m^2) than renewable energy sources (RES). It means that renewable generation requires much more

space than non-renewable for the same generating capacity. To use renewable energy in a sustainable way the electricity generation must be combined with other land uses (buildings, agriculture, roads).

The need to *save energy by not wasting heat* and the *low energy density of RES* are the two drivers that caused generators to reduce in size and become spatially distributed, closer to the point of consumption of both heat and electricity [3]. Of course, it goes without saying that the main driving force to expand both centralized plants and distributed generation (DG) is the worldwide increase in electricity demand. The distinction between centralized plants and DG depends on the adopted definition, plant size, location, ownership, as well as several other factors that vary from country to country [4]. A compromise would be to say that DG ranges from several kW up to 100 MW and connects at distribution system level (customer's side of the meter) while centralized plants have >100MW ratings and are connected at transmission system level. In addition to solving the efficient production and transmission of electricity and heat, there are other benefits of opting for DG instead of centralized plants:

- *Rapid deployment*. Instead of several years' work for centralized plants the DG can be deployed within weeks or even days.
- *Scalability*. The DG can be bought, built and operated with less capital due to smaller size. Coincidentally, the world regions with greatest electricity needs are also the least financially capable to afford large plants, so DG is an excellent alternative.
- *Resilience.* With smaller, spatially dispersed DG, locally organized in micro-grids, the power system becomes more resilient in natural disaster scenarios, both in terms of power system survival and restoration.

- *Environmental benefits*. Due to small size, the DG has greater feasibility without risking large, permanent modification of natural environment.

The investments in DG are on the rise globally. The annual investment projections by 2020 are $206 billion. The DG will account for 42% of global capacity expansion[5]. The DG technologies include: reciprocating engines, gas turbines, fuel cells, solar PV, and small wind turbines. Among these, the most technologically and commercially mature are reciprocating engines and gas turbines, which can be found in standalone or combined heat and power generation (CHP). Interestingly, they are immediately followed by solar photovoltaic (PV) systems (Figure 1.2).

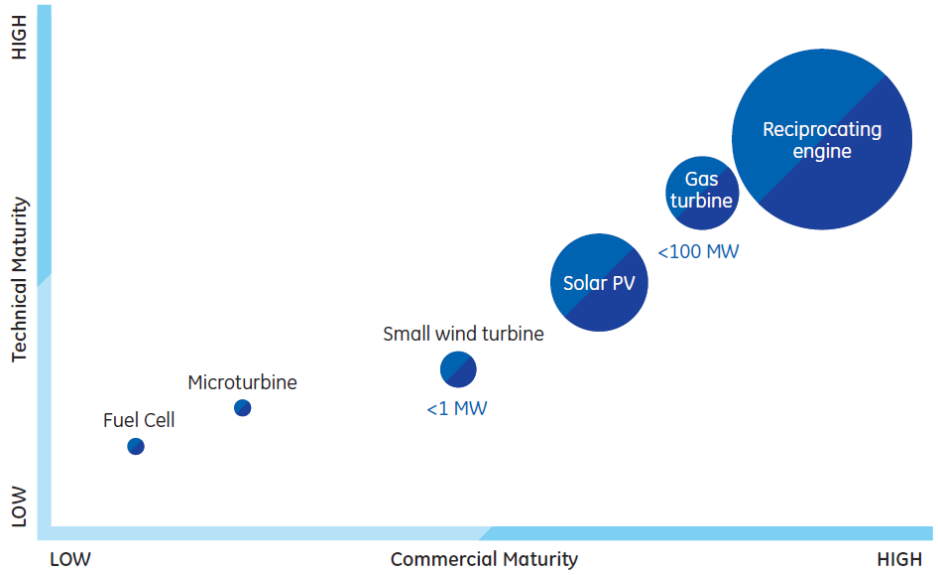

Figure 1.2: Distributed power technologies (© 2014, General Electric Company)

1.2.1 Advantages of small-scale solar PV

Of all DG technologies only hydro, wind and solar PV systems don't require fuel which makes their application particularly attractive. The solar vs. wind energy debate is still ongoing, but there are indications that in small-size, building-integrated applications the PV is more feasible than wind. Wind speeds in rooftop application are generally much lower which decreases efficiency[6].The obstacles such as buildings and trees can create turbulence which

increases the variability of generated power compared to that of exposed areas and higher altitudes. The wind turbulence can increase turbine vibrations and the built environment can amplify them creating unacceptable noise levels[7]. Unlike wind, small solar is not so location-sensitive and can be installed almost anywhere. The PV can experience partial module shading problems, however in site surveying this is much easier to predict than inefficiencies of small wind turbines. Even in large-scale applications, where wind does become more competitive, the solar PV can get even twenty times higher energy density[1][8].

1.2.2 Net zero and net positive energy buildings

To efficiently exploit the DG, the built environment must be utilized in combination with energy efficient materials and building methods. Because of good possibility of roof utilization and building integration, the PV modules are often the preferred DG choice in residential grids. The homeowners do not have to sacrifice the dwelling space like incase of CHP or get involved in a highly unpredictable investment in rooftop wind. Communities, driven by attractive incentives for installing renewable energy generators, are equipping buildings with grid-tied PV. Such trends are heading towards neighborhoods with nearly 100% PV penetration (generation to demand ratio). So called *net zero energy buildings* (NZEB) combine energy efficiency and PV generation to achieve an annual zero net exchange between energy received from the grid and injected into the grid [9], [10]. Also *net positive energy buildings* (NPEB) exist. Such buildings on annual level behave like generators, supplying the grid with electricity. The principal difference is that NZEB concept can be

[1] Power density is calculated as a ratio of plant capacity and the surface of contracted land.

realized by stronger emphasis on energy efficiency rather than presence of PV system, while NPEB requires PV system even larger than in NZEB [11], [12].

1.3 Traditional operation of electricity grids

The electrical grid is an infrastructure built to transfer the electrical power from the producer to the consumer of electricity. The producers (generating plants) and the grid form the power supply system. To overcome various engineering problems related to power transfer, as well as to satisfy the ever-growing energy demand, the electrical grid evolved into a top-down operated system with a multi-level voltage transformation scheme. Figure 1.3 illustrates the organization of European grid into: high voltage (HV) grid, operating in the range of 380-50kV; medium voltage (MV) grid mostly operating at 10kV; and the low voltage (LV) grid at 400V/230V. The power supply operation itself is divided into transmission (HV) and distribution (MV and LV), although in some varieties of grid design the MV can take on the sub-transmission role at different voltage levels (3, 6, 20 or 25kV)[13].

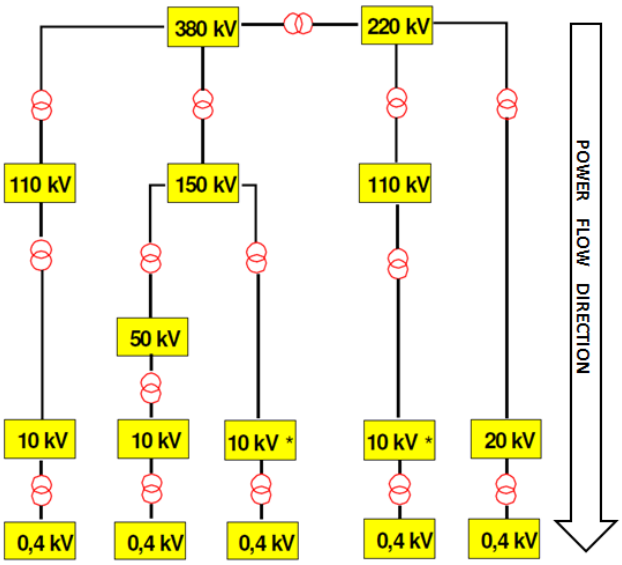

Figure 1.3: Voltage levels in Dutch grid. The 10kV step can also be 20kV.*

What makes the historical grid operation "traditional" at all voltage levels is the *unidirectional* power flow. The power always flows from producer to consumer, where large-scale centralized power plants are connected at HV level and consumers at MV and LV levels. Up until last two decades, there was no true market for electricity. The prices were fully regulated by government agencies. Such an economic setting certainly contributed to maintaining the unidirectional power flow approach. This one-way interaction between producers and consumers, imposed over a historically dominant form of electricity conversion using synchronous generators, has shaped the engineering solutions used in frequency/voltage control and protection operations.

The electricity cannot be stored in large quantities cost-effectively. It is a unique product because it has to be produced and consumed simultaneously. A stable power transfer through the grid is primarily dependent on balancing supply and demand. The measure of this balance is frequency. The frequency control strategy has three levels: primary, secondary and tertiary control[14]. Voltage is also controlled using this three-level approach, but frequency

deviation impacts the whole interconnected power system while voltage has a regional/local impact.

Protective system is designed to detect overcurrent (overloading or faults) and isolate the faulted component from the system. Protection needs to act relatively fast in order to limit material damage to the faulted component and minimize supply problems (e.g. outages, voltage dips) for connected consumers. Also it needs to provide personal safety for maintenance personnel working on power restoration and for customers connected to the network. Conventional overcurrent protection is triggered only by current magnitude without considering flow direction because traditionally it is assumed that fault current can only flow in one direction [15].

The monitoring and control are entrusted to transmission system operators (TSO) and distribution system operators (DSO). The essential operator tool is the supervisory control and data acquisition (SCADA)[16]. The SCADA master station extends its remote monitoring and control operations by linking with remote terminal units (RTU), which are locally linked to substations and generators. As the impact of faults reduces with voltage level, so does the number of RTUs and operator's monitoring and control capacity. At HV, being the backbone of power generation and transfer, the reliability requirements are highest so having monitoring and control capacities is most important at this level. It decreases down through MV levels and practically stops at MV/LV substation. The location and detection of faults at LV level still predominantly relies on customer complaints and maintenance crew reports rather than remote data acquisition [17].

1.4 DG grid integration problems

The expansion of DG technically required the enabling of grid connection, first at MV level, and with full market liberalization, at LV level as well. The market liberalization

created the conditions for both businesses and individuals to participate in the electricity supply, therefore making the DG even more dispersed. The consumer was given the chance to produce electricity, hence the term "prosumer" was coined. The DG has changed the power flow from unidirectional to *bidirectional* in a grid that was designed to operate as unidirectional.

A large portion of DG uses wind and solar PV energy. Increasing wind and solar RES practically means increasing the presence of intermittent, uncontrollable prime movers. Reducing fossil and nuclear fuels practically means reducing controllable prime movers and losing synchronous generator rotating inertia which is desirable to have in situations with destabilized power system. The frequency and voltage control is then contradictorily becoming more dependent on the uncontrollable prime movers. The intermittent RES mostly cannot be synchronously coupled to the grid as conventional sources. They require power electronic converters as a coupling and synchronization interface. The bidirectional power flow along with increasing presence of power electronics converters creates a new supply-demand interaction which is impacting the power quality, control and protection in new ways. The impacts that occur can be classified as local and system-wide as in Table 1.1.

Table 1.1: Local and system-wide impacts of DG on power system.

Local impacts	**System-wide impacts**
Node voltages	Power system dynamics and stability
Fault currents and protection (incl. overloading)	Reactive power and voltage control
Harmonic distortion	Frequency control and load following
Flicker	

In addition to producing active power for supplying loads, both centralized and distributed generators must ensure that node voltages are kept within boundaries, so that transmission and distribution operations (and connected installations) may run efficiently. If

the node voltages are out of limits, the new generator is not allowed to connect. This is why every generator should have some reactive power control and provisioning capability. Conventional synchronous generators are quite flexible in providing reactive power due to their wide loading range. The variable speed wind turbines, PV and small CHP are interfaced through power converters and can control node voltages by reactive power variation. This capability is determined by characteristic of power converter and controller. There are exceptions. In case of constant speed ("squirrel cage")wind turbines there is no power converter interface and reactive power is externally compensated[18]. During faults, they accelerate and draw high amount of reactive power. This slows down the voltage restoration and increases voltage and rotor speed instability unlike synchronous generators that provide reactive power support during voltage restoration.

The power electronics is more sensitive to fault currents than synchronous generators, but can detect abnormal currents/voltages rather quickly and disconnect. In a high DG penetration scenario such behavior can be counterproductive in case of transient voltage drops as it may cause large instantaneous loss of generating capacity and deteriorate power system stability more than the original voltage drop that triggered the disconnection. For this reason low voltage ride-through (LVRT) capability had to be introduced. The LVRT voltage level and duration requirements vary depending on the application and are subject to local regulation, as illustrated in Figure 1.4 [19].

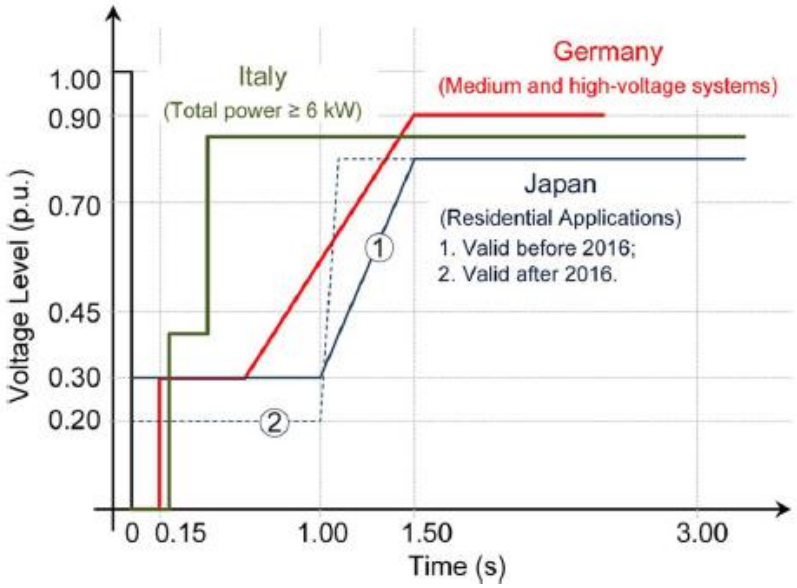

Figure 1.4: LVRT requirements defined in different countries (© 2013, IEEE).

Even more important is the frequency ride-through (FRT) because of its system-wide effects. In Germany, very well known for high penetration of PV at distribution level, the FRT retrofit of PV inverters was necessary because of the imbalances resulting from power trading at transmission (cross-border interconnection) level. The problem is known as "50.2Hz problem" and was threatening to cause massive disconnection of plants at distribution level unless FRT was introduced[20].

Depending on the placement of DG in the feeder the fault current contribution changes, which can impact the protection selectivity - disconnecting the correct feeder once the fault occurs. Some of the selectivity problems caused by DG are: false tripping, blinding of protection and recloser problems [21]. Figure 1.5 portrays a typical false tripping scenario caused by changes in generator fault current magnitude. The fault will cause overcurrent $I_{oc\text{-}DG}$ which can exceed the default relay setttings at $I_{oc\text{-}grid}$ and cause the healthy feeder to be disconnected before clearing the fault.

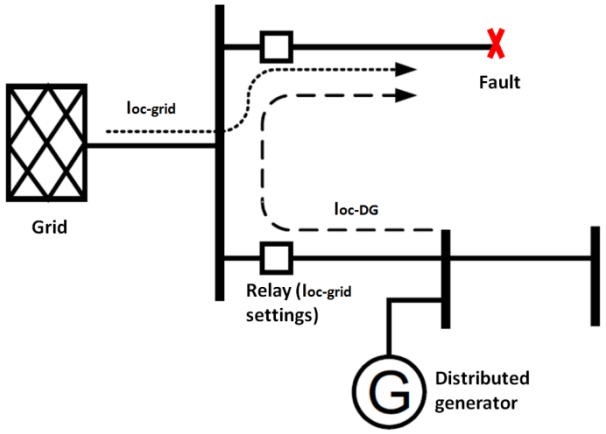

Figure 1.5: DG fault current contribution.

Higher trip settings could be applied as a solution, but that would also cause smaller magnitude faults to become undetectable. More permanent solution would be the use of directional relays however they are more expensive and have slower reaction. Therefore, protection selectivity problems give another reason why quick disconnection of DG is required. Once DG is isolated the circuit becomes unidirectional again and protection can act according to original design.

The power converters are known to inject voltage and current harmonics into the grid which can deteriorate the power quality[22]. The total harmonic distortion will depend on the type of DG and its converter interface, as well as on the number of units and their placement in the grid [23]. In modern converters the switching frequencies have increased considerably providing smoother output voltages and currents, but high frequency currents can also cause electromagnetic compatibility issues. Advances in active filtering capabilities are also contributing harmonic mitigation[24].

The fluctuation seen in light bulbs is known as *flicker* and causes psychophysiological stress in humans. Of all DG types, flicker is typically associated with constant speed wind

turbines as prime mover fluctuations are not buffered by power converter by directly translated into electric power fluctuations[25].

The issues presented in this introductory section provide the reader only with a brief glance on the general DG integration problems. The focus of this thesis is solar PV DG and its integration problems and solutions will be dealt in more details later on.

1.5 Smart grid transformation with support of ICT

The potential of power electronics that enables grid connection of various RES technologies is not fully realizable without exploiting advances in modern information and communication technologies (ICT). With the increasing presence of DG at distribution level, new challenges arise for DSO such as: local load balancing, demand side management, power flow optimization and voltage control. These operations require better coverage of MV, but especially LV grid with sensors and actuators in various degrees of real-time requirements. The Advanced *Metering Infrastructure (AMI)* should provide that. In simplest terms it is a two-way communication platform that combines automatic meter reading and automatic meter management [26]. The smart meters connected through AMI can now be used to remotely read consumption, power quality indicators and switch the load on/off. DSO cannot always financially afford all of these smart meter functionalities. The future tendency of AMI development is expansion beyond smart metering and integration of DG and electric vehicle charging monitoring and control (Figure 1.6).

At distribution level the number of network nodes increases, meshed topologies increase in complexity and so do the self-healing and optimization procedures. This calls for increase of distributed computing applications. The need for more reliability and redundancy requires more autonomous decision making at node level. *Multi-agent system* is a distributed computing platform that originally found its application in multi-objective robotics problems,

but is also expanding in power systems domain with the goal of helping to transform the distribution system from passive into active [27].

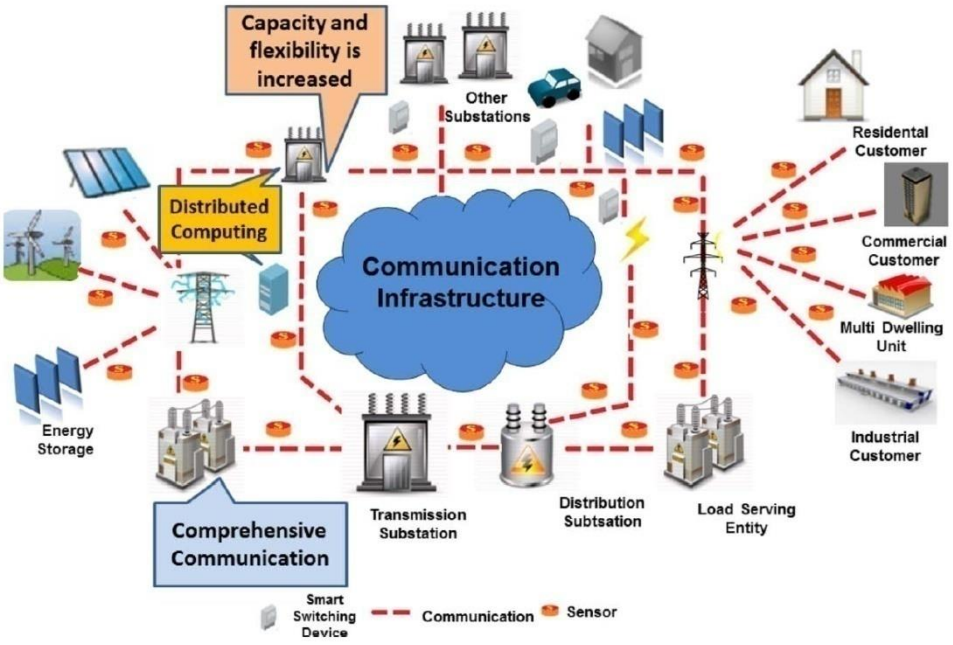

Figure 1.6 Smart grid concept (© 2011, IEEE).

Traditional SCADA system relies on analogue circuits and modems with specific protocols. Reconfiguration of such systems requires rewiring, which is time consuming, costly and requires specialized skills. Typically SCADA modems use 3kHz voice bandwidth which limits the integration potential of SCADA with high bandwidth substation automation, distributed computing and advanced metering infrastructure. The increase in complexity of power system operation calls for a more integrated approach where all aspects could be covered by a single network. Although Transmission control protocol/Internet protocol (TCP/IP) was not immediately considered as it first appeared because of its non-deterministic behavior, the advances in *Quality of Service* are making migration of SCADA to TCP/IP a more likely scenario [28]. The benefits that drive such migration is much easier system

expansion and reconfiguration due to worldwide adoption of internet, well developed hardware and software market and resiliency of IP routing.

The future vision of a smart grid is yet another Internet of Things concept extended into the energy arena, actually, the term "*Internet of Energy*" is already widespread [29]. Today there are very little technological barriers for such realization. The smart home/home automation industry has already made the technology available. Rather, it is a problem of declaring responsibilities devising policies, clarifying business models and solving the problem of privacy and information security before smart grid can truly take off at that very bottom level. The technology currently suffers more from the lack of standardization when it comes to interoperability of devices coming from different vendors and using different communication protocols[30].

CHAPTER 2

Research Goals and Scope of the Thesis

The term "utility-interactive" or "grid-interactive" is used to describe a PV inverter capable of feeding power to the grid in a safe and reliable manner, respecting the regulatory boundaries set by DSO. Not more than several years ago the term "smart inverter" became a more prominent word in both the academia and industry. The term signifies the introduction of new control capabilities that exceed the basic protection existing in most inverters deployed in the world today. The transition from low to high PV penetration era comes with increased complexity of the inverter-grid interaction. More inverter control flexibility and situational awareness is required in order to maintain an efficient, safe and reliable grid feeding operation. In this thesis, being oriented on inverter-based solutions for integrating PV into the grid, the title phrase "*improved grid interaction"* signifies the transition from the "old", grid-interactive inverters to the new, smart inverters as means of expanding grid-connected PV capacities in a seamless, sustainable manner.

2.1 The SELECT+ "Positive Energy House" Project

The SELECT+ is a joint doctoral research program in the area of sustainable energy technologies, sponsored by European Commission. The program combines the scientific research with the development of innovations that have a market potential. The PhD candidates are strongly encouraged to shape their research so that it becomes suitable for technology transfer and commercialization. Also, the participants are obliged to spend one year of their research in the industry, focusing more on the commercialization aspects of the research. The "Positive energy house" was a name given to the project of 2012 that unified nine PhD candidates from nine universities, one of them being the author of this thesis. The

project goal was conceptual development and practical implementation of NPEB. The grid-connected solar PV generators are instrumental to this task.

2.2 Research Objective

The problem of high PV penetration scenarios in residential LV grids forms the backbone of this research. The research goal is to provide a solution for increasing the PV grid hosting capacity, while avoiding changes in the primary equipment. Given the strongly industry-oriented nature of the SELECT+ project, the underlying goal was to provide a practical, easy to implement solution that meets the following objectives:

- distributed solution that can be seamlessly integrated within the built environment without disrupting the lifestyle of NPEB inhabitants
- sustainable - the solution must consider not only the new PV systems, but also the possibility of retrofitting the old systems instead of replacing them
- the solution should be reliable

2.3 Approach and thesis structure

The introductory Chapter I provided a brief glance over a wide range of DG grid integration problems. In Chapter III, according to defined objective, the problem is narrowed down to overvoltage problem due to PV exceeding the grid hosting capacity. A range of centralized and distributed solutions is reviewed to provide the reader with a wider perspective on the problem. At the focus of this research is the interface between the grid and PV, the DC/AC inverter. Specifically, the micro-inverter is selected as the most suitable inverter technology to carry out the solution implementation and answer the entire scope of objectives. Chapter IV introduces the reader with micro-inverter benefits and reviews the designs and technologies that made micro-inverter practically realizable. Achieving grid

support functionalities, such as active power curtailment, only by inverter software retrofit is presented in Chapter V as an important tool in sustainable transition towards smart inverters. An innovative micro-inverter feed-in management system designed to mitigate overvoltage is described in Chapter VI. Once the control algorithm was developed it was implemented in a LV grid model and tested in power flow simulations of high PV penetration scenario. The grid modeling and power flow simulations are covered in Chapter VII. A techno-economic comparison of the proposed solution against known alternatives, as well as reliability prediction study to confirm the proposed reliability advantages are contained in Chapter VIII. Finally, a laboratory demonstration is presented in Chapter IX with final discussion and synthesis in Chapter X.

CHAPTER 3

Review of PV Integration Problems and Solutions

Of all the DG, solar PV is the least controllable source (Figure 3.1). Changes in irradiance in a constrained grid capacity scenario can cause fast voltage ramp-up within seconds, eventually leading to overvoltage[31]. Furthermore, overvoltage is not a solitary problem and can be accompanied by problems of unequal feed-in losses and voltage unbalance.

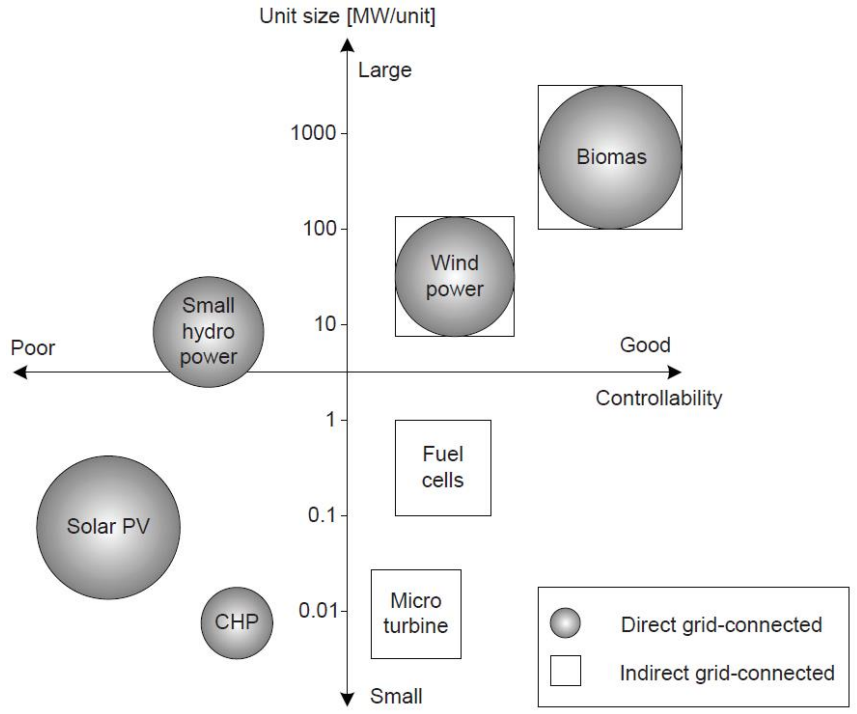

Figure 3.1: Unit size and controllability characteristics of some distributed generators[27]

3.1 Overvoltage problem

The overvoltage due to exceeded hosting capacity is one of the most immediate problems in large-scale integration of PV. Overvoltage deteriorates power quality, reduces the lifetime of electrical components, and presents a potential fire/electric shock risk in case of

insulation breakdown. What really compounds the problem and makes it "visible" to prosumers is the economic aspect. The inverter overvoltage protection acts to prevent the aforementioned problems by disconnecting PV from the grid. These inverter downtimes translate into feed-in energy losses. In a radial distribution feeder the feed-in loss is lowest at the beginning of the feeder and highest at the end. For example, a 6 kW system can experience 0-12.5% annual feed-in loss rise as its location moves towards the end of the feeder. The rise of feed-in loss prolongs the PV system payback time 0-18%. For a larger system of 30 kW this annual loss can get even up to 70% of energy yield [32], [33].

In residential grids, the PV generation profile is known to be poorly matched to the household load profile. Especially during noon hours, low load is correlated with high PV production peaks (Figure 3.2). A significant portion of generated electricity remains unused by the household loads. As the load increases towards the evening hours the solar energy is no longer available and power must be consumed from the grid. Most critical cases for this mismatch represent summer months in high-latitude areas [34]. The excess (net generated) power that cannot be load-matched causes occasional overvoltage. The higher the unmatched generation the more likely is the probability of overvoltage happening.

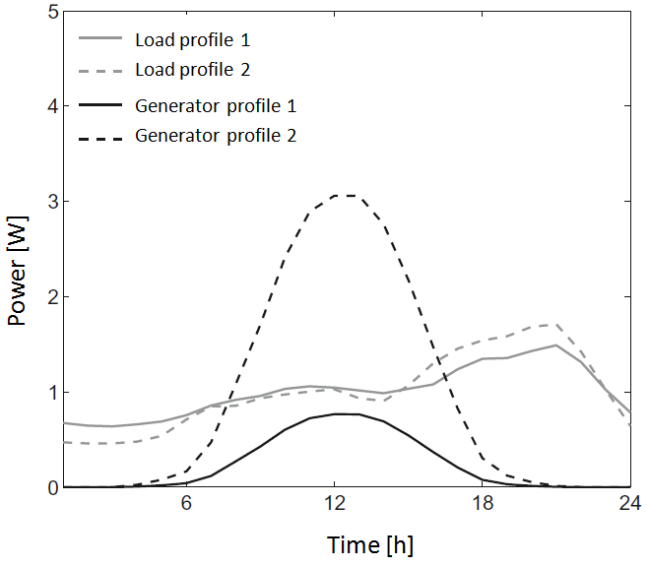

Figure 3.2: Hourly correlation between residential load and PV generation profiles[34].

The voltage rise is also a function of the grid supply impedance, both in terms of its magnitude and electrical characteristics. The impedance magnitude grows with the line length. The rural grids are more likely to experience overvoltage problem due to long lines creating high supply impedances. Figure 3.3 household load profile changes from net consumption to net generation impact the voltage profile as a function of line length (distance from transformer). This portrayed voltage variation is simulated for a Canadian suburban grid [35].

Suburban and rural grids are supplied with overhead lines more often, while in urban grids underground cables are more convenient. Usually cables are shorter than lines so impedance magnitude is reduced. However, the choice of line/cables changes the impedance characteristics which also impacts the voltage variation behavior. The overhead lines tend to be more inductive in nature while underground cables are more resistive. Even if urban grids might have shorter cables, the resistance-reactance ratio will actually be higher. Figure 3.4 shows how voltage variation magnitude increases with resistance-reactance ratio (R/X) under unity power factor and different loading conditions.

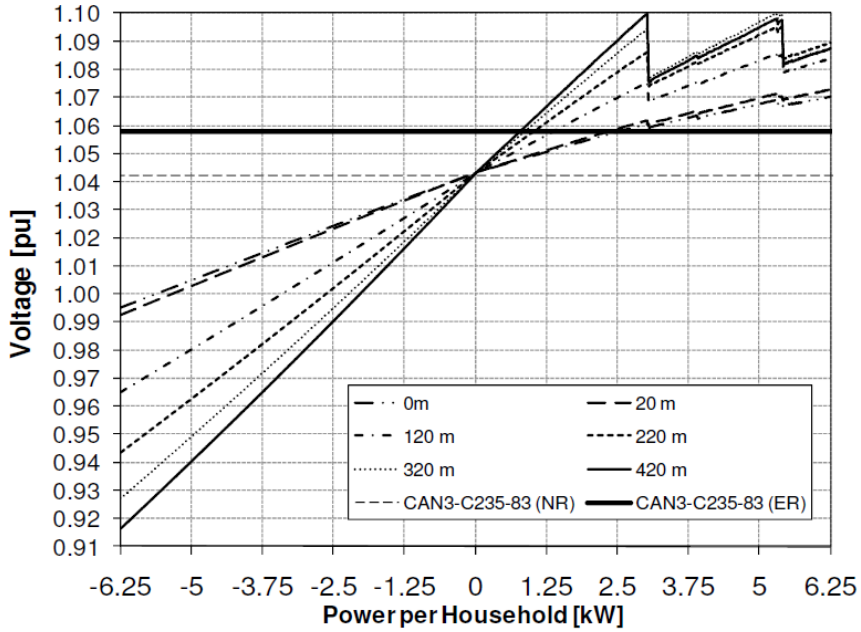

Figure 3.3: Voltage variation depending on line length (© 2012, IEEE).

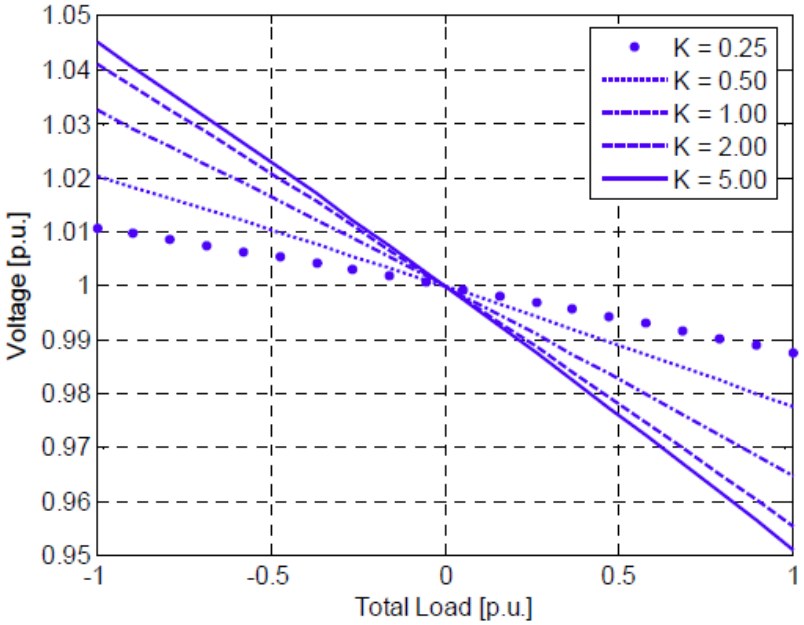

Figure 3.4: Voltage variation depending on R/X ratio K (© 2008, IEEE).

Another observation can be made from Figure 3.3. The Canadian DSO defines the normal operating voltage (0.917-1.042 pu) and extreme operating voltage (0.88-1.058 pu) range. If a corrective action is not taken in 1.042-1.058 pu range, the voltage eventually hits the 1.1 pu threshold at which the inverter disconnects. Only two inverters farthest from transformer experienced overvoltage. Voltage levels along the feeder vary due to increase of impedance from transformer toward the end of the feeder. With no PV (net consumption), the end of the feeder has the highest voltage drop, but with PV presence the situation is reversed and overvoltage first occurs at the end of the feeder. With equal trip settings in all inverters, but with unequal voltage rise levels this creates unequal distribution of feed-in losses.

An overview of simulation studies for determining the level of PV penetration at which overvoltage occurs is given in Table 3.1. These studies were performed for single family houses in urban and rural LV grids of several countries. In a Swedish scenario simulated with 5kW PV per household (rating that can satisfy the Swedish NZEB requirement) a 100% penetration was achieved before overvoltage started happening at 1.05 pu [36]. This however is still far from 1.1pu defined by EN 50160 power quality standard. For an actual standard violation an extreme 325% penetration could be tolerated [37]. Both cases yielded such good results due to Swedish grid being specifically designed to handle heavy heating loads. Such high penetration levels are favorable for the development of residential neighborhoods with NZEB or even NPEB. Rather similar voltage levels were achieved in UK and Canadian grids, yet with a much lower PV penetration. It can be concluded that not every grid in every country is equally prepared for high PV penetration scenario.

Table 3.1: Power flow simulations in LV networks under high PV penetration scenarios.

Country	LV grid type	PV capacity [kW/household]	Voltage/voltage limit [pu]	PV penetration level[%]
Finland[38]	Urban	2	1.055 /1.025	200
United Kingdom[39]	Urban	2.16	1.028/1.02	50
Canada [35]	Suburban	2.5	1.068/1.042	75
Sweden [36]	Urban	5	>1.05[1]	100
Sweden [37]	Rural / Urban	Not stated	>1.1[1]	325

3.2 Voltage unbalance problem

The voltage in a 3-phase distribution network is considered unbalanced if differences in magnitudes and/or angles between phases exist.[40]. Voltage unbalance(VU) can cause a decrease in efficiency of the induction motor, sub-optimal operation of power electronics and reduced capacity in transformers, lines and cables[41]. In the hierarchy of power transmission and distribution system, the three-phase LV grids are most susceptible to voltage unbalance (VU). The main causes are large presence of randomly distributed single-phase loads and, following the latest trends, the increasing presence of single-phase PV. At HV and MV level, loads are mostly three-phase and balanced, but at LV level many single-phase loads exist and randomness of load profiles is greater. Despite the best practices of LV grid planning, some increased unbalance is always experienced compared to MV and HV level. The trends of increasing single-phase DG can further promote the increase of unbalance at LV levels. In most residential applications PV is single-phase. Studies were performed on PV impact on VU[42], [43]. Unlike overvoltage the VU doesn't have a direct economic consequence on the feed-in losses, but indirectly, VU can induce overvoltage and vice versa. One phase can have more PV connected and magnitudes could rise therefore causing unbalance. High PV

[1]Small, finite probability of voltage crossing above utility levels.

penetration in an unbalanced network is especially problematic as it can cause cascaded overvoltage tripping [44].

3.3 Review of mitigation solutions

The capacity of lines, cables and transformers is typically oversized for peak loading. The peak load represents a minor part of the daily load profile, but must be accounted for in order to prevent undervoltage. This leaves the grid infrastructure under-utilized most of the time. This traditional approach would also be applied in an increased PV penetration scenario: during the time of peak generation, voltage goes above limits, and reinforcing lines and adding more transformers will mitigate the problem. It requires intensive involvement of DSO, local authorities' permissions, and encumbering administration. In case of underground cables it requires dig works and digging might be restricted in some areas. Additional transformers might require dedicated land surfaces. It is by nature, a disruptive and slow intervention that could leave prosumers waiting for a long time before they are allowed to connect. The grid infrastructure changes can be delayed or even avoided if other solutions are employed[45].

3.3.1 Centralized solutions

The centralized solutions are implemented and managed by DSO:

- On-load tap changer (OLTC) transformers
- Custom power devices (CPD)
- Utility-scale energy storage

The voltage regulation at LV side of the MV/LV transformer is achieved by manually adjusting the setpoint mechanism called the "tap". This is a traditional approach where DSO must send personnel to the field and power for the entire LV circuit must be interrupted

during the tap change operation. Most MV/LV transformers are still operated like this today. The dynamics of bidirectional power flow requires faster, more automated solutions. The OLTC technology is slowly making its way towards LV from MV and HV grids where it is regularly used. The benefit of OLTC is that it can regulate voltage automatically and without supply interruption[46].The rural grids already face the undervoltage problem due to long cables/lines. The practical approach is to raise the tap from 1.0 to 1.05 pu. This might prevent undervoltage, but it can also increase the chances for overvoltage in high PV penetration scenarios. The OLTC does not offer complete solution and would have to cooperate with PV systems to ensure acceptable voltage levels [47].Still, OLTC is not something that can be yet counted on large scale. Out of five million MV/LV transformers in Europe only about 50-100 thousand is automated [48]. Because of the high number of LV substations, a large-scale automation would be costly.

The custom power devices (CPD) are advanced power electronics devices belonging to the family of so-called *flexible AC transmission system* (FACTS) or flexible *AC distribution system* (FACDS) devices. The CPDs are placed in strategic locations on the feeder to perform a variety of functions: voltage regulation, reactive power compensation, unbalance mitigation and harmonic elimination. In [43] two CPD types, a dynamic voltage restorers (DVR) and a distribution static compensator (DSTATCOM) were applied in VU mitigation caused by unequal distribution of single-phase PV among the three phases. In [49] a DSTATCOM was successfully used to assist the suboptimal OLTC handling of over/under voltage. The application of CPDs in LV grids is in infancy and due to their custom design they are not commercially available in high numbers. This makes them a costly solution for the time being, but promising in the future.

Probably the least considered solution due to the cost and the maturity of technology, the large-scale energy storage is intended for multi-objective purpose with grid support being one of them [50], [51]. The batteries whose capacity measures in MWh could certainly commit part of its capacity to solve the overvoltage problem for the entire feeder or LV node.

3.3.2 Decentralized solutions

In section 3.1. of the current chapter, a distributed character of overvoltage and voltage unbalance problem was described. Unlike the frequency deviation the overvoltage doesn't occur simultaneously in all connection points, but rather manifests at different times and locations. This implies that centralized solutions are not solving the problem optimally and that distributed solutions should be considered. A distributed solution requires a local intervention, either at load side or at PV generator. Some limited effect on voltage decrease can be achieved by demand side management or changing the PV module orientation to improve the load matching capability [34], but comprehensive solutions require direct voltage control by PV balance-of-system components such as inverters. The inverters control voltage by active power curtailment (APC)[52]–[54], or reactive power control[55]–[57]. Mitigation of overvoltage by APC is simultaneously acting beneficially on VU reduction[58]. Another balance-of-system component that could be used is a battery. The batteries are primarily intended for use in self-consumption, but they can prevent overvoltage by absorbing the excess active power [59]. Battery usage for overvoltage prevention can be optimized in combination with other solutions such as inverter reactive power control [60].

3.3.3 Coordinated solutions

The enhanced problem solving requires a combined and coordinated effort of resources at disposal. The coordination may exist between centralized and/or distributed

solutions. The OLTC can optimize its setting points in coordination with DG active /reactive power control using a dedicated multi-agent communication platform [61]. In [62] the APC is engaged as a secondary measure when DSTATCOM is unable to solve the problem by absorbing reactive power. In situations where the distributed energy storage is used to prevent overvoltage, the combined effort with PV inverters supplying reactive power can reduce the battery capacity needed for such an application and improve the overall economics of the solution[63].

The coordination is required to handle the techno-social inequality arising from the problem of the unfair feed-in loss sharing. In making DG cost-effective the application of ICT should be minimal. The coordination based on voltage sensitivity to active and reactive power is researched. It can achieve a relatively good equalization of losses in all buses on the feeder. The coordinated sensitivity-based approach can equalize the feed-in losses of PV inverters [64], but it can also equalize the use of distributed storage capacities for excess PV power absorption[63].

3.3.4 Voltage unbalance mitigation

Most basic and most limited solution is to improve the grid planning practices. Equal distribution of generators on each phase can reduce VU. But the process of purchasing PV systems is random, and 3-phase connection is not always available at prosumer site which makes the planning a limited option. Further solutions that can come from DSO side are application of specialized transformers and fast-acting power electronics devices[41]. In [43], a VU mitigation by DSTATCOM and DVR was analyzed. There are also proposals for an active involvement of distributed generation. In [65] a PV with storage is used to mitigate unbalance. The new control designs for PV inverters are integrating the unbalance mitigation[66]–[68].

3.3.5 Real world case studies and surveys

Technical surveys done in USA, Japan and several developed EU countries show a successful large-scale integration of PV communities. Installed capacities range 0.9-6 kW/house and 4.8-34 kW/building [69]. It should be kept in mind that these surveys are in developed countries with good grid infrastructure and in urban areas. But even so, in some PV communities in Japan with 2.6-5 kW/household, utilities did have to intervene with capital investments like reinforcing distribution lines and adding more transformers. In another case in Japan, 553 PV systems (3-5kWp/system) had to install batteries for matching the excess power [70]. Several utilities in developed EU countries were surveyed and they experience no overvoltage problem in communities where PV was introduced at a high level, but nearly all of them are expressing concerns for voltage rise in the future when PV penetration increases [71]. Concern is expressed specifically for weak and rural grids with higher voltage variations.

Lack of real monitoring data that can support the power flow studies can force the DSO to take a rather conservative approach and ban further connection of PV plants. In Hawaii, a cooperation took place between HECO (local DSO) and Enphase, a micro-inverter manufacturer that has a large product fleet installed across Hawaiian islands. The Enphase allowed HECO to access its monitoring network and use micro-inverters as sensors to obtain a better grid awareness. This resulted in additional 4,000 prosumers being allowed to connect PV on Oahu island alone[72].

Queensland has seen significant increase in PV penetration. In southeastern part alone, more than 22,300 PV were installed in the first three months of 2011 compared to 9,000 installed in the 2009-10. It became difficult for DSO to keep voltage within limits on circuits where some houses had PV and others did not. This resulted in rejection of new applications

to connect PV until it is proven that the installed system does not threaten the operation of the grid[73]. In 2014 the applications for PV counted in 1800/month, which forced the local DSO to cope with the problem by limiting the PV capacity to 5kW per prosumer [74].

Based on these selected examples it can be seen that DSOs aren't proactive about selecting solutions described in previous section. They favor the approach of limiting or rejecting new connections as it is non-disruptive to the business-as-usual scenario. However, that does not stop the growth of new applications in regions with good PV incentives. The backlog of prosumers pending approval on one hand, and the inertia of DSO on the other can give off an impression that almost there is a confrontation between the two parties. This doesn't have to be so, as long as technology providers keep an open dialog with DSO and strive to create seamless PV integration solutions. A cooperation between DSO and a micro-inverter supplier in Hawaii is a good example how DSO, by working together with an inverter manufacturer, can obtain proper instruments to allow more PV to connect to the grid.

CHAPTER 4

From Central Inverters to Micro-inverters

The inverter is a power electronics interface between the PV array and the grid. It takes a special place among the solutions described in the previous chapter, because it is the only component without which the PV cannot operate at all. It means that with every new PV system connected, there is a new inverter deployed, unlike storage which is completely optional component in a grid-connected system. The sheer number of inverters that are already deployed in the field and the even greater number of inverters to be deployed in the future, are direct contributors to grid integration problems. This research is within the scope of single-phase, current source PV inverters as they are the most common type used in LV grids.

4.1 Basic functionalities and industry drivers

In order to perform a successful grid feeding operation, the PV inverter must implement these functionalities: maximum power point tracking (MPPT) for DC power harvest maximization; DC voltage boost for voltage conditioning before conversion; modulation of DC current to AC sinusoidal current; synchronization of AC sine wave to the grid phase angle and frequency; protection/connection of inverter circuit and the grid (Figure 4.1).In addition, electromagnetic interference (EMI) filtering and anti-islanding are standard nowadays.

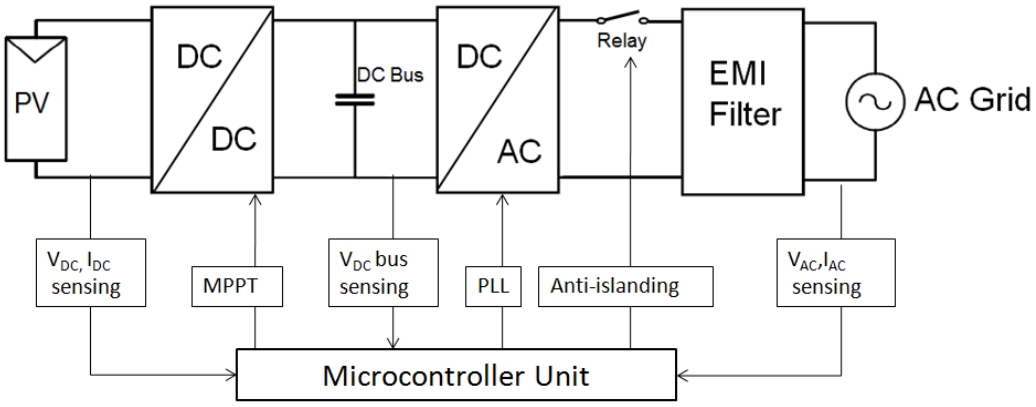

Figure 4.1: Basic inverter schematic with fundamental functionalities.

The main drivers of the PV inverter industry are:

- cost reduction
- efficiency increase
- reliability increase

Cost reduction can be realized by selecting components made of new materials with the same rating, but smaller in size and therefore cheaper. A significant cost reduction can be achieved by eliminating certain components, entire circuits even, by applying new design topologies, while maintaining the same or even better level of functionality. The increased efficiency is practically realized through more accurate MPPT and higher DC/AC conversion ratio. The approach for reliability improvement is similar to cost reduction approach: selection of components with longer life span, reduction of components through design has a cumulatively positive impact on reliability. Other important drivers are reduced cost of installation and safety from fire and electric shock which will also be touched upon in the following sections.

4.2 MPPT

The MPPT is the most distinct feature that differentiates PV inverter from inverters in other applications. At any point in time, under constant irradiance, the PV is outputting power according to its current-voltage (I-V) characteristic. There is an ideal maximum power point (MPP) at which both current and voltage exhibit maximum value (Figure 4.2). However, this point is not fixed, but oscillates with variation of irradiance, temperature and load. It needs to be tracked by microcontroller with MPPT algorithm. The more accurate MPPT means more efficient MPPT. Various algorithms are proposed, but most widely used in the industry is perturb-and-observe due to its high efficiency [75]. In addition to creating a good algorithm, another challenge to overcome is the PV *module mismatch* problem.

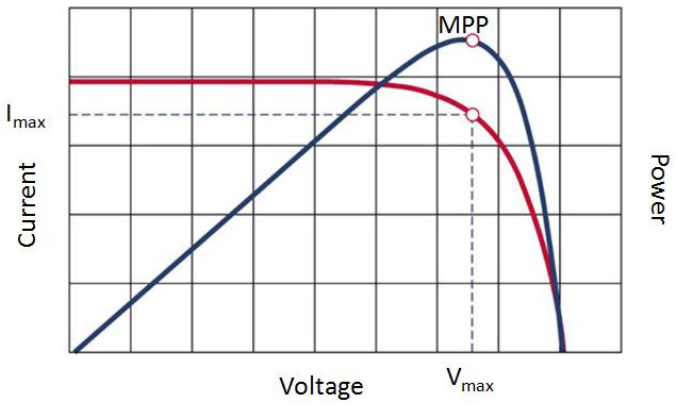

Figure 4.2: I-V characteristic of PV with maximum power point.

4.2.1 PV module mismatch and MPPT efficiency

In simplest terms the module mismatch problem can be described as follows: if one module fails or underperforms, the maximum power point of the entire plant will drop [76]. Possible causes of module mismatch are: partial shading, soiling, differing rates of module degradation and manufacturing tolerances. The partial shading is more pronounced in residential areas due to roof orientation/design constraints and localized shading from the tree

canopy [77]. The "domino effect" of one module affecting the entire array is a combination of how MPPT works, module wiring topology, and inner design of a single module. The PV modules are conventionally connected in series in order to raise the inverter input power by summation of voltage across the array. The PV modules have bypass diodes whose function is to bypass the current flow from the shaded cells in order to protect the cells from "hot spots". The shading of PV cell will reduce its short circuit current and if the incoming current of unshaded cell is higher, it will cause the shaded cell to overheat eventually causing permanent damage. To avoid damage, the bypass diode of shaded module will become forward-biased and create alternative flow through the unshaded cells. This will cause the voltage drop across the bypassed area and the MPPT will shift according to lower voltage (Figure 4.3).

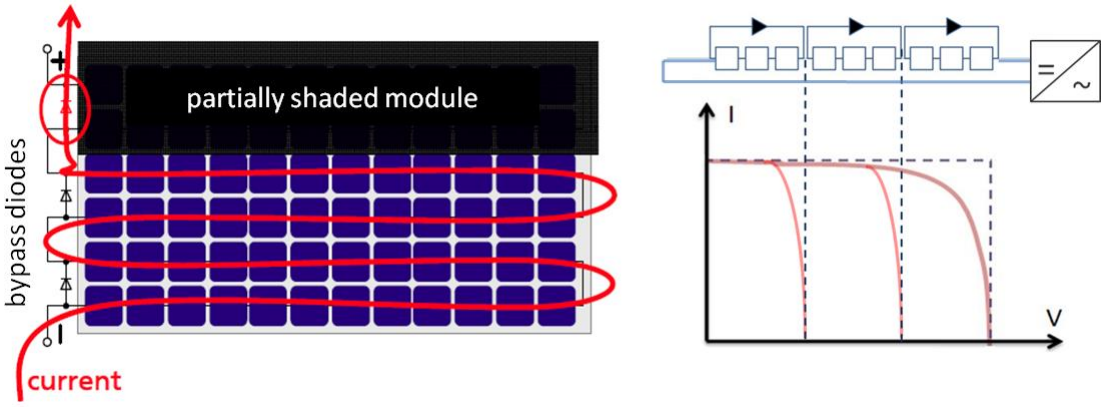

Figure 4.3: Bypass diodes protect the shaded cells, but also reduce MPPT efficiency.

As bypass diodes increase the price of modules, they are scarcely deployed so large number of cells get bypassed. Modules are connected serially into arrays. Longer arrays create higher input losses. It is necessary to segment the array in order to increase the MPPT efficiency.

4.2.2 MPPT and modular inverter topologies

The need for more efficient MPPT has driven the PV plants to become more modular. Hence, three major topologies are distinguished today: central inverters, string inverters and micro-inverters (Figure 4.4).

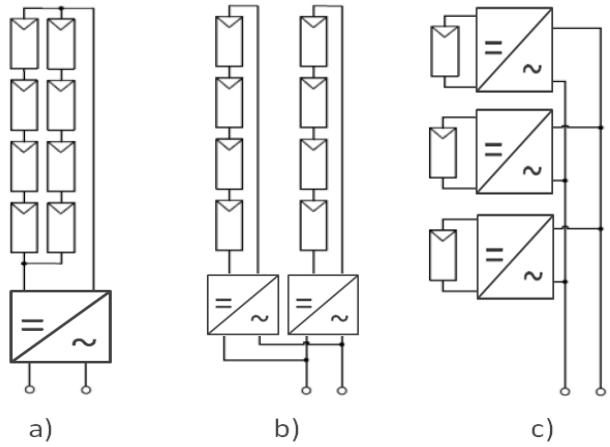

Figure 4.4: Inverter topologies: central (a), string (b) and micro-inverter (c).

Historically, first PV inverters appeared in 1980's. In the beginning it was a simple transfer of technology from the drive systems industry to the solar PV industry [78]. The idea was that only one inverter can be used to harvest the DC power of the entire PV plant as long as it is properly sized. Hence the name "central" inverter as it represented the central point of connection to the AC grid. It soon became apparent that central inverters don't provide optimal MPPT, due to PV module mismatch problem. The PV array was divided into strings. Series connected strings would then be connected in parallel to the grid (Figure 4.4, b)). The multi-string systems isolate the MPPT efficiency problem down to string level, but the problem remains at module-level.

The module-level power conversion better handles the MPPT efficiency problem than central and string inverter topologies. Module-level MPPT can surpass the mismatch problem and provide increase in energy harvest. In studies that only focus on an estimation on the basis

of partial shading, estimated yield gain is 10%-19.5% [79]–[81]. Actual measurements in a large field study involving 143 sites equipped with micro-inverter systems have shown an average of 16% energy yield gain compared to string inverter systems[82].

4.3 Micro-inverters

Module-level conversion, more specifically micro-inverters, is becoming increasingly popular alternative to central inverters especially in residential, building-integrated PV applications. In a fixed rooftop or a building-integrated application the PV modules are more susceptible to shading and module mismatch, so it is these applications that micro-inverters excel in. The term "micro-inverter" is most widely used in the industry and refers to the most common, externally mounted version (Figure 4.5, right). The term "AC module" is also frequently used, but more related with a module-integrated version (Figure 4.5, left).

Figure 4.5Module-integrated (left) and externally mounted micro-inverter (right).

The idea of module-level power conversion dates back to seventies, but there were many technical limitations for its realization at the time. The first micro-inverters begin to appear in the early nineties, however they soon disappeared from the market due to high cost

and high failure rates. However, technology has advanced significantly and from 2009 onwards micro-inverters, made a strong return to the market [83].

4.3.1 Benefits of micro-inverter topology

The MPPT efficiency is not the only benefit that caused the popularity of micro-inverters to rise. It was fast realized that highly modular approach to PV system design brings about additional and important benefits [84], [85].

It became much easier to pinpoint the problem in the PV array. Central inverter used to be the only point of data acquisition for the entire array making it almost impossible to spot which module has the problem. With each module equipped with a sensor and providing data via remote access, this has revolutionized the maintenance practices.

If the central inverter owner would want to expand the PV system capacity, re-wiring of the system and replacing the inverter would be necessary. Micro-inverters allow very gradual and easier system expansion. The installation procedure itself become easier and cheaper as there is no complex DC wiring involved and the use of more expensive DC protection switches. The plug-and-play approach offered by AC module allows less skilled person to install the system.

With micro-inverters DC voltages became several times lower (i.e. up to 60 VDC compared to string system with 400 VDC). This reduces fire risk from DC arcing and minimizes impact from electric shock.

The micro-inverters provide increased system-level reliability. In case of a central or a string inverter failure there is 100% plant/string loss while in case of a micro-inverter the failure it is limited to only one module.

4.4 Technological trends: How inverters became smaller?

The increase in modularity to reach higher MPTT efficiency would not be feasible without reduction in inverter unit size, weight and cost. This section highlights several technological advances in components and design that support practical realization of smaller inverter (including micro-inverter), taking into account the key industry drivers: efficiency, cost and reliability.

4.4.1 Film capacitors in active power decoupling designs

It was mentioned in Section 4.2 that MPPT depends on irradiance, temperature and load variations. There is nothing that can be done to influence the environmental variations, but it is possible to influence load to appear more constant from perspective of MPTT algorithm. Very important part of the inverter design is the decoupling of DC power produced by PV from the AC load power. The efficiency of MPPT is increased by providing a more constant load current. Larger capacitance gives better decoupling capability, but also increase the cost, weight and size of the inverter [86].The component reliability can be improved with film capacitors, which are more expensive than electrolytic, but also have a longer life span. At micro-inverter scale it is cost effective to employ them to increase reliability. Film capacitors are therefore used in active power decoupling (APDC)applications[87]. Reliability is enhanced in two ways: by using longer life span capacitor and by elimination circuitry through improved power decoupling designs[88]. In Figure 4.6 two micro-inverter APDC designs are shown. In both cases the idea was to reduce the size of electrolytic C_{DC} by implementing APDC circuits with much smaller C_x film capacitor. In the bottom design APDC is achieved with using only one switch while top uses four switches.

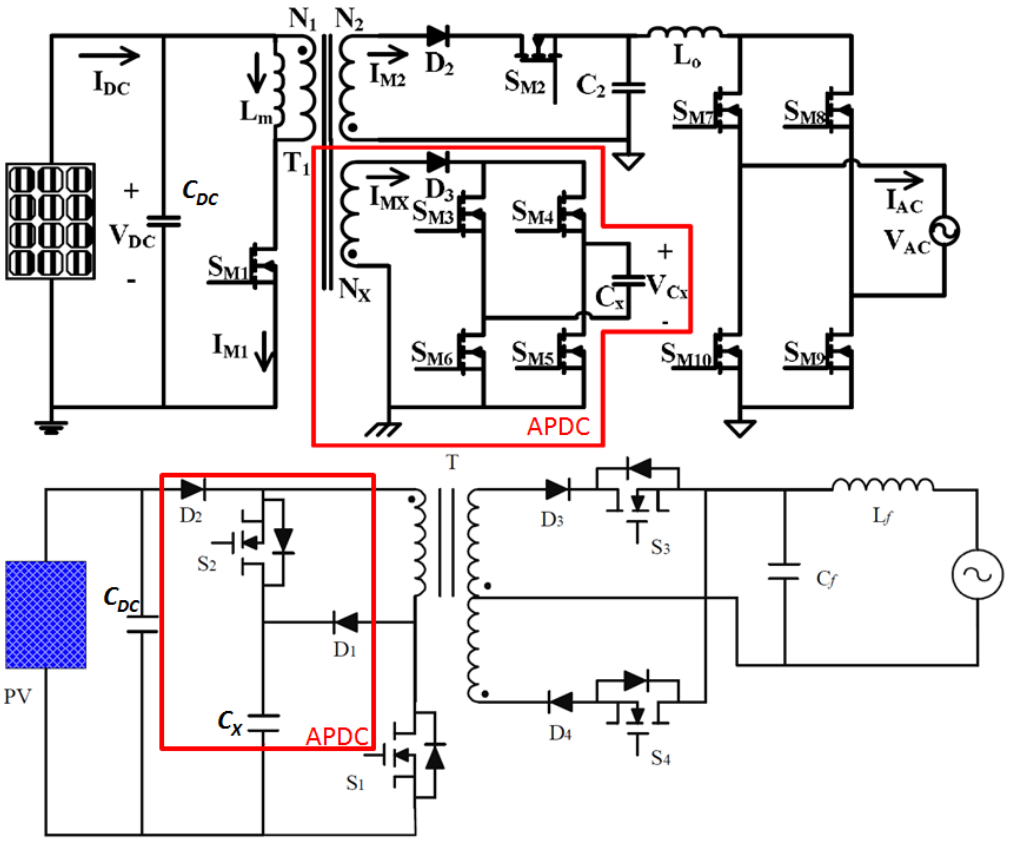

Figure 4.6: Two micro-inverter designs with APDC circuits and C_x decoupling film capacitors (2011, IEEE).

4.4.2 Transformerless inverters

One approach in reducing weight and size is using *transformerless* inverters. Inverters without grid connection transformer are generally more efficient and cheaper compared to inverters with transformers. This is especially true for line frequency (LF) transformer which are the bulkiest and add most weight to the inverter. Instead of stepping up voltage with LF after the DC/AC stage, the voltage is boosted using DC bus section of transformerless inverter (Figure 4.7).Their only disadvantage is having no galvanic isolation, however different studies show that transformerless inverters have a negligible impact on the electromagnetic interference and electric shock hazard [78].

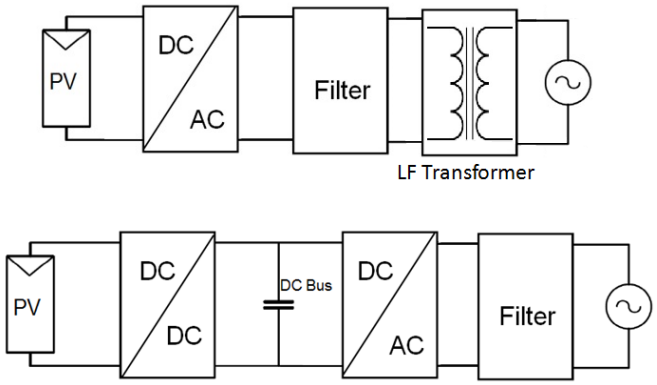

Figure 4.7: Inverter with LF transformer and transformerless inverter.

4.4.3 Resonant inverters and HF components

The resonant inverters operate at high frequencies (HF), several hundred times higher than the line frequency. The HF operation results in reduced size, weight and cost of components. The reduced size results in lower switching losses, reduced semiconductor stresses, etc.[89]. Therefore, in a micro-inverter application a HF transformer can provide galvanic isolation while meeting the smaller size requirements unlike the line frequency transformer. This reduces the inverter size and weight, saves on component materials and even increases inverter efficiency by 2% [90].An important design objective is to realize a HF transformer with a low leakage flux. Practically this means having a low turns ratio, so to compensate the smaller voltage stepping range, a DC bus capacitance is placed after the transformer (Figure 4.8). The HF transformer is placed after the DC converter stage as a first step of the DC voltage boost, then the DC bus capacitors finalize the boost[91]. In Figure both micro-inverter designs utilize HF transformers. In fact in [88], the APDC circuit is multipurpose: it improves MPPT efficiency and uses its decoupling capacitor to store the transformer leakage energy, therefore eliminating the need for extra dissipative circuits.

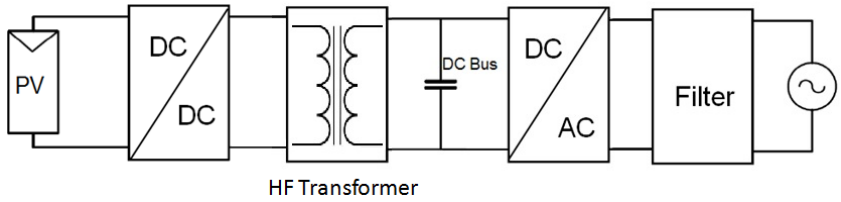

Figure 4.8: Inverter with HF transformer.

4.4.4 Z-source and quasi-Z-source inverters

Two-stage topology consisting of separated DC boost converter and inverter dominates the inverter design. The Z-source inverter (ZSI) offers the possibility of having boost and conversion as a single stage. The boost functionality is achieved passively using impedance (Z) network instead of active switches [92], [93]. The impedance network is realized with capacitors in X shape across inductors (Figure 4.9). Not only that reduction in size and cost is achieved by eliminating the DC stage, but reliability is considerably improved with having no switching components and shoot-through current is much better tolerated by passive components.

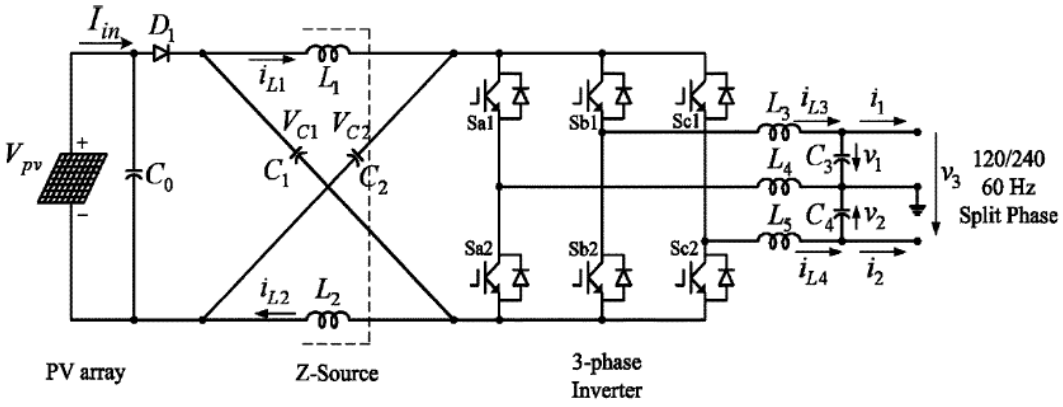

Figure 4.9: Z-source inverter (2006, IEEE).

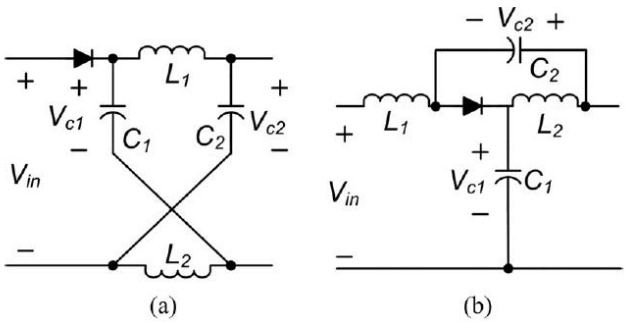

Figure 4.10: LC configurations of voltage-fed ZSI family (a) ZSI, (b) qZSI (2013, IEEE).

The quasi-Z-source (qZSI) inverter (Figure 4.10, (b)) has a LC configuration and is essentially providing the same benefit as ZSI, but with an added value - the capacitance required for the passive impedance network is smaller [93]. The micro-inverter described in [94]was realized with 30% reduced rating of electrolytic capacitor when qZSI was applied instead of ZSI.

CHAPTER 5

Transition to Smart Inverters

The PV inverter designs for LV networks did not immediately anticipate network capacity problems. Historically, the focus was on making use of feed-in incentives by maximizing power output. This is why most inverters deployed in the world today only have MPPT function and basic anti-islanding protection. However, the connection requirements are evolving and becoming more demanding in terms of inverter capabilities [98]. APC and reactive power support are new functionalities (ancillary services) that define the so-called "smart inverter" [99]. Not only new inverters that come of an assembly line must become smart. The new grid interactions affect both old and new inverters simultaneously. The introduction of smart inverter must be treated holistically otherwise transition to high PV penetration will not be optimal, nor sustainable.

5.1 Anti-islanding

The PV inverters operate mostly as current sources. As long as they sense the referent grid voltage and frequency they continue to supply power. When specific conditions meet, during a supply interruption the inverter might not detect it and will continue to supply power. This will happen either when inverter power output and load are closely matched or if there are inverters or other devices on neighboring circuits that continue to act as grid reference sources. Such an event is called *islanding*, because an "island" of electricity has formed in a "sea" of isolated circuits. Islanding can cause several incidents: damage to customer loads, improper functioning of protective equipment, and, most importantly, risk of electric shock for maintenance personnel. Therefore, anti-islanding is protective function that allows the inverter to detect an interruption, stop feeding power and prevent the mentioned incidents

from happening. Frequently used term for an inverter with anti-islanding function is *utility-interactive* or *grid-interactive* inverter [95], [96].

Two major categories of anti-islanding methods exist: passive and active [96]. Passive anti-islanding is based on monitoring grid parameters such as voltage and frequency and disconnecting the inverter when they are out of defined range. Active anti-islanding requires the inverter to inject a disturbance and monitor the response of the circuit in order to determine if the grid is present or not. Both categories can be divided in further subcategories shown in Figure 5.1.

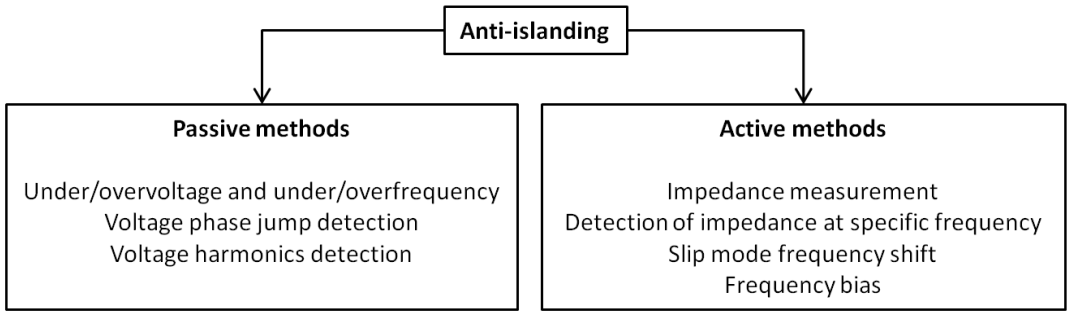

Figure 5.1: Passive and active methods of islanding detection.

Of further interest is the undervoltage/overvoltage protection (UVP/OVP) because it is the simplest, most widely applied method in the industry, and it is an important starting point for understanding the solution described in the next chapter. According to VDE-AR-N4105 interconnection standard the UVP/OVP must disconnect the inverter from the grid if voltage goes below 0.9 pu or exceeds 1.1 pu [97]. The real-time requirement is maximum 0.2s *clearing time*, but in case of Dutch grid code the requirement is 2s. After this follows the production downtime defined by *reconnection time* parameter during which the voltage must remain within allowed limits and only after this time is the inverter allowed to reconnect. According to German VDE-AR-N4105, the standard reconnection time has minimum duration of one minute, IEEE1457 requires five minutes and IEC61727 is flexible ranging

from twenty seconds to five minutes [97]. The DSOs can impose longer reconnecting times and stricter voltage limits if they find it necessary. The inverter manufacturer is then obliged to update the firmware accordingly.

5.2 Enabling smart inverters via software retrofit

Most inverters installed in the world today meet only basic protection like UVP/OVP and rarely have a remote communication capability. For a smart inverter the UVP/OVP is too basic and non-optimal for the power flow dynamics of future grid with high PV penetration. More intelligence is required in form of voltage and frequency regulation by dynamic control of active (P) and reactive (Q) power. A remote access is necessary in order to turn the inverter into a DSO asset. So P/Q control and remote access capability is what makes a distinct difference between a smart inverter and what is typically understood as a grid-interactive inverter.

The transition towards high PV penetration can also be viewed as a transition from the already deployed, MPTT-only inverters towards smart inverters. The process of transition is driven by the adoption of new grid codes. Usually a commissioning date is established after which every new inverter must have smart functionalities while inverters installed prior to that date must either be replaced or retrofitted with new functionalities. In some cases it is possible to perform retrofit only by modifying inverter firmware (software retrofit).

Large-scale software retrofits are already reality. Such is the German directive VDE-AR-N-4015[98]. Under this directive, an ordinance for FRT (Systemstabilitätsverordnung-SysStabV) was issued, requiring a retrofit of 315,000 PV plants. The total estimated retrofit costs are: €65-175 million for retrofitting and €20 million for administration, all borne by the electricity consumers [20]. The three technical guidelines including frequency-controlled APC were given. A four year period was assigned for the completion of this retrofit.

Another, much effective example of large-scale software retrofit is the 800,000 micro-inverters retrofit on the island of Oahu, Hawaii [99]. The retrofit concerned the FRT and VRT for 140MW of installed micro-inverter capacity. This retrofit was completed in a single day. Such an express performance is owed to a strong remote communication support that accompanies micro-inverters. A comprehensive outlook on software inverter retrofit was discussed in [100] and takes into account four aspects depicted in Figure 5.2.

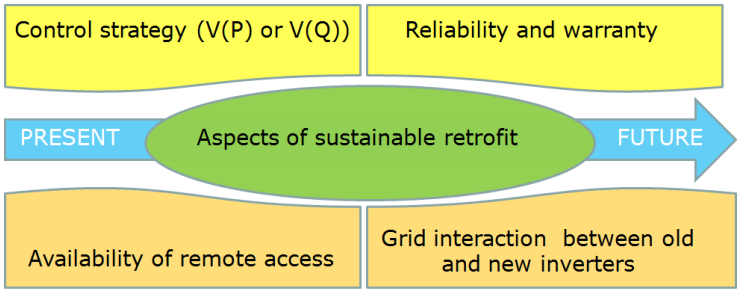

Figure 5.2: Four aspects of sustainable inverter retrofit.

5.2.1 Active vs. reactive power control

The impedance of LV networks is predominantly resistive (R>>X). As a consequence, voltage is more sensitive to variations of active than reactive power, so using reactive power to regulate voltage in LV is not as effective. A comprehensive voltage sensitivity study for radial LV/MV feeders was performed in [101] and its results are reused in Figure 5.3 for the purpose of this discussion. A typical LV feeder can be characterized with impedance ratio of R/X=5, while R/X=1 and lower is more applicable to MV. In case of LV feeder even when power factor is lowered to 0.8, dV/dP is still three orders of magnitude higher than dV/dQ. This suggest that in LV feeder, a reactive power could compete against active power in voltage control effectiveness only by cumulative action of multiple inverters. In an inverter unit vs. unit competition, the one using active power control would be much more effective. It

is only at R/X=1 and with non-unity power factor that reactive power control would become competitive on a unit vs. unit basis.

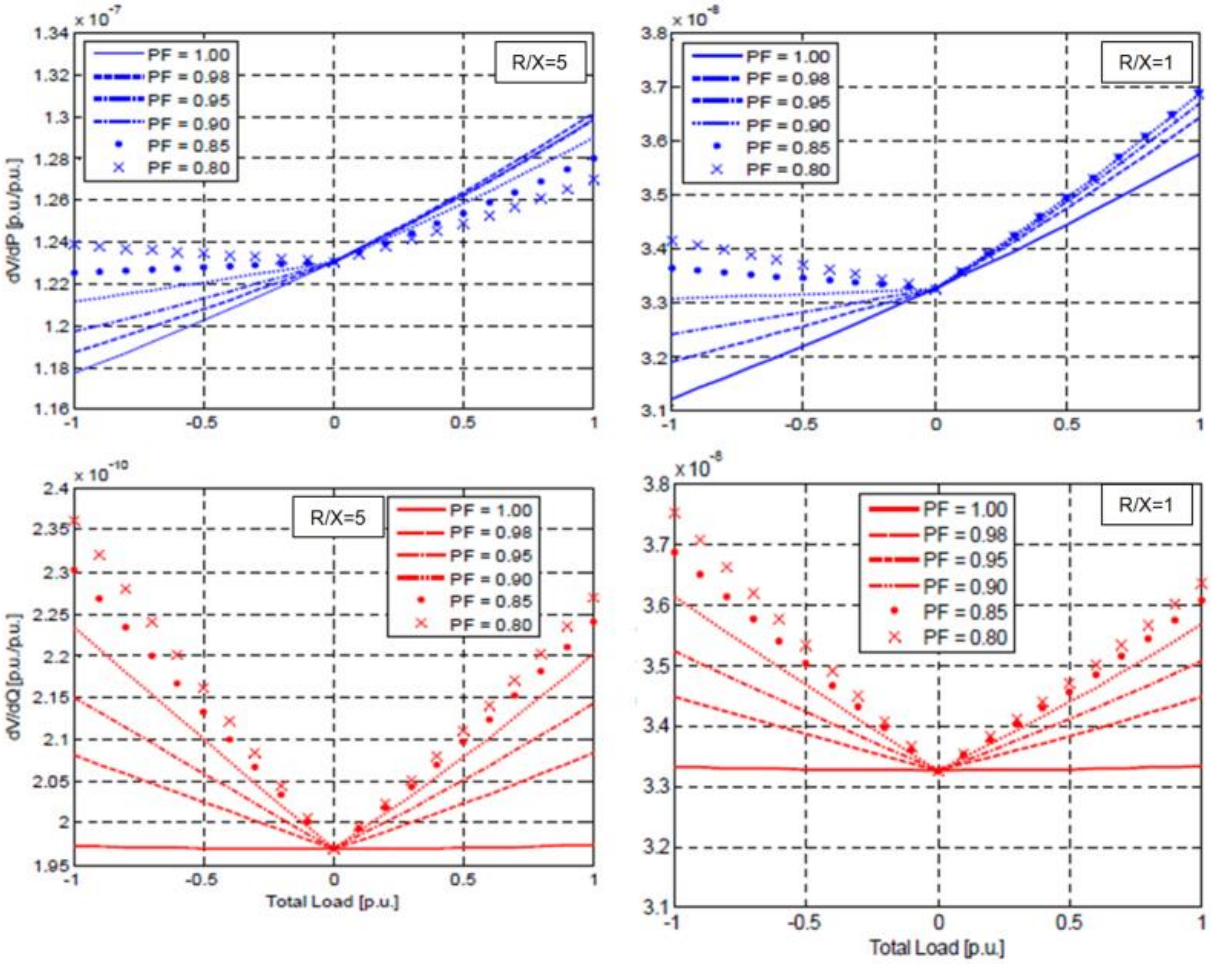

Figure 5.3 Voltage sensitivity to active and reactive power variation depending on R/X, power factor (PF) and net loading (© 2008, IEEE).

The Dutch LV grid is mainly supplied with cables with R/X ratio between 3 and 5. Even at Dutch MV levels, when cables are used the R/X=2 while in case of MV overhead lines R/X gets about 0.5 [102]. So at distribution (LV and some MV) levels where cables are used voltage drop primarily depends on active power.

The inverter would have to be largely overrated for reactive capacity and it would work with low power factor which contributes to losses and deteriorates power quality. Active power variation can control voltage more effectively, but since the inverter by default

operates in MPPT mode, voltage can only be lowered by curtailing power. Despite its effectiveness in voltage control, APC is always considered as a last resort and advantage is given to reactive power control, because curtailing active power produces feed-in losses and has direct economic consequences for the PV owner[54], [62]. Nevertheless, if the overvoltage probability is low, curtailment can be profitable, because it allows PV to feed some amount of power, rather than having no feed-in at all, due to inverter trip.

In [45] the reactive power control was assessed as the most cost-effective option however authors state that they have assessed it as a "green-field" project, meaning there are no already deployed systems involved and that inverters are oversized for reactive power from the beginning. Old inverters would have to reduce active power output in order to accommodate reactive power otherwise failure is likely to happen due to exceeding their rating. Therefore, in a software retrofit scenario reactive power will also lead to feed-in losses as shown in Figure 5.4.Only an oversized inverter can support the same amount of active power (P).

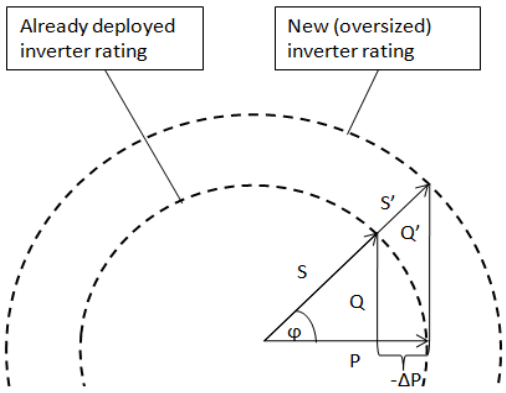

Figure 5.4: Retrofit for reactive power (Q) comes at the price of active power loss (ΔP).

5.2.2 Reliability and warranty

In the present day most inverters are digitally controlled which enables easier implementation of various MPPT algorithms [75]. The expectation is that control algorithms

for software retrofits should also be relatively easy to implement. However, from the manufacturer's viewpoint this is not just a software domain problem. These software changes can impact the reliability of existing components, especially if the inverter application is in severe environmental conditions. Industrial survey on the reliability of power converters portrays capacitors and transistors as the most fragile components, whereas extreme ambient temperatures are the main source of environmental stress [103].

The APC implementation requires varying the transistor duty cycle in the DC-DC boost section while reactive power control requires the same in the DC-AC section [31]. In addition, the latter increases voltage stress on the DC link capacitors [104]. Retrofit for APC is less invasive, however it is still a new, untested functionality. Inverters manufactured prior to the grid code change went through accelerated life tests, but only for MPPT regime. It can be suspected that implementing active and, especially, reactive power control in the environmentally worn-out inverters, could produce unforeseen failure mechanisms and warranty could be questioned. Some manufacturers will openly state that already deployed inverters cannot be retrofitted for reactive power control[57].

5.2.3 Availability of remote access

Implementing remote communication with distributed PV is important for the operational efficiency of the grid. Two-way communication for the purpose of monitoring and control is an integral part of smart grid technology. In Germany in 2012 it became mandatory for inverters to have a remote control access enabled for DSO. All inverters under 30kW must have it otherwise they would have to limit active power down to 70% regardless of grid conditions [45].However, remote access is not always available and depends on the inverter age (commissioning date). In the German case, a sensitivity analysis of retrofit cost to inverter

size and commissioning date was performed. The cost trend is presented in Figure 5.5, based on data provided in [20].

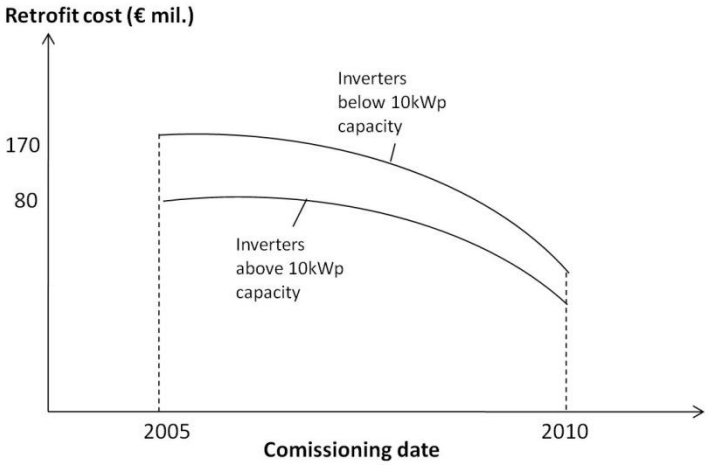

Figure 5.5: Software retrofit costs as a function of inverter commissioning date and capacity.

It can be observed that:

- In the same capacity category, older inverters will incur more cost
- For the same commissioning date, smaller inverters will incur more cost

Such trends are result of high number of small inverters with lack of remote communication. If only local interfacing is available then installers must spend fuel for transport to and back from the PV plant location. Also, the cost of administering fieldwork operation grows. Remote access would reduce the fuel costs and CO_2 emissions associated with transport. Focusing on inverters with more recent commissioning date that already have remote access as part of the standard commercial package is the low-hanging fruit of sustainable retrofit and the Hawaiian micro-inverter retrofit proves it.

5.2.4 Grid interaction between old and new inverters

Different generations of inverters and different manufacturers can exist in the same feeder. Inevitably this leads to having a mix of inverters with and without new functionalities, connected to the same LV circuit. This is a rarely discussed transitional problem, very similar

to the unequal distribution of feed-in losses already described in Chapter III. When multiple PVs on the same feeder engage in a voltage control, unequal sharing of feed-in losses occurs. As the feeder length increases, so does voltage sensitivity to active power. The same amount of power injection will cause higher magnitude voltage variation in points farther from transformer (Figure 5.6). If all inverters use the same voltage limit to trigger the curtailment, then inverters towards the end of the feeder will trigger earlier than inverters closer to the transformer. The inverters A and B export at peak power and both have curtailment functionality. Inverter B engages curtailment at two instances in time. Curtailment at B also has an effect on lowering voltage at inverter A, which doesn't engage its curtailment. In other words, voltage rise that is caused by both inverters gets to be solved by only one of them at the price of unequal feed-in opportunity. Identical situation (from a system state point of view)

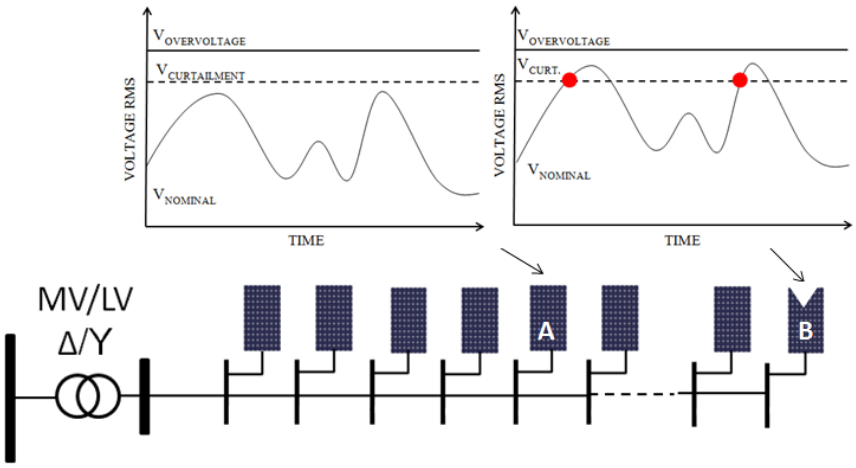

Figure 5.6Interaction between inverters on the same feeder: unequal voltage-controlled curtailment.

is when inverter B is curtailment-capable and A is not. The same network state and variables, only the context of the problem is different. The position in the feeder can only make it worse or better for the engaged inverter, but the fact that one inverter starts curtailment and the other doesn't is enough to cause the problem. Without information and communication technologies

(ICT) infrastructure equally available and unified communication standard between different inverter brands this problem is difficult to optimize in practice. Some DSOs don't necessarily view the unequal curtailment as a problem and intend to solve it by financially compensating the prosumer who got curtailed.

5.3 Summary

The retrofit is an important aspect of smart inverter implementation, hence it was made on of the objectives of this thesis. The active power has a much more dominant effect on voltage control in LV networks and is more retrofit-friendly orientated compared to reactive power control. Large-scale retrofit in Germany opted for active power control and Hawaiian case demonstrated the micro-inverter technological maturity to execute FRT and VRT in a fast and efficient manner. The next chapter follows with proposal of retrofit-friendly APC solution with objective of preventing grid overvoltage.

CHAPTER 6

Micro-inverter Feed-in Management System

The micro-inverter benefits mentioned in Chapter 4 were mostly of interest to the system owner, but it is the system modularity that inspired the control design proposed in this thesis. The feed-in power is the active power. The term "feed-in management" used in this thesis is a form of APC. Conventionally understood, the APC is a linear ramp control, better known as *droop* control. Typically in HV and MV grid there can be either frequency/active power droop, or voltage/reactive power droop [105]. As mentioned previously, in LV networks, due to more resistive character of the impedance, it makes sense to apply voltage/active power droop. The curtailed power quantity is dependent on the voltage sensitivity to active power change which changes with the location of the inverter in the feeder. This is expressed using droop coefficient. The droop APC is a linear ramp-down of power injection from the MPPT point to a power point associated with desired voltage level (Figure 6.1).

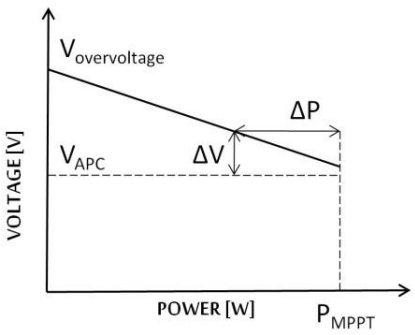

Figure 6.1: Linear characteristic of active power-voltage droop control.

Transition from MPPT to droop mode works without interruption of feed-in operation, therefore inverter is in a continuous operating state as long as PV modules generate power. Ramp slope can be determined from the following equation [64]:

$$\Delta P = P_{MPPT} - \frac{dP}{dV}\Delta V \tag{6.1}$$

where ΔP is curtailed power injection, P_{MPPT} is maximum power injection, ΔV is the voltage level above which APC is engaged, and the dP/dV is the droop coefficient.

In PV inverters, power ramp-down is implemented by reducing the MOSFET duty cycle in the DC-DC section [31]. By reducing duty cycle the junction temperature should drop too [106]. Furthermore, by reducing duty cycle, the DC bus voltage is also reduced which acts beneficially on the voltage stress of capacitors. However, in a software retrofit scenario droop functionality might pose a reliability risk for MOSFETs not tested for dynamic variations and wide range of duty cycle gains issued by the droop controller. There is an opportunity to increase the cool-down benefits of reduced temperature and voltage stress while implementing APC in a more retrofit-friendly, yet competitive way compared to droop.

6.1 Sequential module-level tripping

In this thesis, a new control concept called sequential module-level tripping (SMT) is proposed, that implements APC on a PV plant level, but unlike droop, it avoids using DC-DC MOSFETs to execute APC. On an individual inverter level it does not exist, because instead of being implemented on DC-DC or DC-AC power stage switches, it is implemented in the AC protection switch just behind the filter (Figure 6.2). This is achieved by exploiting the modular design of micro-inverter PV plant and an existing OVP function within each micro-inverter. The OVP was described in previous chapter as part of the mandatory anti-islanding functionality in all PV inverters. At a defined voltage threshold it operates by disconnecting the PV plant from the grid, causing 100% feed-in loss for the duration of defined reconnection time (5 minutes). This interruption is known as "voltage trip". If voltage is normalized after

5min, the inverter resumes the feed-in operation. In a series (string) connected module topology it is unavoidable to lose the entire PV string during voltage trip. Via micro-inverters each module can be tripped independently, causing only partial loss (module-level trip).

The SMT is designed to be competitive with droop. Figure 6.2 shows that each droop function can be approximated by a staircase function, where each discontinuity represents a single micro-inverter trip.

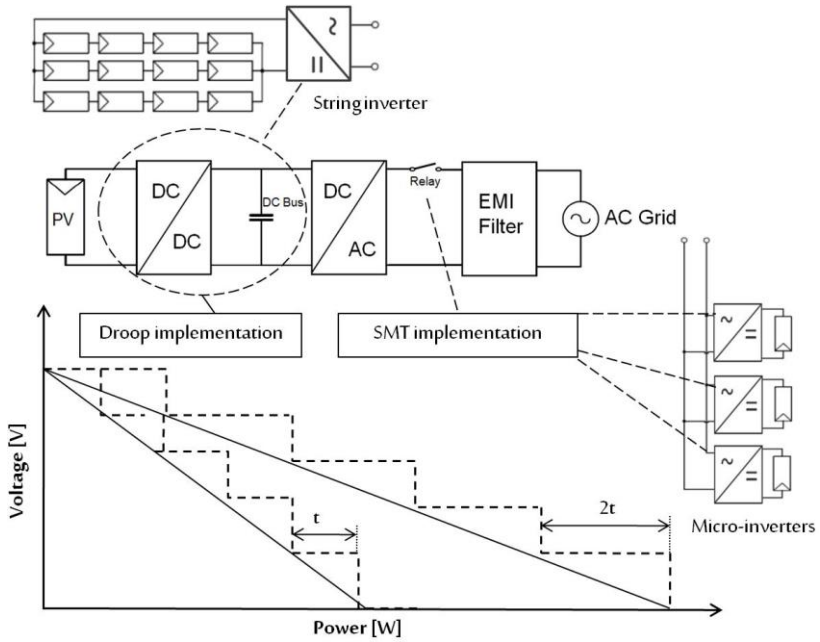

Figure 6.2: Droop and SMT methods: design and implementation comparison.

Different trip time steps (t, 2t, etc.) allow the "ceiling" of different droop lines. Each droop line has its own corresponding trip sequence, hence the name "sequential module-level tripping" was given. The outcome of SMT approach is that APC is virtually implemented on system level, but without creating new functionality at unit level, making it a more reliable and software retrofit-friendly alternative to droop. The assumption of SMT's design-for-reliability is that reconnection time provides some cool-down to MOSFETs and capacitors, whereas the cool-down resulting from droop-scheme would be less, as it is still an operating state. The SMT relieves MOSFETs from unknown functionality allowing them to be engaged

only in default MPPT operation. While droop is applicable for all inverter ratings and topologies, the limitation of SMT is that it is economically sensible only for small-sized inverters (250W-500W). Applying SMT on a larger string inverter would be no different than executing OVP and losing 100% plant capacity.

6.2 SMT algorithm

The SMT concept was first proposed by this thesis author in [107] and further developed in [108]. Most recent version of the algorithm is shown in Figure 6.3.

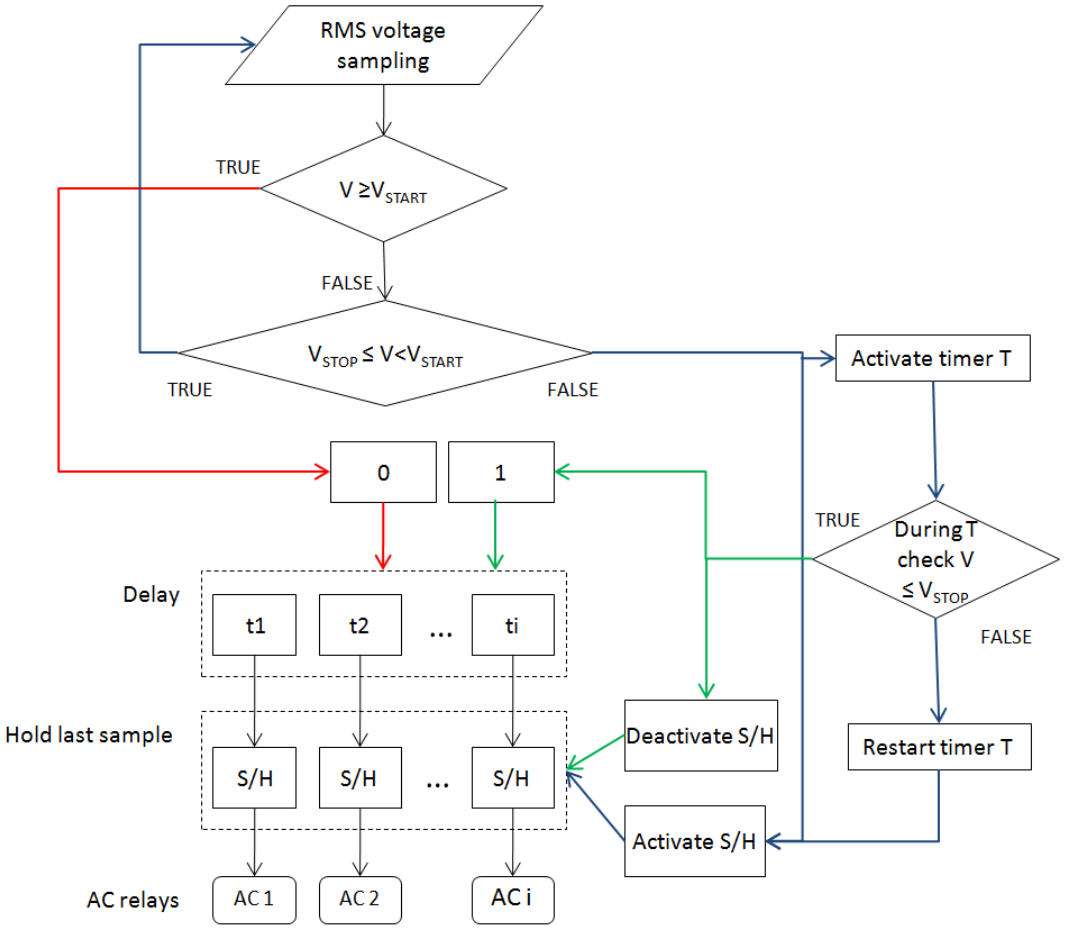

Figure 6.3: SMT algorithm.

Control range boundaries are determined by V_{START} and V_{STOP} parameters. V_{START} is kept slightly below the mandatory overvoltage threshold (i.e., 1.09pu). The RMS voltage is

checked in closed loop with every trip, until V_{STOP} is reached. Such a modified overvoltage protection scheme produces a "staircase" voltage response depicted in Figure 6.4. Just as conventional OVP, the SMT uses its own reconnection timer T. However since SMT operates below overvoltage threshold its timer is not restricted by any standard and can be set according to dynamic behavior of voltage at PCC. If the voltage successfully remains below control range during time T, the power will gradually ramp-up in the same staircase manner.

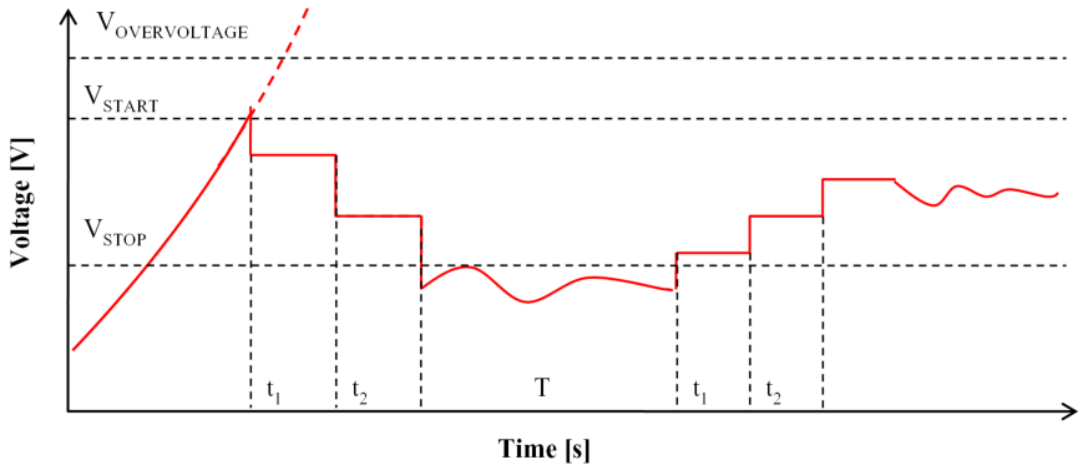

Figure 6.4: Conceptual representation of overvoltage prevention by SMT.

6.2.1 Algorithm parameterization

The algorithm parameters can be configured both locally (single PCC) and over a wide-area (multiple PCCs along the feeder). Locally, these parameters only consider the voltage rise problem from perspective of a single PV system, while wide-area configuration allows the DSO to balance between voltage requirements and energy export at feeder level, coordination with their own protection gear and/or OLTC, optimization of unequal feed-in losses in different feeder points, etc. For example, a two-way parameterization as shown in Figure 6.5 could be applied to balance between voltage requirements and energy export. One way is to change the width of the V_{START}/V_{STOP} control range. In case of V_{STOP1} only two micro-inverters would be disconnected, while V_{STOP2} requires disconnection of five micro-

inverters. Therefore V_{STOP1} would be used if green energy export is more favored than voltage level and V_{STOP2} in case of more strict voltage requirement. Another way to favor energy export over voltage level is to increase the delay time step. Figure 6.5 on the right shows that shorter step produces less energy (represented by hatched surface), but it will bring voltage to required level faster. In similar way reconnection time T could be set longer or shorter, depending on what is being prioritized.

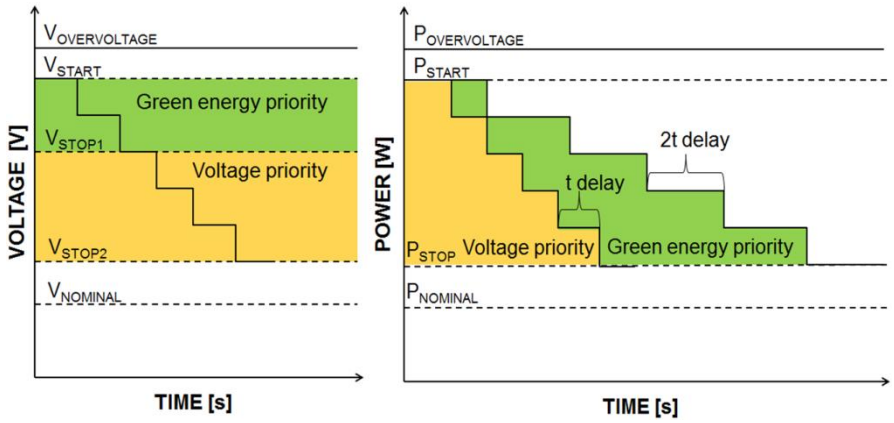

Figure 6.5: Exported energy maximization vs. voltage priority by changing control range (left) and/or by changing delay time step (right).

6.3 Determination of delay time step

The SMT cannot control power change (*dP)* directly, because it does not engage the inverter power switches like droop control. Instead, it engages the protection switch and can only execute control by setting the duration of trip delays t_1, t_2...t_i (dt steps). But since the objective is to control voltage, a theoretical relation must be established between the droop and SMT concepts.

The voltage-power dependency expressed as a droop coefficient dV/dP is obtained from a voltage sensitivity analysis. The droop coefficients are determinants of submatrices of the inversed Jacobian matrix $\underline{J}^{-1}$, which is derived from Newton-Raphson power flow solution.

The power flow is considered solved when the bus voltages (V) and phase angles (δ) are known. The active and reactive power flow equations are solved in the form of

$$\underline{P} = \underline{P}(\underline{\delta}, \underline{V}) \tag{6.2}$$

$$\underline{Q} = \underline{Q}(\underline{\delta}, \underline{V}) \tag{6.3}$$

where

$$\underline{\delta} = \begin{bmatrix} \delta_1 \\ \dots \\ \delta_{b-1} \end{bmatrix} \tag{6.4}$$

$$\underline{V} = \begin{bmatrix} V_1 \\ \dots \\ \delta_{bpq} \end{bmatrix} \tag{6.5}$$

where *b* is the number of buses, and *bpq* is the number of PQ buses. The equations are solved iteratively

$$\begin{pmatrix} \underline{\delta}^{k+1} \\ \underline{V}^{k+1} \end{pmatrix} = \begin{pmatrix} \underline{\delta}^{k} \\ \underline{V}^{k} \end{pmatrix} + \underline{J}^{-1} \begin{bmatrix} \underline{P} - \underline{P}(\underline{\delta}^k, \underline{V}^k) \\ \underline{Q} - \underline{Q}(\underline{\delta}^k, \underline{V}^k) \end{bmatrix} \tag{6.6}$$

with *k* being the number of iterations and $\underline{J}$ is the Jacobian matrix. The sensitivity matrix $\underline{S}$ is obtained

$$\underline{S} = \begin{bmatrix} 1 & 0 \\ 0 & |V| \end{bmatrix} \begin{bmatrix} \frac{\partial \underline{P}}{\partial \underline{\delta}} & |V| \frac{\partial \underline{P}}{\partial \underline{V}} \\ \frac{\partial \underline{Q}}{\partial \underline{\delta}} & |V| \frac{\partial \underline{Q}}{\partial \underline{V}} \end{bmatrix}^{-1} = \begin{bmatrix} \frac{d\delta}{dP} & \frac{d\delta}{dQ} \\ \frac{dV}{dP} & \frac{dV}{dQ} \end{bmatrix} \tag{6.7}$$

where *dV/dP* and *dV/dQ* are voltage sensitivity and *dδ/dP* and *dδ/dQ* phase angle sensitivity to active and reactive power injection, respectively. The SMT is concerned only with *dV/dP*. The *dV/dP* can be expressed differently as

$$\frac{dV}{dP} = \frac{\frac{dV}{dt}}{\frac{dP}{dt}} \tag{6.8}$$

where *dV/dt* and *dP/dt* represent voltage change rate and power injection rate. The *dV/dP* increases with feeder length, suggesting that the same power injection rate produces higher voltage change rate. The success of SMT response depends on whether the voltage drop rate (dV_D/dt) caused by curtailment is equal or higher than the voltage rise rate caused by excess grid power (dV_R/dt):

$$\frac{dV_R}{dt} \leq \frac{dV_D}{dt} \tag{6.9}$$

or in power rate change notation

$$\frac{dP_R}{dt} \leq \frac{dP_D}{dt} \tag{6.10}$$

Assuming that dP_D represents a power drop resulting from disconnecting a single micro-inverter, then d*t* on the right side of (6.10) can be renamed as dt_D representing the delay time step, while dt on the left side represents a referent time step used to monitor dP_R. The optimal time delay step is

$$dt_D \leq \frac{dP_D dt}{dP_R} \tag{6.11}$$

Implementing the delay time step optimization in a real-time control system runs into both theoretical and practical problems. The theoretical *dV/dP* is derived from offline computation based on the knowledge of static power flows and voltages in all of the buses at fundamental frequency only. The SMT is limited to power and voltage data coming from micro-inverter sensors only. The delay time step computation has to be computed online in a dynamic power flow, time domain environment. The digital signal processing (DSP) would be crucial in obtaining a correct *dV/dP* under these conditions. Such a solution that could successfully replace an offline *dV/dP* (obtained from a fully known power system state) with an alternative parameter obtained through online DSP (with only knowing the local bus state),

is not known to the author. The practical problem is obtaining dP_D and dP_R physically. Despite these optimization limitations, the delay time step can be set in an arbitrary way while respecting certain constraints and still have a very high success rate in preventing overvoltage.

6.4 Controller design

The SMT controller is considered in two varieties for two scenarios: software retrofit and hardware retrofit. The software retrofit allows seamless integration with zero cost involved. Given the rising importance of massive smart grid inverter retrofits in the future, the software retrofit should be given priority whenever possible.

6.4.1 Software retrofit using existing gateway infrastructure

The micro-inverters are probably the most mature inverter niche in terms of availability of remote access which allows extensive exploration of software retrofit opportunities. The implementation of power electronic converters at module-level expanded the opportunity for monitoring power parameters from a single PCC point to each module/micro-inverter in the PV plant. This generates a lot of data. In high PV penetration areas there can be hundreds of PV modules and their data needs to be aggregated and presented to the application or the end-user in a meaningful way. Most of the micro-inverters available on the market today are sold in package with a data concentrator device, more often called "gateway". They communicate to micro-inverters via mesh radio or power line communication while remote communication with an application is done via internet [109], [110]. One gateway can cover from several tens to several hundreds of micro-inverters. PV owners use them for monitoring and easy troubleshooting; manufacturers use them for more complicated troubleshooting and firmware updates (Figure 6.6). At request of DSO the

manufacturer will change the trip settings remotely if the PV owner experiences frequent overvoltage.

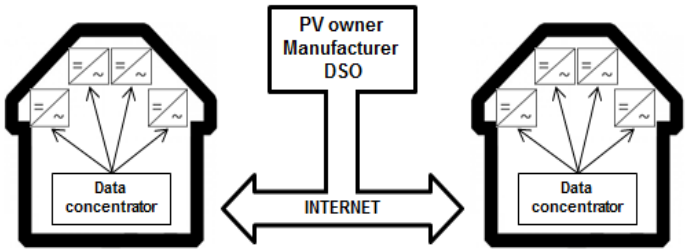

Figure 6.6: Multiple parties accessing the micro-inverter communication infrastructure.

Similarly, the SMT trip delay and voltage control parameters can be assigned to micro-inverters via gateways. The actual voltage monitoring and control loop remains internal to the micro-inverter while the gateway only manages the behavior of micro-inverter (Figure 6.7).

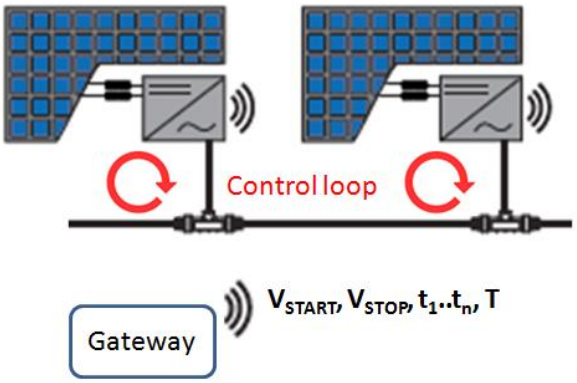

Figure 6.7: Figure SMT controller implemented in the existing gateway.

This is what inspired the usage of term "feed-in management" instead of "control". This approach ensures that control loop is not affected by communication issues that might occur between the gateway and micro-inverter. Secondly, system reliability is not affected as even if the gateway fails, the last settings remain active in all the micro-inverters. The only downside is that voltage drop along the micro-inverter branch creates a minor offset that would have to be accounted for when setting V_{START} values.

6.4.2 Hardware retrofit with a dedicated controller

There is no unified standard in micro-inverter development platforms and communications used in gateways. Secondly, micro-inverter market is very competitive and from author's industry experience as a system integrator, the manufacturers are generally not open to the idea of sharing their firmware with 3rd party integrators to implement new functionalities. This complicates the idea of unified SMT retrofit for different manufacturers and, depending on the urgency of enabling power curtailment, hardware retrofit would be faster, but more expensive solution. Independence from micro-inverter technology is achieved by adding external slave relays instead of targeting inverter's internal protection switches (Figure 6.8). There is fixed added cost due to dedicated master controller and voltage sensor at PCC point (distribution panel). Furthermore, the slave relays present a growing cost due to inverse economies of scale - the bigger the PV capacity the more relays will be needed. There is only one voltage monitoring point so there is no problem with branch voltage drop offset, but with the failure of master device, the whole controller is inoperable. Additionally the delay and timer setting for relays would have to factor in the inverters own anti-islanding settings, since from the inverter side, an external interruption executed via relay would be viewed as a loss of mains.

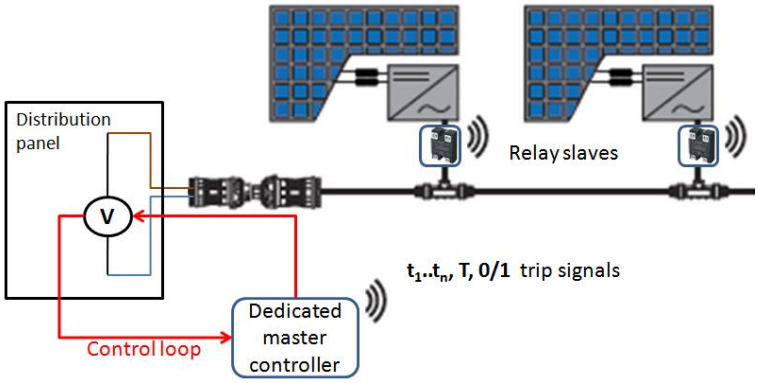

Figure 6.8: Dedicated SMT controller with external slave relays.

CHAPTER 7

Modeling and Simulation

In this chapter several types of power flow simulation are performed. For general demonstration of SMT effects on the voltage regulation, a *worst-case scenario*, constant power flow is performed. In this simulation two wide area curtailment schemes were tested. The better performing scheme is then applied in an annual power flow simulation with variable load and generation profiles. In both constant and variable power flow the objective is to mitigate overvoltage using SMT and preserve certain percentage of generation as opposed to 100% disconnection. Of secondary interest is an assessment of micro-inverter gateways for voltage unbalance monitoring. For that purpose Monte Carlo stochastic power flow is simulated. The modeling and simulation is performed in Matlab/Simulink.

7.1 SMT in worst-case constant power flow simulation

The worst-case approach is known to be used by DSO for determining the maximum DG capacity allowed to connect to LV grid [111]. This deterministic approach sets the grid model with no load/low load and high generation. The generation capacity is then increased until overvoltage is achieved, marking the limit of grid hosting capacity. A power system with constant load and generation is used for easier discernment of SMT effects on the voltage profile. With variable power flow it would be more difficult to discern between SMT effects and oscillations coming from power flow variations. Thirdly, the simulation is *initialized with overvoltage* - a massive overvoltage scenario in all buses is created. As a consequence, the SMT is triggered in all buses simultaneously which is useful for demonstrating the effect of voltage-coordinated curtailment and feed-in loss sharing.

7.1.1 LV grid model

Typical Dutch three-phase LV grid is used to build the grid model [112]. Four feeders extend radially from a 400kVA delta-star transformer (400/230V, X/R ratio=3.2, no OLTC), each feeder having 14 supply buses. In most MV/LV transformers in the Dutch grid, the transformer tap is set to 1.05pu to compensate for voltage drop along the feeder. This prevents undervoltage during peak demand hours, but increases the chances for overvoltage during peak generation hours, so it was included in the model. Each bus provides three-phase supply where each phase supplies one house. It is computationally demanding to simulate curtailment on 168 houses with PV, so the model was reduced to one 14-bus feeder (Figure 7.1) with 42 houses, while the other three feeders were represented as occupied transformer capacity based on lump calculation of load and generation. Cables are modeled as RL branches and their characteristics given in Table 7.1. Total feeder length is 0.49km.

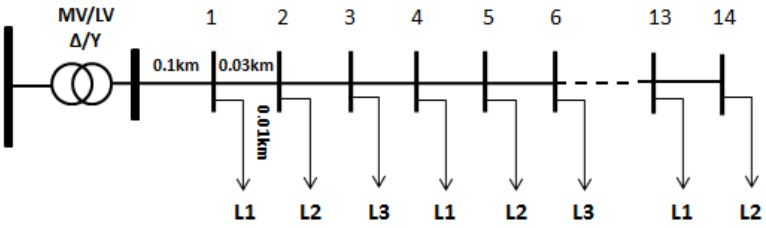

Figure 7.1: One-line diagram of typical Dutch LV feeder with three alternately distributed load types.

Table 7.1: Cable characteristics and lengths.

Cable type	Resistance [mΩ]	Inductance [μH]
0.1 km main cable	23.5	75
0.03 km bus-to-bus	7.05	7.5
0.01 km service connection	20.82	2.8

7.1.2 Generation and load models

The micro-inverters are modeled as single-phase PLL-controlled AC current sources (Figure 7.2). The current amplitude is constant 1A, which is realistic maximum AC output current for a 250W micro-inverter.

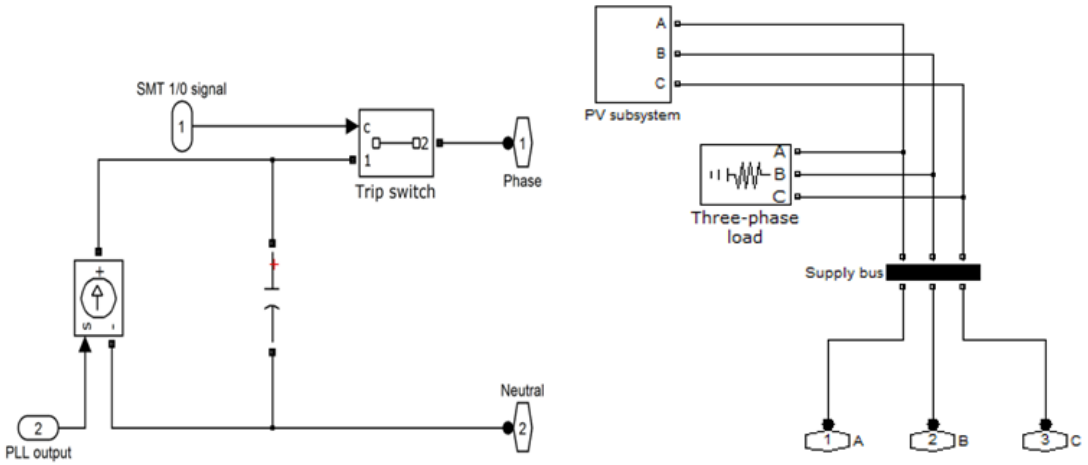

Figure 7.2: Single-phase micro-inverter model (left) and 3-phase supply (right).

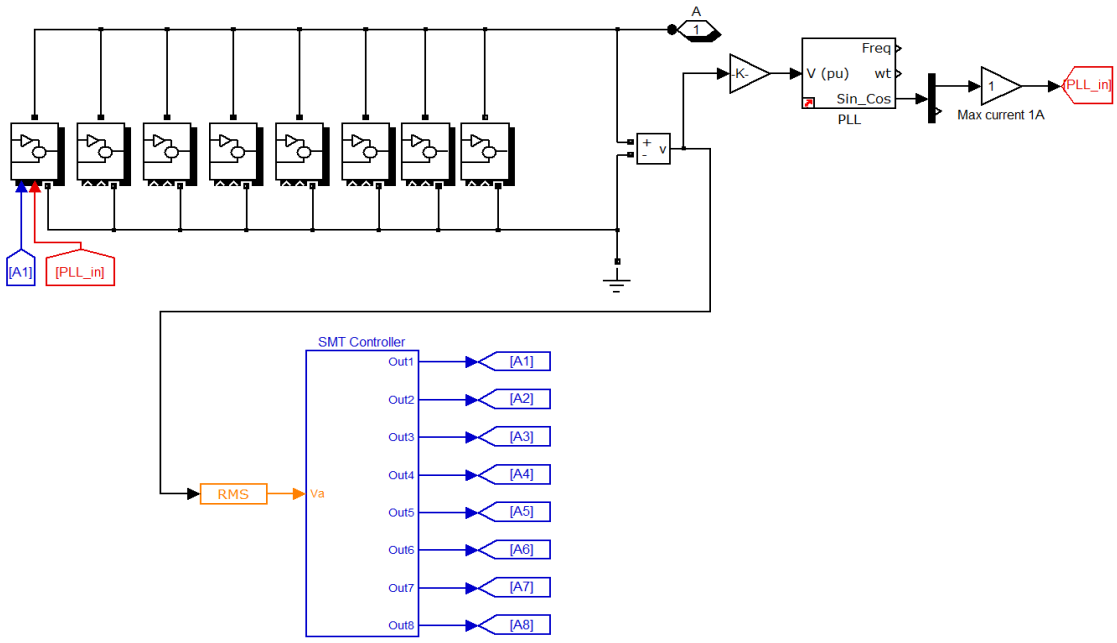

Figure 7.3: Simulink model of 1.8 kW system with SMT controller.

Each house in the test feeder is equipped with eight micro-inverters (8A). To optimize the model for faster computation a common PLL block drives all the micro-inverters belonging to the same house (Figure 7.3).

The load at each bus is represented as a 3-phase resistive load to account for three houses per bus. Three different load types (L1, L2 and L3) are used and alternately distributed along the feeder as shown in Figure 7.1. L1 and L2 are 360W and 650W, respectively. This data was derived from[113].To create a low load situation, a 12:00 pm work day of month of June is used. To create load diversity, L3 of 1200W is introduced and it represents average household peak demand according to[112]. Both generation and load are at unity power factor.

The assumption is that each of 168 houses has an equal PV capacity installed. Voltage trip limit is 1.1 pu. Under these conditions, a maximum allowed injection per phase is 5A at each house. At 6A overvoltage would occur on multiple buses along the feeder. All supply points in the test feeder are populated with 8A PV systems like the one in Figure 7.3, while the other three feeders remain populated with 5A PV systems. The test feeder is simulated for two scenarios: a uniform low load (L1) used in all buses and all three load types alternately distributed.

7.1.3 Wide-area SMT delay schemes

In the model outlined in previous section there are 42 houses with 8 micro-inverters, which gives DSO a maximum granularity of 336 power steps for wide-area control. The granularity of control depends on wide-area distribution of trip delays and whether there is overlap of identical delay setting in different micro-inverters.

Two SMT delay schemes are proposed: *branch trip delay* (BD) and *branch-and-bus trip delay* (BBD). In both schemes voltage control range is kept constant at each bus along

the feeder in order to flatten the voltage and minimize the distribution losses. In previous chapter it was mentioned that an ideal time step optimization was out of scope due to theoretical and practical limitations, however certain optimization boundaries can be applied. Since SMT uses RMS voltage, a minimum delay value must not be less than the running average window for RMS calculation. Otherwise, the power stepping might happen faster than RMS voltage calculation after each step, causing more disconnection steps than necessary. In this study, the default Simulink averaging window is over one cycle of 50Hz fundamental frequency or 0.02s, hence a delay step of 0.03s was assigned, while respecting the RMS calculation constraint.

Branch delay scheme

The branch delay (BD) scheme is straightforward as it is just a copy of local setup of the last bus onto all buses. Delays only exist within local micro-inverter branch, but they will execute simultaneously on buses where voltage crosses the V_{START} threshold. This means that V_{STOP} is reached with fewer power steps and in shorter time, therefore BD should be used for strategies requiring fast response. Table 7.2 shows delay setup for each micro-inverter in the feeder. In this example, since the idea is to increase penetration to 8A per phase, there are eight micro-inverters with 1A maximum output. Note how delay sequences, although having the same progression, are phase-rotated on each bus (ABC, BCA, CAB, etc.). Since micro-inverters are single phase devices connected to 3-phasenetwork, having no phase rotation at each bus could increase unbalance. Having low granularity of control with maximum 24 steps (3 phases x 8 micro-inverters) is expected to lead to excessive curtailment, but also to faster execution.

Table 7.2: Branch trip delay scheme [s]

	1	**2**	**3**	**4**	**5**	**6**	**7**	**8**
A1	0.03	0.12	0.21	0.3	0.39	0.48	0.57	0.66
B1	0.06	0.15	0.24	0.33	0.42	0.51	0.6	0.69
C1	0.09	0.18	0.27	0.36	0.45	0.54	0.63	0.72
B2	0.03	0.12	0.21	0.3	0.39	0.48	0.57	0.66
C2	0.06	0.15	0.24	0.33	0.42	0.51	0.6	0.69
A2	0.09	0.18	0.27	0.36	0.45	0.54	0.63	0.72
C3	0.03	0.12	0.21	0.3	0.39	0.48	0.57	0.66
A3	0.06	0.15	0.24	0.33	0.42	0.51	0.6	0.69
B3	0.09	0.18	0.27	0.36	0.45	0.54	0.63	0.72
…	…	…	…	…	…	…	…	…
B14	0.03	0.12	0.21	0.3	0.39	0.48	0.57	0.66
A14	0.06	0.15	0.24	0.33	0.42	0.51	0.6	0.69
C14	0.09	0.18	0.27	0.36	0.45	0.54	0.63	0.72

Branch-and-bus delay scheme

Table 7.3 shows the branch-and-bus (BBD) delay setup. This particular BBD scheme is created with maximum granularity of control, which is achieved by not having any of two micro-inverters in the feeder trip simultaneously. Instead, the sequence is time shifted across each bus and phase creating 336 possible power steps (42 houses x 8 micro-inverters). The shortest delay starts at the end of the feeder (0.03s at A14) and increases towards transformer ending with 10.08s delay at C1. Such delay distribution ensures faster SMT execution at the end of the feeder where *dV/dP* is higher.

Table 7.3: Branch-and-bus trip delay scheme [s]

	1	**2**	**3**	**4**	**5**	**6**	**7**	**8**
A14	0.03	1.29	2.55	3.81	5.07	6.33	7.59	8.85
B14	0.06	1.32	2.58	3.84	5.1	6.36	7.62	8.88
C14	0.09	1.35	2.61	3.87	5.13	6.39	7.65	8.91
A13	0.12	1.38	2.64	3.9	5.16	6.42	7.68	8.94
B13	0.15	1.41	2.67	3.93	5.19	6.45	7.71	8.97
C13	0.18	1.44	2.7	3.96	5.22	6.48	7.74	9
A12	0.21	1.47	2.73	3.99	5.25	6.51	7.77	9.03
B12	0.24	1.5	2.76	4.02	5.28	6.54	7.8	9.06
C12	0.27	1.53	2.79	4.05	5.31	6.57	7.83	9.09
…	…	…	…	…	…	…	…	…
A1	1.2	2.46	3.72	4.98	6.24	7.5	8.76	10.02
B1	1.23	2.49	3.75	5.01	6.27	7.53	8.79	10.05
C1	1.26	2.52	3.78	5.04	6.3	7.56	8.82	10.08

It can be seen from Table 7.3 that micro-inverters are disconnected in groups of three per branch position at each bus and when they finish one cycle from bus 14 to bus 1, the curtailment cycle is repeated on the next branch position. Cycles repeat from branch position 1 to 8. This pattern allows both phase balanced curtailment and sharing of curtailment losses among PV owners.

7.1.4 Simulation results

The control parameters and Simulink configuration are presented in Table 7.4. After applying SMT curtailment, the bus voltage levels are equalized between buses. Comparing to massive overvoltage without curtailment (Figure 7.4).Significantly longer cable between the transformer and bus 1 creates a steep voltage rise compared to that between the buses. Both BD and BBD used V_{STOP}=1.08pu and their effect on voltage flattening is almost identical.

Table 7.4: SMT parameters and simulation setup

Parameters	**Simulink configuration**
V_{START}=1.09pu	Solver: Ode45, variable step
V_{STOP} =1.08pu	Simulation type: discrete
Delay time step: 0.03s	Simulation step: 0.5ms
BD delay range: 0.03-0.72s, BDD delay range: 0.03-10.08s	

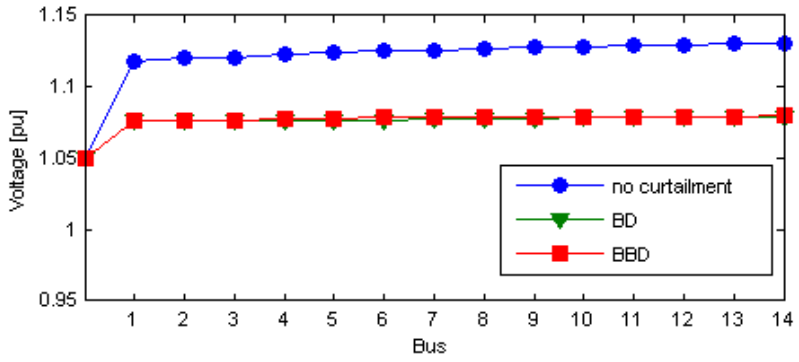

Figure 7.4: Effects of SMT curtailment on bus voltages.

Figure 7.5-7.9 show three-phase RMS voltage response to BD and BBD schemes with different loads at bus 14. Note that in all four cases curtailment starts in the overvoltage range, although control range is 1.09-1.08pu. This is due to model being initialized with overvoltage state in all buses. The multi-point overvoltage is synchronizing the SMT curtailment action in all buses. The curtailment has a one-time delay of 0.5s due to PLL model initialization that takes 0.3s to complete. During the PLL initialization there are voltage transients that could be mistaken for voltage rise by the curtailment system.

The BD executes faster in both load schemes, but it shows slight tendencies to create unbalance, especially in case of alternately distributed loads. Biggest voltage unbalance of 0.12% was recorded after BD scheme execution for different loads (Figure 7.6). When it comes to achieving voltage level accuracy relative to $V_{STOP,}$ both curtailment schemes perform well, BD with maximum error of 0.48% and BBD, having higher granularity of control, with maximum error of 0.32%. BBD having smaller power steps allows a smooth voltage ramp (Figure 7.7 and 7.8), but it takes longer to execute. It is very similar to typical droop control response, however, it is achieved not as an action of a single inverter, but as a resulting response from sequential tripping of multiple micro-inverters. This is demonstrated in Figure 7.9: there is an ongoing curtailment between 4-6s with 21 power steps, although according to

Table 7.3, only three micro-inverters at bus 14 (branch position 5) are scheduled between 4-6s (5.07s, 5.1s and 5.13s). This shows how the entire fleet of distributed micro-inverters could be engaged to carry out complex requests coming from a single bus.

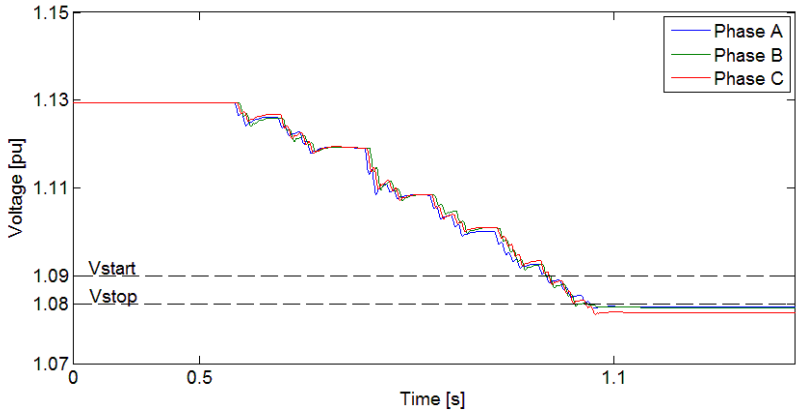

Figure 7.5: Bus 14 voltage response to BD under uniformly distributed load.

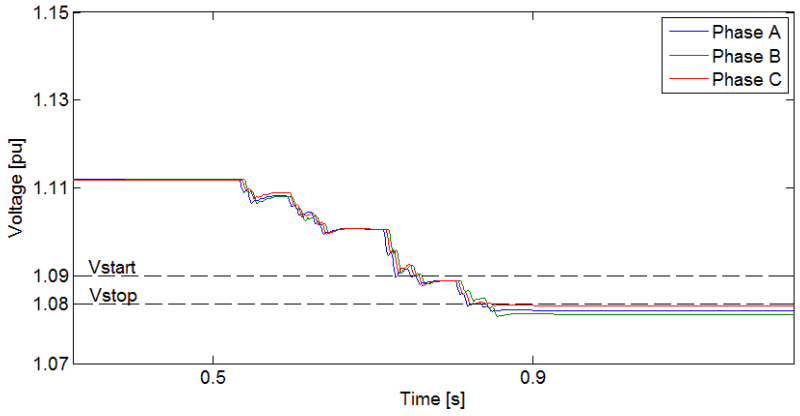

Figure 7.6: Bus 14 voltage response to BD under alternately distributed load.

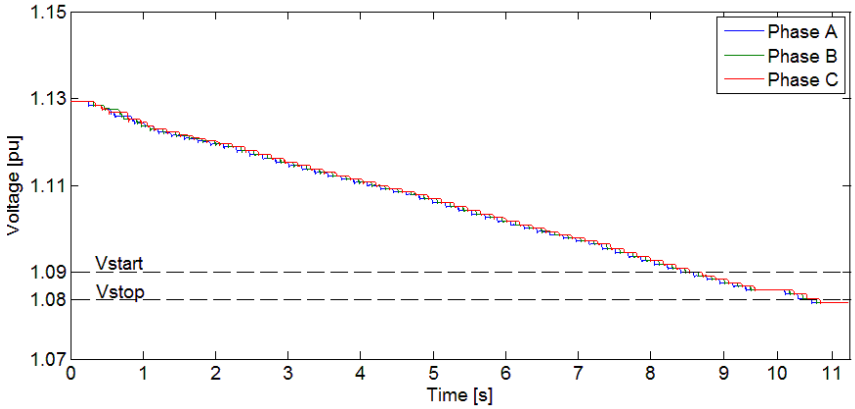

Figure 7.7: Bus 14 voltage response to BBD under uniformly distributed load.

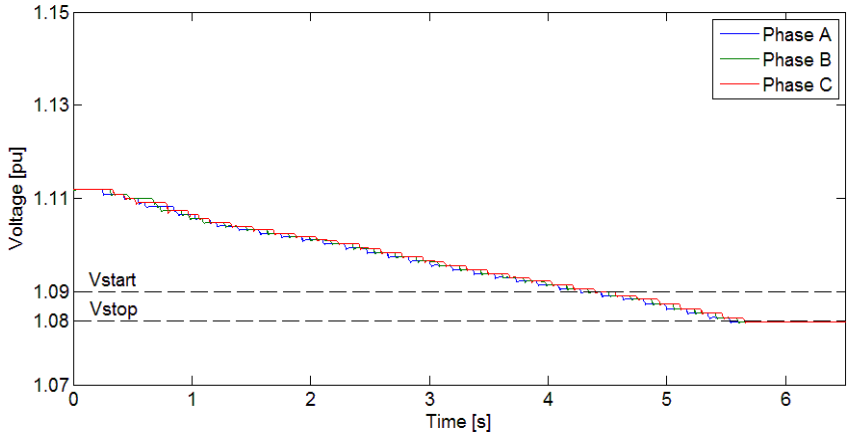

Figure 7.8: Bus 14 voltage response to BBD under alternately distributed load.

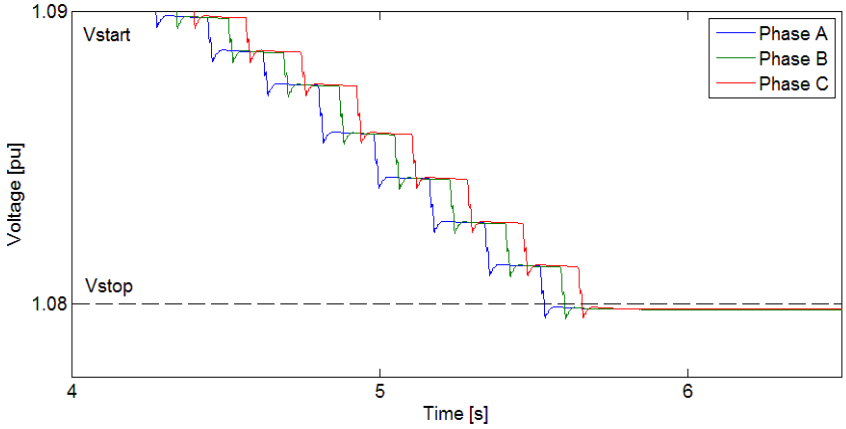

Figure 7.9: Zoomed bus 14 voltage response to BBD.

The effects of BD and BBD on the preserved generation after all buses reached 1.08pu level are shown in Table 7.5 for uniform load and in Table 7.6 for different loads case. The

BBD provides 4A more than BD output on a feeder level. More indicative is the ability of BBD to curtail less power while preserving phase balance better than BD, and creating less economic inequality among PV owners.BD has four categories of curtailed users (2A, 3A, 4A and 5A) and preserved generation ranging 25%-63%.BBD has three categories of curtailed users (3A, 4A, 5A) and preserved generation ranging 38%-75%.

In case of different loads presented in Table 7.6, BBD maintains its advantages. Less power is curtailed due to more load being present. Another important observation is that variable load along the feeder has a beneficial effect on equalization among PV owners with both BD and BBD having only two curtailment categories of 5A and 6A. This is encouraging considering that in reality some level of stochastic variation is always present and it would be extremely rare to have a situation of 42 houses having same low load at the same time.

Table 7.5: Preserved generation in amperes [A] for uniform load.

	BD				**BBD**			
Bus	**Phase A**	**Phase B**	**Phase C**	∑	**Phase A**	**Phase B**	**Phase C**	∑
1	4	3	5	12	5	5	5	15
2	5	4	3	12	5	5	5	15
3	3	5	4	12	4	4	4	12
4	4	3	5	12	4	4	4	12
5	5	4	3	12	4	4	4	12
6	2	5	4	11	4	4	4	12
7	4	3	5	12	4	4	4	12
8	5	4	2	11	4	4	4	12
9	2	5	4	11	4	4	4	12
10	4	3	5	12	4	4	4	12
11	5	4	2	11	4	4	4	12
12	2	5	4	11	3	3	3	9
13	4	2	5	11	3	3	3	9
14	5	4	2	11	3	3	3	9
Total	54	54	53	161	55	55	55	165

Table 7.6: Preserved generation in amperes [A] for different loads.

	BD				BBD			
Bus	**Phase A**	**Phase B**	**Phase C**	**∑**	**Phase A**	**Phase B**	**Phase C**	**∑**
1	6	6	5	17	6	6	6	18
2	5	6	6	17	6	6	6	18
3	6	5	6	17	6	6	6	18
4	6	6	5	17	6	6	6	18
5	5	5	6	16	6	6	6	18
6	6	5	6	17	6	6	6	18
7	6	6	5	17	6	6	6	18
8	5	5	6	16	6	6	6	18
9	6	5	6	17	6	6	6	18
10	5	6	5	16	5	5	5	15
11	5	5	6	16	5	5	5	15
12	6	5	5	16	5	5	5	15
13	5	6	5	16	5	5	5	15
14	5	5	6	16	5	5	5	15
Total	77	76	78	231	79	79	79	237

7.2 SMT in variable power flow simulations

Unlike the previous time domain simulation, the variable power flow is performed as a *phasor* simulation. The assessment of the overvoltage problem over long intervals (i.e. annually) is mainly concerned with impact on voltage magnitudes. Annual simulation of a full electrical state in a detailed model would take months of real-time simulation. The phasor simulation assumes only one (fundamental) frequency and algebraically solves circuit voltages and currents as phasors. This means that only magnitudes and phase angles are solved for the selected frequency; there is no concept of sine wave/zero crossing; no impact of RLC elements on frequency response, which results in much faster simulation execution.

7.2.1 Generation and load models

The grid model and the SMT schemes remained the same as in previous time domain simulation, but the generator and load models are further optimized (Figure 7.10).The PV

generator model can be represented by a current source without PLL since there is no sine wave to synchronize with. The generator and load are not separately modeled as in previous simulation. Instead, an integrated *net flow* approach is used: a single current source reference is driven by the net power flow data(generation and load power values already subtracted)[114]. Depending on net export or net import state the current sign is either positive or negative. The net flow approach is convenient as it further reduces the model and simulation time. The load data is obtained from [113] and actual inverter power measurements were taken from a PV site in Amsterdam, both provided in a 15-minute time steps.

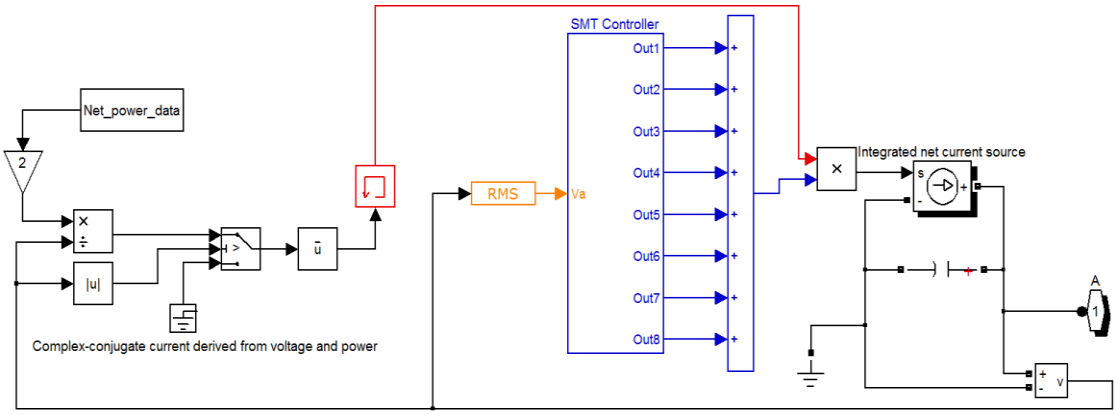

Figure 7.10: Optimization of model with net power flow and elimination of switches.

Second optimization was achieved by eliminating switches from the previously analyzed constant flow model. In that model there were 336 switches creating a stiff simulation problem. The alternative is to send 1/0 controller signals to the sum block and then multiply with base net power data of a single micro-inverter. Whenever SMT output changes to "0" the staircase response of voltage/power will be emulated as if an actual switch was used.

7.2.2 Simulation results

The worst-case analysis revealed that BBD scheme brings more benefits including more yield, hence it was chosen to be applied in the annual simulation. Figure 7.11 shows power flow and voltage measurements taken at bus 14 during several random overvoltage/curtailment events that happen throughout the year. The bus 14 was selected for presentation of voltage response as, being at the end of the feeder, it experiences the highest magnitudes and highest number of events. The top plot shows forecasted (unmitigated) voltage data points and their SMT-mitigated equivalents. From the bottom plot it can be seen that SMT maintains better energy yield (green line) in situations where it is otherwise brought to zero due to voltage trip (red line).

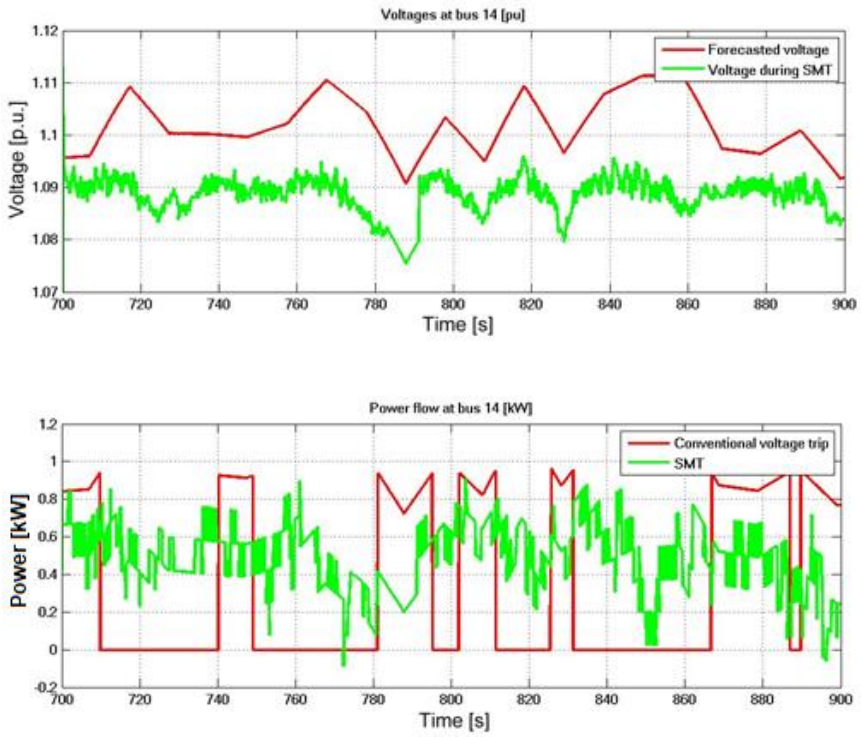

Figure 7.11: Effects of overvoltage on power export and optimization by SMT.

Over the whole year the overvoltage prevention efficiency of curtailment is quite high with only a few events out of 515 that curtailment was unable to successfully resolve (Figure

7.12). The situation at 2.8-3.2s occurred because, occasionally, delay settings of one or more micro-inverters will miss their schedule due to V_{START} level not being simultaneously reached in all buses. This further leads to incidental overlapping of trip delays ending in simultaneous trip of multiple micro-inverters creating bigger voltage dip than usual. Another finding of variable power flow is that in reality, all buses never experience curtailment simultaneously as in the worst-case scenario. The overvoltage/curtailment level is first reached at the end of the feeder and then if not mitigated, it progresses towards transformer. However curtailment action at the end of the feeder will prevent voltage rise to advance upstream and in some buses curtailment will never be triggered. Over the year this creates unequal feed-in loss sharing as shown in Figure 7.13. Nonetheless, the effect of curtailment on feed-in loss reduction is evident, but this economic aspect of curtailment will be more thoroughly analyzed in the next chapter.

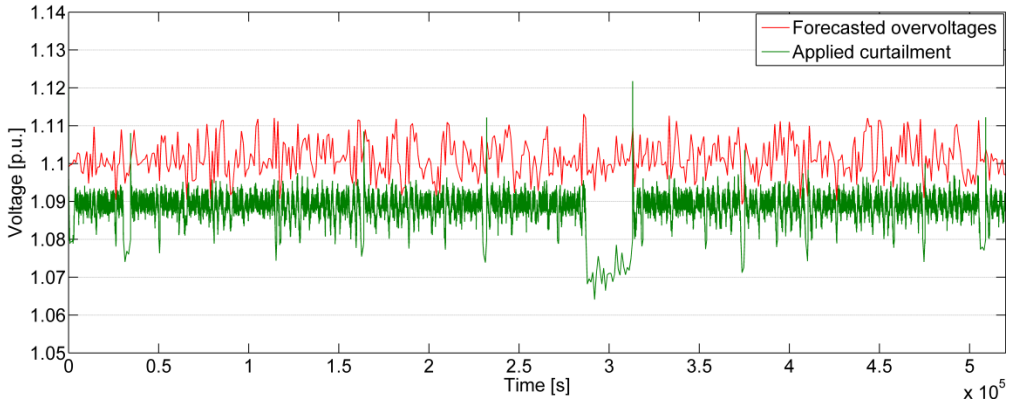

Figure 7.12: Filtered overvoltage and curtailment events for the whole year.

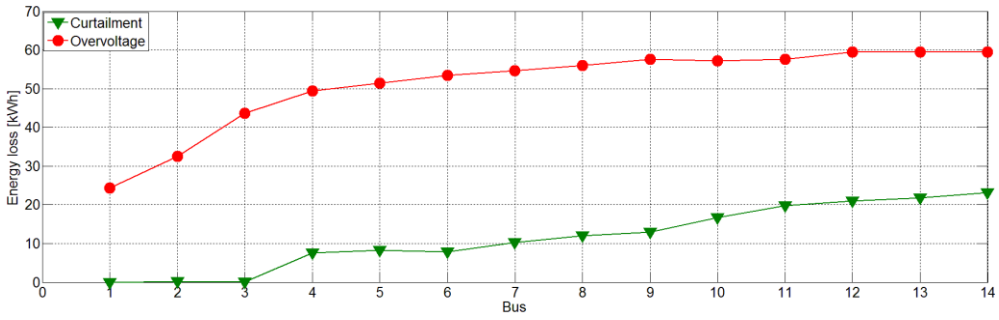

Figure 7.13: Unequal feed-in losses caused by overvoltage protection and curtailment.

7.2.3 Summary

A synchronized curtailment action and fairly good distribution of feed-in losses among customers was demonstrated in a constant power flow, worst-case scenario. The wide area BBD scheme proved a better performance, and as such was applied in a variable power flow simulation. It was capable to prevent almost all overvoltage events on annual level with minor deviation in trip delay execution. The variable power flow showed that the reality of the overvoltage problem is different and instead of massive multi bus overvoltage it tends to gradually appear first at the end of the feeder and then, if not mitigated, it progresses towards transformer. The practical implication for SMT implementation is that PCC voltage level alone could not be relied upon as a means to synchronize the SMT at entire feeder level. A dedicated communication channel would have to be used to coordinate the buses and for that an appropriate gateway infrastructure already exists. Overall, a successful PV penetration increase from 5A to 8A per house, for the case of Dutch LV feeder was achieved without changing the grid infrastructure.

7.3 Voltage unbalance monitoring

The voltage unbalance in synergy with excess generation can additionally escalate the overvoltage problem. Section 1.3 mentioned that LV grids are inherently more unbalanced due to random placement of single phase loads and generators. Micro-inverters are almost

exclusively single phase, and increase the risk of VU occurrence. The DSO has poor awareness of VU beyond MV/LV substation. Having a densely deployed remote sensor infrastructure becomes very expensive at LV level due to high number of nodes that need to be covered. It would be worthwhile to investigate the existing ICT support that comes with micro-inverters before resorting to raising cost further with additional data acquisition devices.

7.3.1 Voltage unbalance definition

Whether only magnitudes or both magnitudes and angles are considered, the VU calculation depends on the adopted VU definition [40]. Most widely accepted is the *true voltage unbalance* definition that takes both magnitudes and angles into account. Quantitatively it is expressed in percentages as the voltage unbalance factor (VUF):

$$VUF(\%) = \frac{V^-}{V^+} \tag{7.1}$$

where V^- and V^+ represent the magnitudes of negative and positive sequence voltages. By applying the method of symmetrical components, positive and negative sequence voltages are obtained:

$$\begin{bmatrix} V_a \\ V_b \\ V_c \end{bmatrix} = \frac{1}{3}\begin{bmatrix} 1 & 1 & 1 \\ 1 & a & a^2 \\ 1 & a^2 & a \end{bmatrix}\begin{bmatrix} V^0 \\ V^+ \\ V^- \end{bmatrix} \tag{7.2}$$

These are complex domain calculations where complex operator a is a function of phase angle: a=e(j2π/3). In order to calculate sequence voltages, the instantaneous three-phase voltages and angles must be obtained simultaneously [115]. Technical implementation of monitoring therefore requires a device directly connected to a 3-phase supply. This is an unsolvable problem for single-phase devices unless an external device acting as their coordinator is used.

7.3.2 Lack of solutions for single-phase inverters

In [66] an external controller at substation level coordinates single-phase and three-phase inverters in order to mitigate unbalance. Three-phase inverter control designs are proposed in [67], [68]. In [116] a three-phase smart meter is used to monitor VU with high accuracy and low cost. What is common for all these referenced solutions is that they all use VUF to assess VU. This is why these solutions are dominantly three-phase. It is evident that without an additional three-phase device, there is an inherentgap in VUF monitoring and control for single-phase inverters. Additional device also incurs additional cost to the PV system, therefore it would be worthwhile looking into single-phase devices whose existing ICT infrastructure could be software-retrofitted for purpose of enabling VUF monitoring and control in LV networks.

In Section 6 it was discussed how a micro-inverter gateway infrastructure could be exploited by DSO for wide area feed-in management of PV generation, only by software retrofit. However, trying software retrofit for the purpose of obtaining VUF would likely face implementation difficulties on the gateway hardware side. The symmetrical components sequence analyzer requires phase detection circuits and complex digital filtering [115]. Such features are found in power quality analyzers which are considerably more expensive devices. The proposed alternative is to try approximating the VUF with a less computationally and technically demanding method.

7.3.3 VUF approximation model

In [40] an overview of three VU definitions and their respective calculations was given: NEMA, IEEE, true definition (VUF). More importantly a new formula was proposed. This is a non-complex calculation formula that doesn't use phase angles but nevertheless approximates VUF by using only voltage magnitudes:

$$AVUF = \frac{82\sqrt{V_{ae}^2 + V_{be}^2 + V_{ce}^2}}{avg\ phase\ voltage} \tag{7.3}$$

where V_{ae}, V_{be} and V_{ce} are differences between phase (a, b, c) voltages and the average phase voltage. The formula was provided in its final form without derivation steps. The authors claimed that it can approximate to VUF better than other definitions even under highly unbalanced conditions, so it was selected, as is, for this study. The modeling is performed in Simulink for both VUF and AVUF. Models are presented in Figure 7.14. For modeling VUF the default Simulink three-phase sequence analyzer blocks are used, one for positive and one for negative voltage sequence at 50Hz. Unlike VUF that uses instantaneous input voltage the AVUF voltage inputs had to be averaged to RMS at fundamental frequency otherwise the AVUF would have sinusoidal component unsuitable for comparison with VUF.

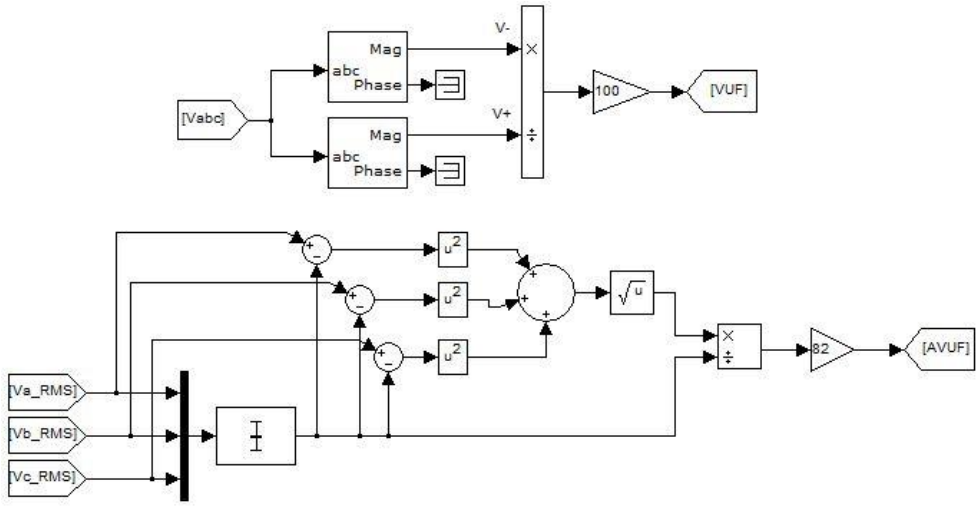

Figure 7.14: Simulink models of VUF (top) and AVUF (bottom).

7.3.4 Limitations of AVUF gateway application

The technical application would be to aggregate micro-inverter output RMS voltages and execute AVUF calculation by the existing gateway microprocessor. Although gateways are capable of sampling RMS voltages, two limitations are currently foreseen. The gateways aggregate from tens to hundreds of micro-inverters simultaneously. Their aggregate sample

rate is limited. For example in Enphase [109]and ABB [110] gateways the sampling rate is limited to 1 minute. Providing AVUF in 1 min interval might be sufficient for a LV monitoring application, but protection/control applications (like fault clearing or dynamic unbalance control) would be more demanding. Compared to dynamics of SMT control which is meant to follow the voltage in a time span of seconds, it would be difficult to adjust it with the minute-based VU sampling. For this reason the VU application was kept at the level of monitoring and was not extended to control application.

Secondly, the AVUF is only applicable in scenarios where all three single-phase PV plants connect to the same 3-phase supply point like in Figure 7.15 (left). In reality PV plants will more likely be scattered (Figure 7.15, right) due to randomness of PV purchase and installation process. If the supply point where only V_a is available, is the AVUF acquisition point, the other two phase voltages are missing. The only available voltages are from the neighboring systems on different phases and supply points (V_b' and V_c''). In this case AVUF would have to be assisted with some kind of state estimation method. Also the technical complexity of acquiring voltages V_b' and V_c'' would increase as they might be out of the gateway communication range.

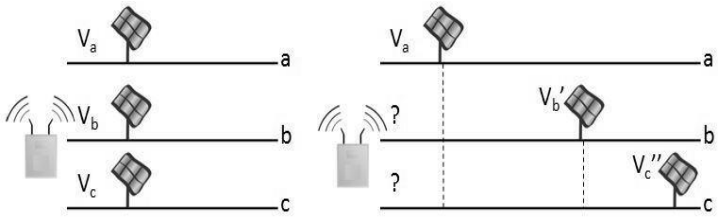

Figure 7.15: Limitations of aggregating voltages from a single supply point due to scattered single-phase PV.

7.3.5 Grid model

The grid model is still based on the same 14 bus 3-phase feeder previously used for SMT simulations, however this time a neutral wire is explicitly modeled in order to simulate a

3-phase, 4-wire unbalanced circuit. There is a common neutral going through each bus with star grounding at transformer. The grounding, neutral and lines are modeled as RL branches. One PV and three load profiles with hourly resolution were created based on profiles in [117]. Peak values of three loads are 1, 1.8 and 4.6kW. They are randomly distributed along the feeder. The PV is modeled as a single-phase AC current with a phase-locked loop. Together, load and generation form the net power flow subsystems (Net flow 1, 2,...,14) as shown in Figure 7.16.

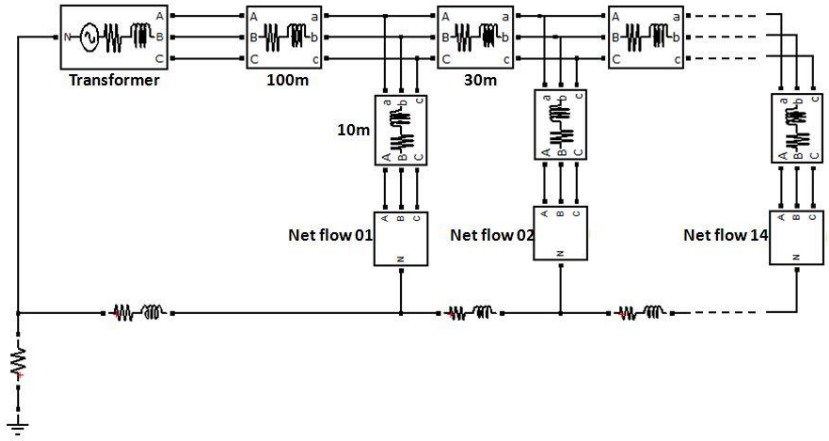

Figure 7.16: Simulink model of three-phase four-wire distribution network.

7.3.6 Monte Carlo simulation

Monte Carlo is a convenient method for simulating stochastic nature of PV generation. In particular it was used in the unbalanced network analysis [117]. Similarly, in this study Monte Carlo is used to vary the PV ratings on all three phases. The limitation of having PV present on all three-phases simultaneously is taken into account. The PV in 1-4kW range is varied following a (0,1) uniform distribution. In Monte Carlo applications in power system studies the coefficient of variance is often used as a convergence criterion or a stopping rule[118]. In this study coefficient of variance $\eta(\overline{VUF})$is used:

$$\eta(\overline{VUF}) = \sqrt{Var(\overline{VUF})}/\overline{VUF} \tag{7.4}$$

where $Var(\overline{VUF})$stands for variance. Simulink load flow is carried out for each iteration until $\eta(\overline{VUF})$ reaches an acceptable convergence. The AVUF and VUF results are retrieved for the entire Monte Carlo set (1000 trials).

7.3.7 Simulation results

The Figure 7.17 shows the outcome of applying two different calculation methods. It can be seen that AVUF results are much more dispersed with a higher density of extreme values compared to VUF. This is attributed to AVUF relying on voltage magnitudes only. Also it can be observed that AVUF almost always resolves in the same fashion being the highest at bus 14 and lowest at bus 1. Given how the load and generation is distributed this should not always be the case. The VUF at bus 7 will often have a slightly higher unbalance than bus 14 especially during the more extreme unbalance cases (over 2.5%), but around 2% the bus 14 will have a higher VUF. Therefore in addition to inflated magnitudes the AVUF will tend to give a voltage magnitude-biased result when the whole feeder is analyzed.

Three extreme cases of VUF peaks and their corresponding AVUF peaks are circled in Figure 7.17 (cases I, II, III). To better understand when AVUF makes a good approximation and when it diverges into extreme peaks, the peaks are zoomed into and compared against three-phase voltage snapshot at the corresponding time (Figure 7.18). Daily three-phase voltage profiles are taken from bus 1 for each of the selected trials. It can be seen that the high AVUF peaks correspond to situations when the load flow resolves into simultaneous two-phase overvoltage. VUF will also experience peaks at this time, but AVUF, relying only on voltage magnitudes, is much more sensitive to overvoltage than VUF.

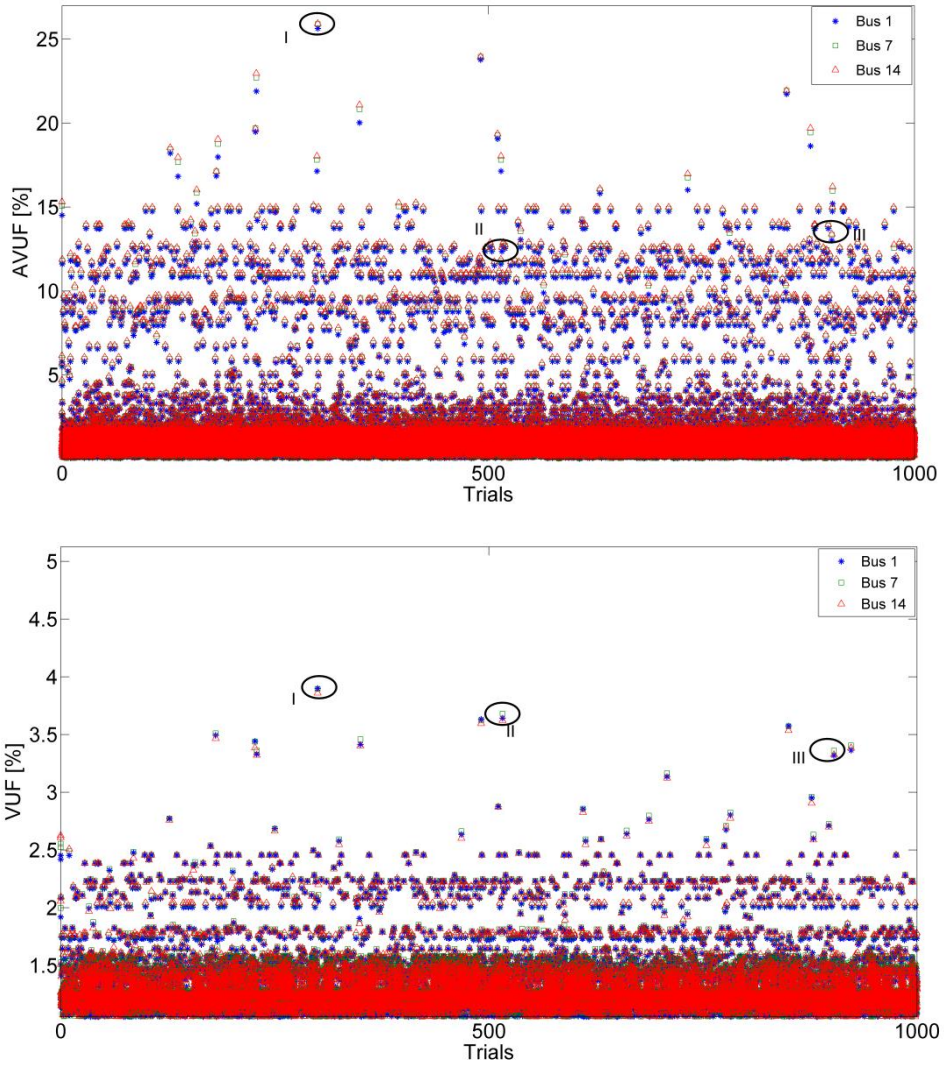

Figure 7.17: AVUF and VUF calculated in 1000 Monte Carlo trials.

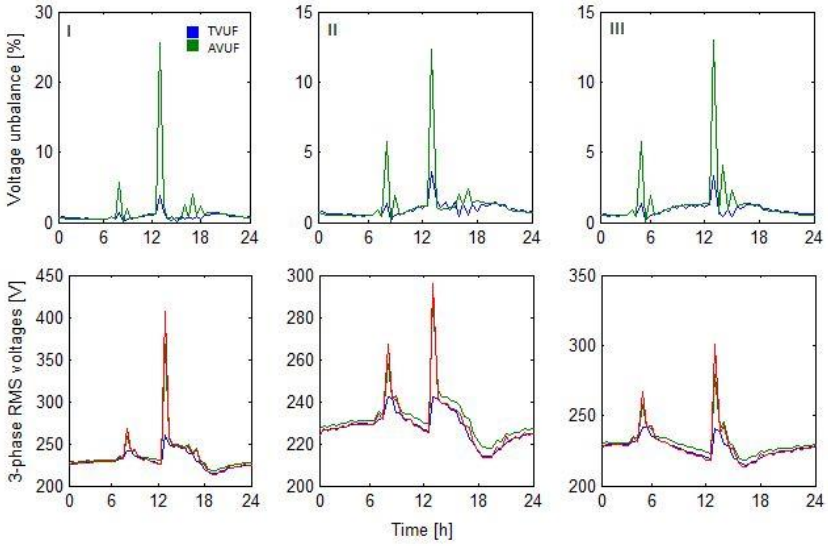

Figure 7.18: Zoomed-in extreme VU cases I, II, III with voltage profiles.

In Figure 7.19 are presented the mean absolute error (MAE) and mean percentage error (MPE) for buses 1-7-14 throughout the whole simulation. Also the converging process of Monte Carlo is presented in the bottom plot. While mean absolute error (MAE) does not exceed 0.4% the mean percentage error is much more sensitive to large peaks being included in the error averaging process. From the aspect of entire feeder both MAE and MPE increase with impedance. The $\eta(\overline{VUF})$ converges between 0.46-0.48 after 300 trials.

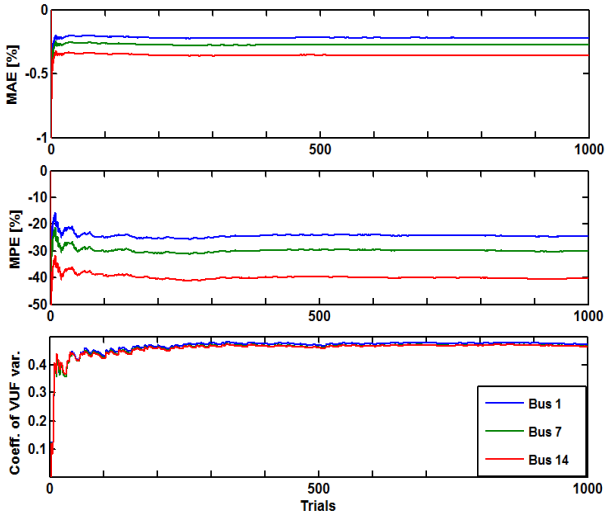

Figure 7.19: MAE, MPE and η (VUF) at buses 1, 7 and 14.

7.3.8 Summary

The daily overvoltage occurrences due to excess PV generation under unbalanced conditions have caused at least two out of 24 AVUF samples per day to give false readings compared to VUF. That makes about 8.3% of recorded AVUF profile. In a power quality analysis it would be possible to filter-out the false AVUF peaks by using their corresponding overvoltage events like it was presented in Figure 7.18, however it is likely that such large peaks would not have the chance to manifest in the first place. The tips of the analyzed voltage peaks reach almost 400V. This is a steady-state voltage change and its rise would be interrupted much sooner due to inverter overvoltage protection (at 253V) or even at a lower level if the inverter has voltage control capability (curtailment, reactive power). The AVUF preceding the trip or the curtailment event would then be smaller. Overvoltage could also occur due to a fault (i.e. floating neutral might cause phase voltage to approach line voltage value), but again the inverter protection would act. It was shown that MAE and MPE increase with feeder impedance.

The AVUF formula cannot always reliably approximate VUF. But, given the lack of remote power quality monitoring capability that distribution operators face at LV level, it might be a worthwhile, intermediary monitoring solution that can add more value to the already deployed micro-inverter systems. The proposed concept is not limited only to single-phase PV. Also home energy management systems consisting of data concentrators and smart single-phase appliances/meters could be considered for the same application.

CHAPTER 8

Techno-economic Analysis

This analysis first considers dynamic APC as a general category among solutions for overvoltage mitigation and projects an APC benefit trend for five EU countries. Secondly, an economic advantage of SMT over conventional overvoltage protection is analyzed with a novel feed-in loss assessment methodology. The final part of analysis concerns the comparison of component reliability impacts against the droop APC. By using a well-known reliability prediction methodology for electronic components, the previously assumed micro-inverter reliability benefits of SMT over droop are quantitatively confirmed.

8.1 Dynamic APC among other solutions

The difference between static and dynamic APC is that the latter can follow either voltage (like SMT) or load in a small time step and therefore regulate power more optimally than the former. The dynamic APC is still experimental and the LV grid codes that so far implemented APC actually implemented a static APC such as the fixed capacity reduction to 70% for plants under 30kW and no remote control capability. A comparative study for the case of suburban LV grid in Germany sheds more light on potential of dynamic APC compared to other solutions [45]. In addition to grid reinforcement-only solution, for additional strategies were considered:

A. Fixed reduction to 70% of installed capacity
B. Static reactive power control
C. Dynamic APC
D. Combined dynamic active/reactive power control
E. Transformer with OLTC

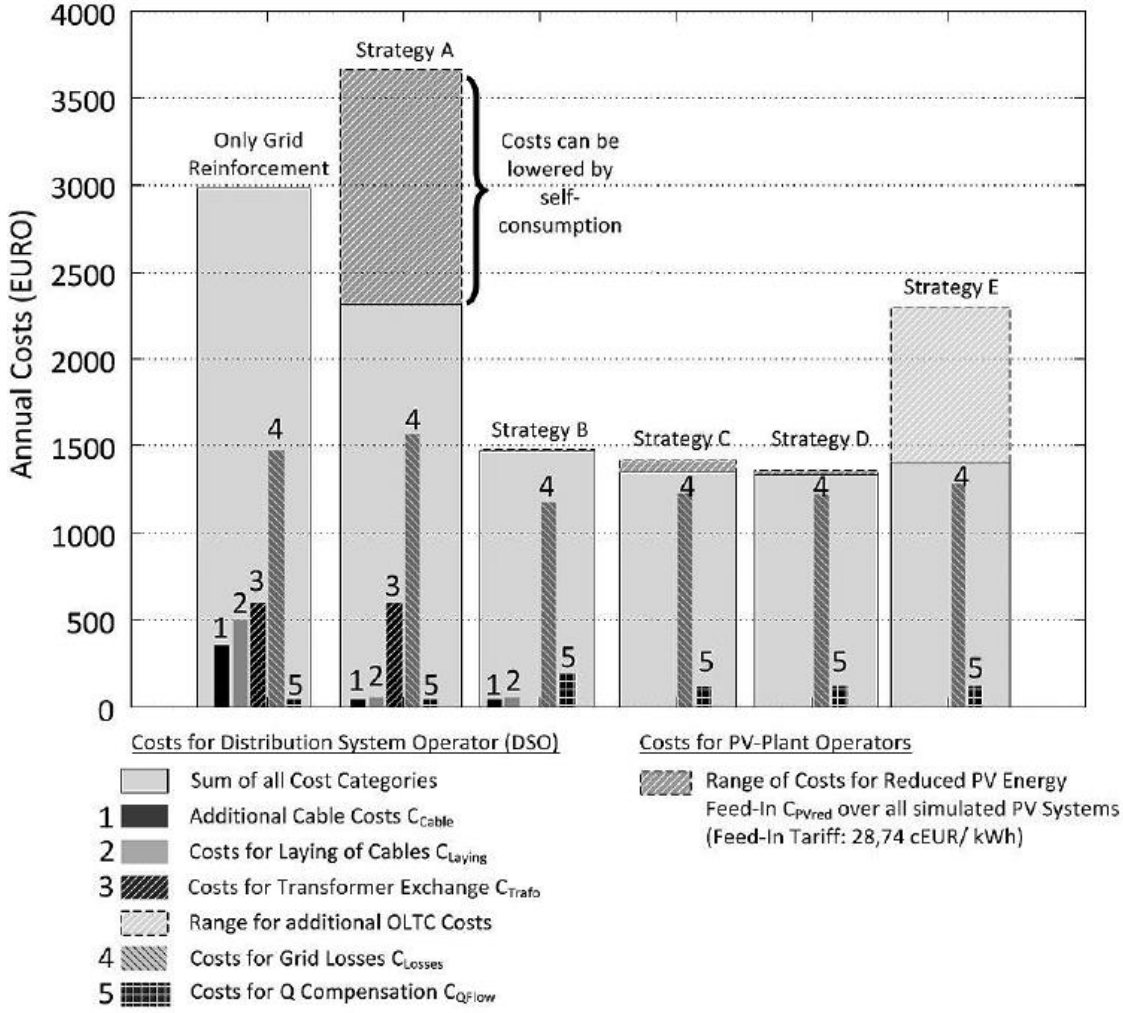

Figure 8.1: Annual costs for different overvoltage mitigation solutions in Germany [45]

Figure 8.1 shows why so much effort is being put to find alternatives to grid reinforcement as it is clearly the most expensive option for DSO. The costs from fixed APC born by the prosumer are very high while dynamic APC performs even ten times better, although a combined dynamic active/reactive power control seems a little bit more beneficial for the prosumer. Fixed reactive power-only control (strategy) seems to almost eliminate the cost to prosumer, but it has negative impact on DSO reactive power compensation capacities. Equipping the transformer with OLTC introduces a significant cost although it is still more

viable than fixed APC. Overall, the dynamic APC has a relatively good positioning among the solutions for overvoltage mitigation in suburban LV grid in Germany.

8.2 APC benefit rating for different EU countries

It would be helpful to have some benchmark information on potential for feed-in loss reduction in different EU countries resulting from APC, but there is no known method to quantify this. Every circuit has a unique topology, impedances, load profiles. This makes it difficult to obtain explicit numbers for feed-in loss projections. Here is a proposal to rate several countries for applicability of APC, based on knowledge of supply impedances so that it can at least be known which countries are more likely to benefit from APC in comparison to others. Table 8.1 contains supply impedances of five EU countries based on impedance measurement report [119].

Table 8.1: Survey of country supply impedances and their respective R/X ratios.

Country	**95% consumers with supply impedance (R+jX) equal to or less than:**	**R/X ratio**
France	0,45 + j0,25	1.80
Germany	0,36 + j0,21	1.71
Poland	1,03 + j0,55	1.87
Italy	0,48 + j0,26	1.85
Netherlands	0,41 + j0,21	1.95
United Kingdom	0,25 + j0,23	1.09

The supply impedances are measured at the end of the feeder for a representative sample of 200 customers, taking into account both urban and rural networks. The focus is on the end-of-the-feeder prosumers as the most critical group in the high PV penetration scenario. Two

criteria can be established: one considers only the resistive impedance part and the other considers the complex impedance expressed as the R/X ratio. The former criterion would indicate that in order to lower or raise per-unit of voltage, the smallest reduction in active power would be required in Poland and the highest in UK.Table 8.1 shows a noticeably higher supply impedance in Poland due to dominantly rural LV grid. It can indicate that a prosumer in Poland would experience more frequent overvoltage events as voltage would ramp up faster due to highly resistive supply impedance. So applying power curtailment would be most beneficial in Poland and the least beneficial in UK. The R/X criterion gives somewhat different results. Resistive impedance is expressed relative to inductive. It can indicate the effectiveness of active over reactive power to regulate voltage. In that case Netherlands takes the first place where curtailment would be most beneficial, Poland is second while UK grid is again the least favorable to curtailment. Figure 8.2 shows the increase in APC trend depending on the criteria used. It is difficult to state which criteria is more correct to follow. Perhaps R/X would be more realistic as it takes into account the complex nature of impedance, however the large difference that Poland demonstrates in resistive part of the complex impedance should not be neglected.

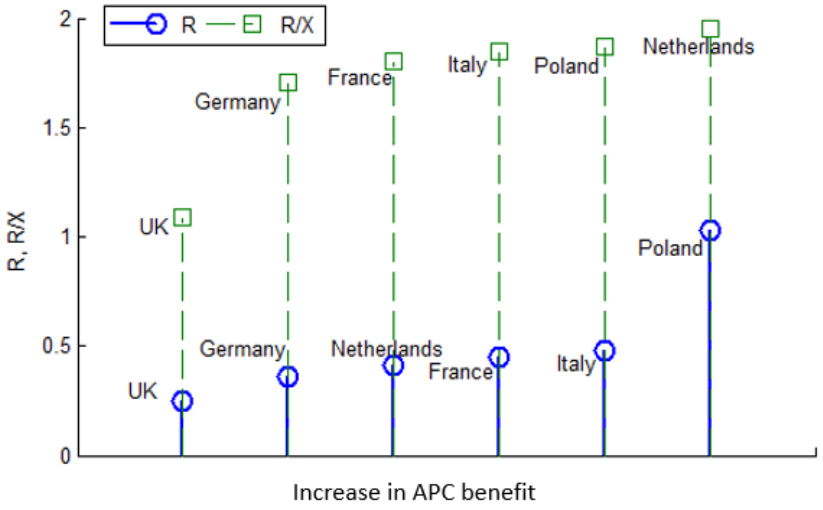

Figure 8.2: Increase in APC benefit for five EU countries based on R/X and R criteria.

8.3 Comparison of SMT and conventional overvoltage protection

By using the same annual power flow model as in previous chapter, a comprehensive annual analysis of feed-in losses is covered in this chapter. The SMT is essentially a modified overvoltage protection scheme, so it was decided to compare the effects of its application against a baseline scenario-conventional overvoltage protection. A new methodology to account and compare the feed-in losses between two solutions is proposed.

8.3.1 Methodology of annual feed-in loss comparison

A comparison is done for the annual load and generation data sets available in 15 min. intervals. The feed-in losses are differentiated as overvoltage losses and curtailment losses (Figure 8.3).

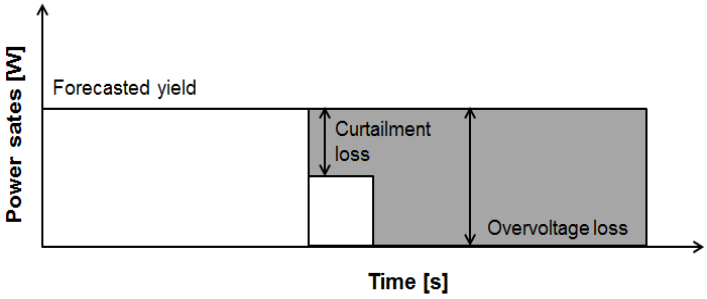

Figure 8.3: Feed-in losses caused by overvoltage protection and curtailment.

With a curtailment control designated to react within seconds, the simulation of annual data set takes unacceptably long. Because of that, a data filtering method is applied: the power flow first runs without curtailment in order to process the raw data set and filter out the power states that correspond to overvoltage and curtailment events. Filter triggers are based on voltage levels, $V \geq V_{MAX}$ for overvoltage events and $V_{START} \leq V < V_{MAX}$ for curtailment events. Next, power flow runs with curtailment using the filtered data set consisting only of event-related power states. Because the measured data was not available in resolution less than 15min, it is assumed that the filtered event is the only event during the observed interval. In reality voltage surge due to change in power output is much more dynamic and can happen in less than 10s, however such high resolution data is difficult to obtain. Conventional overvoltage event represents 100% feed-in loss during inverter downtime. Therefore overvoltage loss can be described as the sum of all annual overvoltage events

$$L_{ov} = \sum_{i=1}^{k} P_i t_{ov} \tag{8.1}$$

where P_i - forecasted power at the moment of overvoltage, k – number of overvoltage events in a year, t_{ov} – event duration (5min reconnection timer). When SMT is active, each overvoltage event is preceded by the *preventive curtailment* event. Therefore the number of annual curtailment events is also k and curtailment loss is

$$L_c = \sum_{i=1}^{k} (P_i - P_{ci}) t_c \tag{8.2}$$

where P_c is power remaining after the curtailment event and t_c is the reconnection time. For the purpose of economic one-to-one comparison, it is assumed that $t_c = t_{ov}$.

The curtailment is engaged at a fixed voltage level $V_{START} < V_{MAX}$. Such setup will produce curtailment events in this range, but not every forecast that crosses V_{START} necessarily leads to V_{MAX}. Every such curtailment is a *wasteful curtailment*. Therefore, to calculate total curtailment loss (L_{tc}), two curtailment event types need to be accounted for: *preventive* and *wasteful* curtailment

$$L_{tc} = L_c + L_{cw} \tag{8.3}$$

The former is already described in (8.2) while the latter is

$$L_{cw} = \sum_{j=1}^{n} (P_j - P_{cj}) t_c \tag{8.4}$$

where P_j – forecasted power during the curtailment, P_{cj} – remaining power after the curtailment, and n-number of the annual wasteful curtailment events. In this case the $t_c = 10s$ because wasteful curtailment is short, unwanted triggering of curtailment and does not directly compare with longer, 5min duration of overvoltage event. The feed-in energy benefit from introducing curtailment is then quantified as the difference between energy lost due to overvoltage and energy lost due to curtailment

$$E = L_{ov} - L_{tc} \tag{8.5}$$

8.3.2 Feed-in loss comparison with overvoltage protection

By applying the proposed methodology on the previously simulated annual power flow data, a feed-in loss comparison was made between SMT and a conventional overvoltage protection. Power flow analysis filtered the preventive and wasteful curtailment events from the annual data set as shown in Figure 8.4.

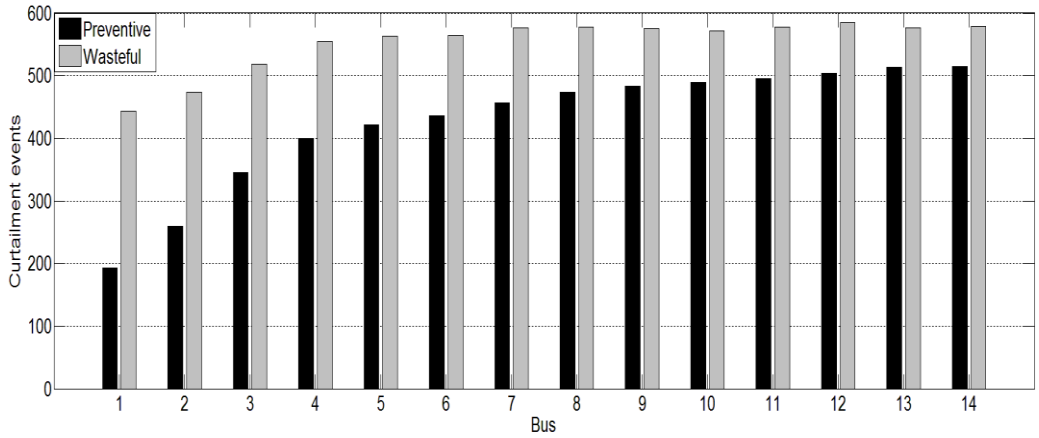

Figure 8.4: Annual distribution of preventive and wasteful curtailment events at each bus.

It can be observed that, with the increased length of the feeder, the difference between the number of preventive and wasteful events becomes smaller. In other words, curtailment actions become more overvoltage-preventive towards the end of the feeder.

The curtailment benefit is visualized in Figure 8.5 as the difference between annual feed-in losses of overvoltage protection and curtailment. Curtailment was able to achieve max yield gain of 99.6%-100% at the first three houses which were practically not curtailed. Minimum yield of 62.3% was achieved at the last bus which experienced most intensive curtailment. In Figure 8.6 it can be seen that the maximum wasteful curtailment does not go above 0.8kWh annually. It can be said that in the presented study, the curtailment has a highly preventive character that doesn't go below 96.8%.

Results for the entire feeder level are presented in Figure 8.7. Curtailment brings 77.4% more yield than the overvoltage protection while wasteful curtailment share is insignificant.

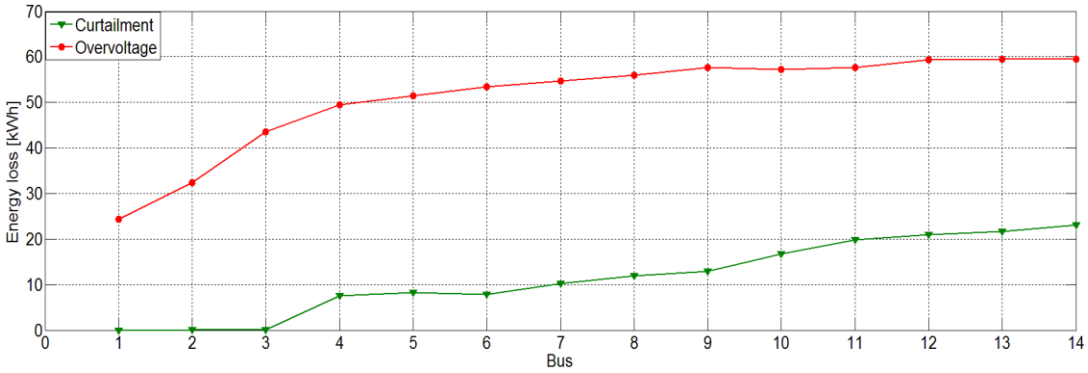

Figure 8.5: Comparison of feed-in losses caused by overvoltage protection and BBD.

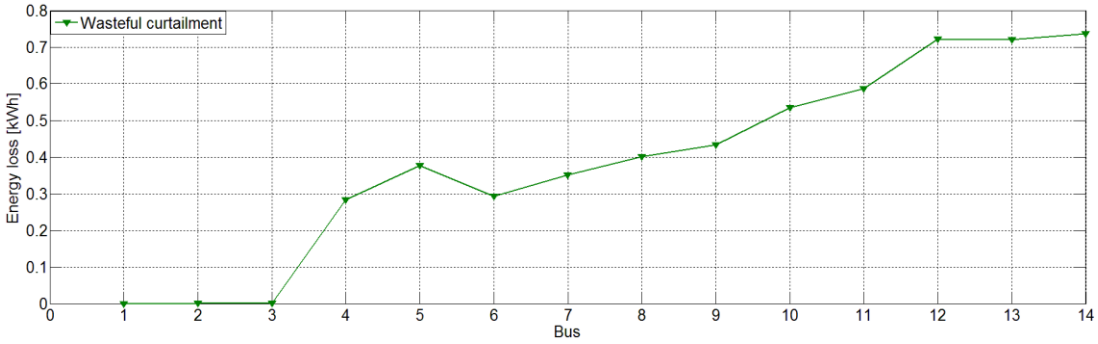

Figure 8.6: Small presence of wasteful curtailment.

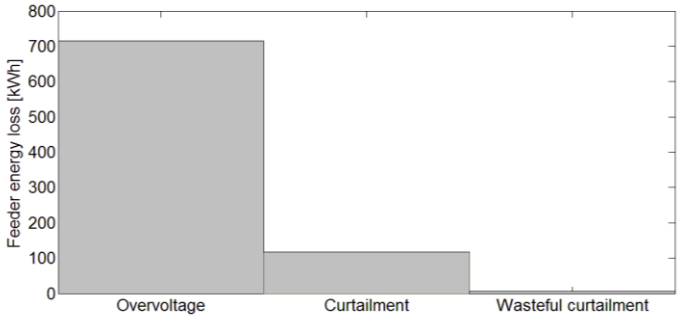

Figure 8.7: Feed-in losses on the entire feeder level.

While proposed curtailment might not be able to handle equality among PV owners it is still a good step forward when compared to the baseline overvoltage protection. On the entire feeder over 550 kWh was saved by curtailment which could easily cover a monthly electricity bill of one household.

8.4 Impact on component reliability: droop vs. SMT

The SMT was proposed as a more reliable and retrofit-friendly curtailment method than droop. In this section, using a 217plus^{TM}reliability prediction methodology, these two control methods are compared. A trade-off analysis is performed to demonstrate how curtailment, although economically undesirable, can actually improve inverter component reliability, especially if SMT is applied.

The reliability of PV inverter components (primarily electrolytic capacitors in a DC bus application) is a well-known problem [120]. The component reliability can be improved with film capacitors, which are more expensive than electrolytic, but also have a longer life span. The micro-inverters represent the peak of the problem as they are applied outdoors and must follow the life time of the PV module (about 25 years) [121]. Their components are directly exposed to the outdoor ambient temperatures and humidity unlike the string inverters that are usually housed indoors. Special design should be taken into consideration to enable long-term, reliable operation. That being said, the implementation of new functionalities only adds more pressure on the design requirements. At preliminary design stage, when no field history is available, the empirical reliability prediction methods can help the designer to choose between competitive designs.

8.4.1 Micro-inverter model and components

The reliability prediction is performed for the components of STEVAL-ISV003V1, a 250W micro-inverter development board [91]. The data from application notes, detailed schematics and bills of materials (BOM) serves as an input to reliability prediction tool, but is generally unavailable from commercial micro-inverter documentation. Hence, a development board was chosen as a reference model. A simplified model of the board is presented in Figure 8.8. It is a two-stage device, an interleaved isolated boost DC-DC converter and a mixed frequency DC-AC converter. The DC-DC MOSFETs Q5 and Q7 are responsible for MPPT and voltage boost operation. They are protected from DC overvoltage by transient voltage suppressor (TVS) diodes. The high frequency transformer (HFT) provides galvanic isolation between DC MOSFETs and the DC capacitor bus. The DC bus consists of two 2.2 µF, 600V plastic film capacitors and four electrolytic capacitors (C8...C11) rated at 22µF, 450V. Two silicon carbide diodes (FWD), are connected in anti-parallel across MOSFETs of one inverter leg and perform the current freewheeling function. The relay (RL1) is placed before the AC filter. Its application is protective and it disconnects the inverter from the grid in an islanding event (over/undervoltage and over/underfrequency protection).

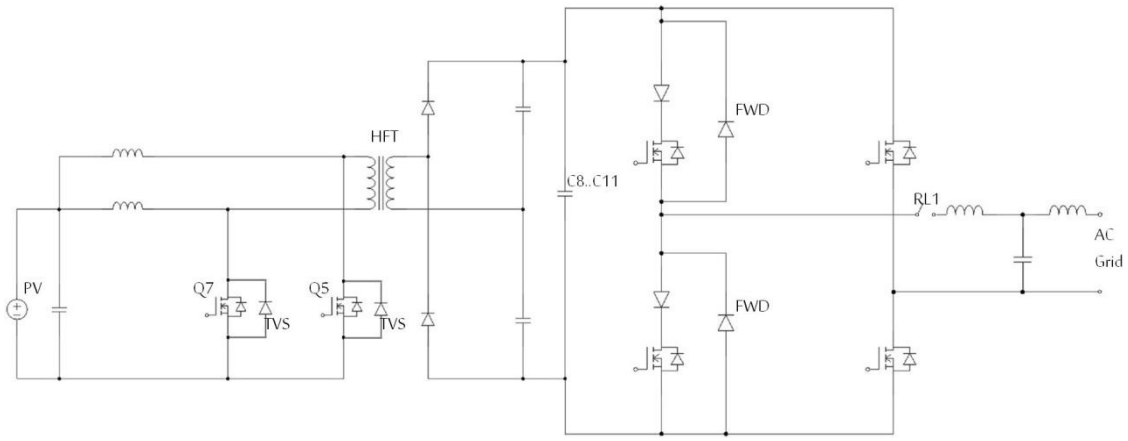

Figure 8.8: DC-DC and DC-AC topologies of STEVAL-ISV003V1 micro-inverter development board.

The droop control implementation requires ramp-down from MPPT and is executed via DC-DC MOSFETs. By reducing MOSFET duty cycle the junction temperature rise is expected to drop too [106]. Further, by reducing duty cycle, DC bus voltage can also be reduced which might act beneficially on the voltage stress of capacitors. These are some of the expected reliability benefits of droop APC.

The SMT, as a modified overvoltage protection, is executed via relay. It should be emphasized that relay is *electromechanical*. It is expected that introducing SMT will negatively impact the reliability of the given relay.

8.4.2 Micro-inverter operating profile

The micro-inverter daily operating profile consists of three states: operating, non-operating and APC (Figure 8.9).

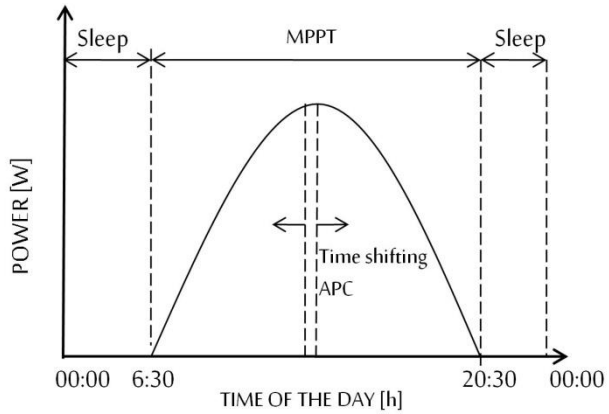

Figure 8.9: Micro-inverter daily operating profile.

The power maximization is the normal inverter operating state (hereinafter referred to as "MPPT"). The state is present in the profile 14 h/day (6:30-20:30). This period is based on the inverter output profile during June in Netherlands. As modules stop generating power towards the night, the inverter eventually gets disconnected until early morning hours. This is the non-operating state that lasts 10 h/day (20:30-6:30, hereinafter referred to as "*sleep"*). Unlike the previous two states, which are determined by the repeating day and night irradiance shift, APC is not present on a daily basis, but has a more stochastic character throughout the whole year. In Figure 8.9 the arrows indicate that APC event could be located anywhere within the MPPT period. The feed-in loss analysis (from Section 8.2), revealed about 600 APC events occurring throughout the year. The same number of events is applied in this study. For consistency with previous states, the annual number of APC events must be expressed as daily presence or h/day (t_{APC}):

$$t_{APC} = \frac{n \times t_r}{60 \times 365} \tag{8.6}$$

where n is the number of events per year and t_r is the reconnection time (5min). This conversion translates 600 events into 0.137 h/day. Depending on which control method is used, APC can be interpreted either as operating state (droop) or non-operating state (SMT).

To assess the reliability impact of implementing APC in a micro-inverter as well as compare the impacts of droop and SMT, three full operational profiles need to be observed: 1) *MPPT,sleep* (which would be the baseline scenario of most inverters today); 2) *MPPT,droop,sleep* and 3) *MPPT,SMT,sleep*.

8.4.3 217plus^{TM} reliability prediction methodology

The 217plus^{TM}is a result of 11 year advancement in the reliability prediction methodology that can be traced since the last update of MIL-HDBK-217 in 1995 until 217plus^{TM} release in 2006 [122]. Although MIL-HDBK-217 is still widely used in both engineering and research studies, the 217plus^{TM} will eventually replace it. Development of both methodologies was sponsored by the US Department of Defense, however today, only the development of 217plus^{TM} is actively supported [123].

With respect to this study there are several advantages to why 217plus^{TM} is used. Firstly, its component models can account for reliability of not only operating states, but also non-operating states. Secondly, the old MIL-HDBK-217 component models are based on the multiplicative approach:

$$\lambda_p = \lambda_b \pi_e \pi_q \pi_s \tag{8.7}$$

where,

λ_p predicted failure rate

λ_b base failure rate

π_e environmental factor

π_q quality factor

π_s stress factor

The disadvantage of multiplicative failure rate model is that values can become unrealistically large or small when the model parameters are at their highest or lowest values. Such model makes it difficult to assess failure mechanisms separately. The 217plus^{TM} takes a hybrid approach with multiplicative-additive failure rate model that allows separation of failure rates associated with different causes.

Finally, the 217plus^{TM} contains failure rate model for relays which was not available until 2006. Since the described micro-inverter model uses electromechanical relay as a trip switch, it was convenient to apply a methodology that has an available relay model supported with empirical data.

8.4.4 Component failure rate models

The scope of reliability prediction presented in this study is limited to following components: MOSFETs, relays and capacitors. This selection was made based on popular micro-inverter reliability issues and components directly involved in the execution of described APC methods. The additive-multiplicative failure rate models for MOSFETs, relays and capacitors are presented respectively in (8.8), (8.9) and (8.10):

$$\lambda_P = \pi_G(\lambda_{OB}\pi_{DCO}\pi_{TO}\pi_S + \lambda_{EB}\pi_{DCN}\pi_{TE} + \lambda_{TCB}\pi_{CR}\pi_{DT}) + \lambda_{SJB}\pi_{SJDT} + \lambda_{IND} \quad (8.8)$$

$$\lambda_P = \pi_G(\lambda_{OB}\pi_{DCO}\pi_{TO} + \lambda_{EB}\pi_{DCN}\pi_{TE} + \lambda_{TCB}\pi_{CR}\pi_{DT}) + \lambda_{IND} \quad (8.9)$$

$$\lambda_P = \pi_G\pi_C(\lambda_{OB}\pi_{DCO}\pi_{TO}\pi_S + \lambda_{EB}\pi_{DCN}\pi_{TE} + \lambda_{TCB}\pi_{CR}\pi_{DT}) + \lambda_{SJB}\pi_{SJDT} + \lambda_{EOS} \quad (8.10)$$

where,

λ_P predicted failure rate (per million calendar hours)

π_G reliability growth rate multiplier

λ_{OB} base failure rate, operating

π_{DCO} failure rate multiplier, duty cycle, operating

π_{TO} failure rate multiplier, temperature, operating

π_S failure rate multiplier, stress

λ_{EB} base failure rate, environmental

π_{DCN} failure rate multiplier, duty cycle, non-operating

π_{TE} failure rate multiplier, temperature - environment

λ_{TCB} base failure rate, temperature cycling

π_{CR} failure rate multiplier, cycling rate

π_{DT} failure rate multiplier, delta temperature

λ_{SJB} base failure rate, solder joint

π_{SJDT} failure rate multiplier, solder joint delta temperature

π_C capacitance failure rate multiplier

λ_{EOS} failure rate, electrical overstress

Table 8.2 lists components along with their base failure rates due to following causes: operating, environmental, temperature cycling, and solder joint. The base failure rates are derived from observed failure rates coming from a variety of sources: testing laboratories, device and equipment manufacturers, government laboratories and equipment users. Base failure rates can indicate which cause statistically carries more weight in the predicted failure rate. Component ids are provided so that the reader can trace them in the application note [91] and in the BOM list [124].

Table 8.2: Selected components of STEVAL-ISV003V1 250W micro-inverter demonstration board. Base failure rates in FIT.

Component ID	**Component type**	λ_{OB}	λ_{EB}	λ_{TCB}	λ_{SJB}
Q5,Q7	Transistor, MOSFET	0.20	0.33	0.26	1.50
C8,C9,C10,C11	Capacitor, electrolytic aluminum	0.47	0.22	0.21	0.95
RL1	General purpose, electromechanical relay	6.34	143.24	10.97	NA

8.4.5 Time fraction weighting factors

The extreme-value operating states such as SMT can produce very inflated or deflated failure rates when assessed separately. In accordance with the multiplicative-additive approach, the proposal is to weight the failure rates of each operating state with a factor of its actual presence in the daily operating profile[125]. The weighted sum of individual state failure rates would then represent failure rate of the full operating profile. The weighting factor of each state is a time fraction of the operating profile in which a particular state is present. That gives the following time fractions: π_{MPPT}=(14-0.137)/24, π_{sleep}=10/24 and π_{APC}=0.137/24. The π_{APC} occurs as a non-operating interruption within MPPT state, hence the subtraction from MPPT hours. Finally, the formula of predicted failure rate for a full operating profile would be

$$\lambda_{full\ profile} = \lambda_{MPPT}\pi_{MPPT} + \lambda_{sleep}\pi_{sleep} + \lambda_{APC}\pi_{APC} \quad (8.11)$$

8.4.6 State parameters

The failure rate models (8.8), (8.9) and (8.10) include a multitude of multipliers (Pi-factors). These factors are calculated from state parameters. The parameters are summarized in four sets for each state: MPPT, sleep, droop and SMT in Table 8.3-8.6 respectively.

Table 8.3: Key parameter set for the MPPT state interpretation.

Component	T_{ao}	T_{ae}	D	CR	S	Tr
MOSFET	40	14	1	0	NA	60
Relay	40	14	1	0	NA	0
Capacitor	40	14	1	0	0.84	0

Table 8.4: Key parameter set for the sleep state interpretation.

Component	T_{ao}	T_{ae}	D	CR	S	Tr
MOSFET	14	14	0	0	NA	0
Relay	14	14	0	0	NA	0
Capacitor	14	14	0	0	0	0

Table 8.5: Key parameter set for the droop state interpretation.

Component	T_{ao}	T_{ae}	D	CR	S	Tr
MOSFET	40	40	1	0	NA	0
Relay	40	40	1	0	NA	0
Capacitor	40	40	1	0	0.84	0

Table 8.6: Key parameter set for the SMT state interpretation.

Component	Tao	Tae	D	CR	S	Tr
MOSFET	40	40	0	0	NA	0
Relay	40	40	0	0	NA	0
Capacitor	40	40	0	0	0	0

For understanding the parameter sets in Table 8.3-8.6, it is necessary to comment on the methodological constraints within 217plus^{TM} and assignment of parameters so that a particular state is realistically interpreted within the given constraints.

Duty cycle and cycling rate

In 217plus^{TM} component duty cycle (D) and cycling rates (CR) are inherited from the system (inverter) level. For example, if the inverter is operating 100% of the time, then D=1 and the MOSFET inside will have D=1 too, although according to electronic calculations in [91], it might have a maximum value of D=0.7. That being said, to interpret the MPPT and droop as the operating states and sleep and SMT as the non-operating, the duty cycle is set D=1 (Table 8.3Table 8.5) and D=0 (Table 8.4, Table 8.6) respectively.

The decision to analyse operating and non-operating states separately rather than within full profile systematically eliminated cycling rate stress in all components (CR=0 in all four states). It can be argued that this is not a good approach, but if the full profile was observed then the states would require both CR>0 and D>0, which would better account for CR, but D>0 would be an inaccurate description of SMT and sleep states.

Ambient operating and non-operating temperatures

Due to the lack of experimental thermal model, the ambient operating (T_{ao}=40^{o}C) and non-operating (T_{ae}=14^{o}C) temperatures are taken from the default 217plus^{TM} empirical values for "*ground stationary, outdoors*" systems [123].

It can be noticed that only MPPT state (Table 8.3) has different T_{ae} and T_{ao}. As this state takes the biggest part of the operating profile it is assumed that temperature cycling from T_{ao} to T_{ae} can occur within 14 hours. That is not the case with droop and SMT because they are short, 5min interruptions within MPPT state during which temperature cannot suddenly drop from 40^{o}C to 14^{o}C degrees. Instead, the assumption is that T_{ae}=T_{ao}=40^{o}C for such short intervals. The sleep state lasts considerably longer (10 hours) and some temperature cycling in 20:30-6:30h period could be expected, but there is a methodological constraint that T_{ae} is not defined for a non-operating state so the assumption is T_{ae}=T_{ao}=14^{o}C (Table 8.4).

Temperature rise

The temperature rise (Tr) refers to the difference between the junction temperature and Tao. For capacitors and relays the default Tr=0, while for MOSFET Tr=60°C. The assumption is that MOSFETs will only experience temperature rise in MPPT state (Table 8.3) as power injection fluctuates with irradiance. For sleep and SMT as non-operating states characterized by Tae, the Tr is not defined, therefore Tr=0°C (Table 8.4, Table 8.6). Even in

droop state the assumption is Tr=0°C because the inverter is forced by voltage droop to reduce the MOSFET duty cycle (Table 8.5).

Electrical stress

The default electrical stress (S) factor for relays and capacitors is not defined/applicable (NA). For capacitors it is defined as the applied voltage stress divided by the rated voltage. In STEVAL-ISV003V1, DC bus capacitors are rated at 450V, but during normal operation DC bus voltage is regulated at 380V [91], therefore S=380/450=0.84 is adopted. The voltage stress is applied on the DC bus capacitors only during operating states (MPPT and droop) while in SMT and sleep, S=0.

8.4.7 Results and discussion

Weighted and non-weighted component failure rates

In Table 8.7 are presented the non-weighted failure rates for each state, while Table 8.8 shows weighted sum of failure rates for the three full profiles as defined in Section 4.

Table 8.7:Non-weighted failure rates (in FIT) for each state in the operating profile.

Component	λ_{MPPT}	λ_{droop}	λ_{SMT}	λ_{sleep}
MOSFET	17.83	11.00	10.99	10.99
Relay	121.06	121.06	2317.07	81.72
Capacitor	3.49	3.20	0.80	0.78

Table 8.8: Weighted sum of state failure rates (in FIT) for three different operating profiles.

Component	$\lambda_{MPPT,sleep}$	$\lambda_{MPPT,droop,sleep}$	$\lambda_{MPPT,SMT,sleep}$
MOSFET	14.98	14.98	14.98
Relay	104.66	104.66	105.19
Capacitor	2.36	2.36	2.36

Depending on the analysed state, variations of the non-weighted failure rate can be large (Table 8.7). It is most pronounced for relays during SMT where it increases almost 20 times compared to the MPPT state. However, SMT is only present for a very limited time, not for the whole calendar time. This is expressed in the weighted calculation (Table 8.8) where it marginally contributes to failure rate increase of 0.53 FIT ($\lambda_{MPPT,SMT,sleep}$) compared to operating without APC ($\lambda_{MPPT,sleep}$). In case of capacitors the non-weighted results show that SMT and sleep states are beneficial (failure rate decreased about 4-5 times compared to λ_{MPPT}), but the weighed profile shows no impact on failure rate. The MOSFET failure rate is showing to be the least sensitive to APC in both weighted and non-weighted variant.

The APC/failure rate trade-off

The baseline scenario for weighted failure rates was 600 APC events/year or 0.137 h/day. To get more insight into the trade-off between presence of APC in the operating profile and failure rate, as well as how reliability impacts of droop and SMT compare, a hypothetical trade-off plot is generated for each component by increasing the number of APC events (Figure 8.10). The trade-off analysis doesn't go beyond $1.2x10^6$ events (11.4h/day) as the available MPPT time is 14h/day, so it would be unrealistic to consider situations where APC is engaged for over 80% of operating time.

The trade-off analysis shows that both droop and SMT act beneficially on reducing failure rate of MOSFETs and capacitors. More specifically, in case of MOSFET, droop and SMT reduce failure rate in almost identical manner with a maximum decrease of 20% at the end of analysis. For capacitors it is evident that SMT is more beneficial than droop. The analysis ends with droop reducing failure rate by 6% and SMT by 54%. The relay is the only component impacted negatively by the introduction of SMT. The end analysis shows a severe,

almost 1000% increase in failure rate. Droop doesn't engage relays and therefore is the same as the baseline *MPTT,sleep* profile.

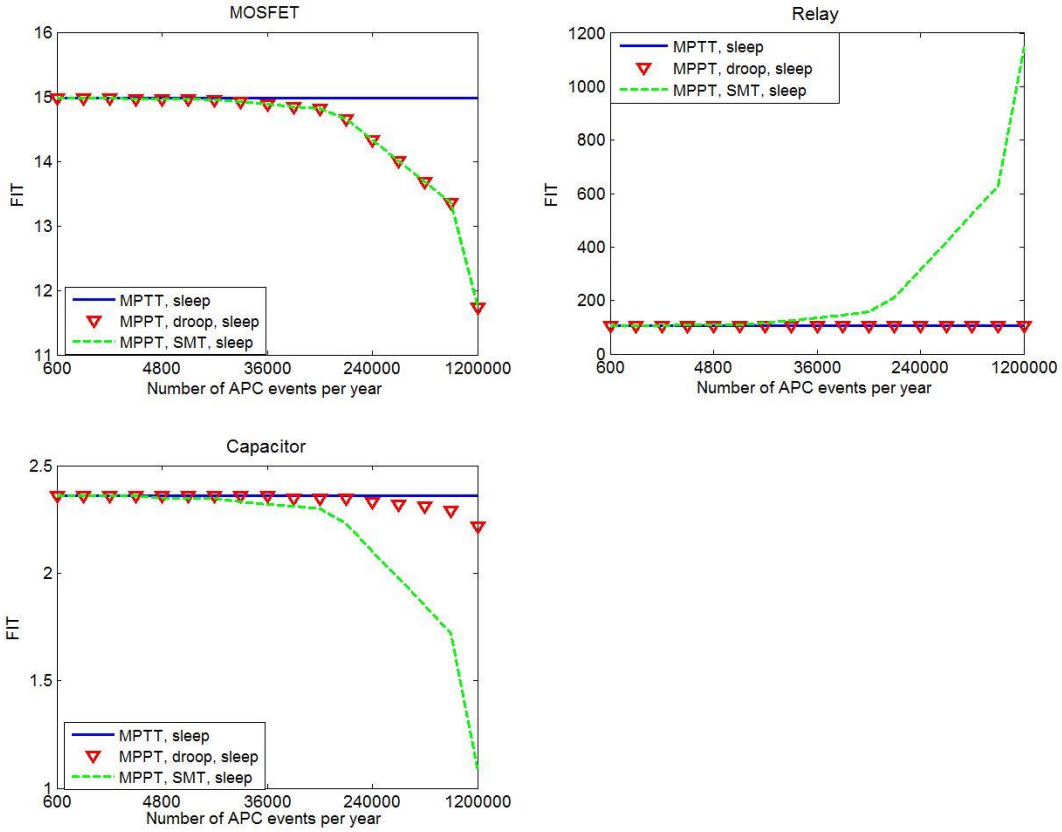

Figure 8.10: Hypothetical trade-off between APC and component failure rates.

Critical Pi-factors and potential causes of failure

Based on the state parameters declared in Section 5.4, all Pi-factors contained in the component models are computed for each of the states and plotted in Figure 8.11. Out of ten Pi-factors altogether present in failure rate models, only three of them are independent of operating states (growth, cycling rate and capacitance failure) , while the rest are state-dependent variables. In MOSFETs both droop and SMT reduce operating temperature stress as well as solder joint temperature stresses. In capacitors there is no noticeable effect of either APC methods on reduction in temperature stress however they do reduce operating duty cycle stress as well as solder joint temperature stress. The added benefit of SMT is voltage stress

reduction which is second critical factor in case of capacitors. For the relay the main issues are temperatures, both operating and ambient. Duty cycle stresses of operating and non-operating states are about the same, but not nearly as critical as temperatures.

The 217plus™ does not provide the user explicit data about the causes of failure. That would requires a physics-of-failure analysis supported with experimental data. However, the base failure rates in 217plus™ incorporate failure causes by mapping empirical failure mode data to failure cause categories. So base failure rates along with knowledge of critical Pi-factors could imply potential causes of failure. For example, in relays the base failure rate attributed to the environment (λ_{EB}) is 13-23 times higher than the other two rates (Table 8.2). In Table 8.8 it can be seen that its multiplier is the environmental factor (π_{TE}) which is also the most critical Pi-factor in Figure 8.11. This relation between the base failure rate and a Pi-factor can suggest that the likely cause of a relay failure is the environmental temperature.

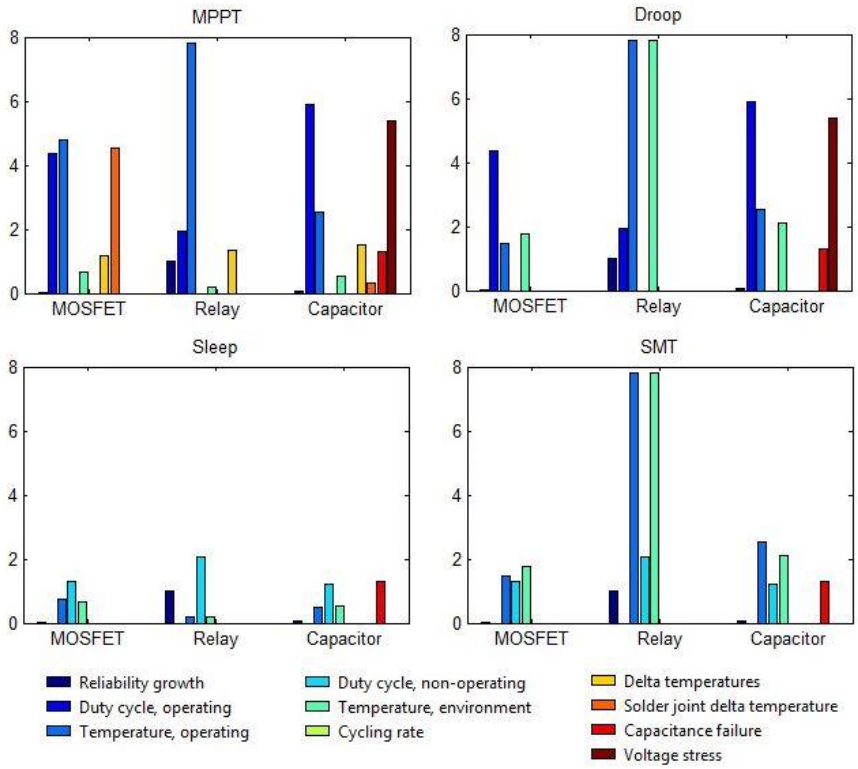

Figure 8.11: Failure multipliers (Pi-factors) influenced by operating and non-operating states.

8.4.8 Summary

This section evaluated the reliability impact of implementing two different APC methods (droop and SMT) in a micro-inverter design. By using 217plus^{TM} reliability prediction methodology, the study reveals that, depending on the applied APC method, the interests can be conflicting from design-for-reliability point of view. While SMT might be favored over droop due to reducing failure rate of electrolytic capacitors, it might significantly increase the failure rate of AC protective relays. This doesn't mean that this conflict cannot be avoided. The author is familiar from private communications with micro-inverter designers that, for the sake of increased reliability, in a commercial micro-inverter moving parts should be avoided and instead of electromechanical relays, the solid state solutions should be used. In other words, MOSFET instead of relay should perform the protective switch function. That

being said, from this study a design recommendation can be derived: for micro-inverters with APC capability, SMT should be a more preferred over droop because of the more beneficial impact on DC bus capacitors, provided that AC protective switch is not electromechanical, but a solid state.

CHAPTER 9

Hardware-in-the-Loop Validation

During the course of research the idea was to field-test the effects of retrofitting an existing, commercial PV micro-inverter system with a new grid support functionality. Instead of just focusing on the proposed SMT method it would be more value-adding to investigate a wider range of voltage support strategies. Specifically the idea was to investigate the possibility of active and reactive power control retrofit. While a 1kW PV system was procured, the remoteness and restricted access of test site and the outdoor (roof) application posed an accessibility problem for conducting tests efficiently and thoroughly. The micro-inverters were off-the-shelf solution so opening the enclosure for setting up probes in order to measure internal effects was not possible. Also manufacturer does not allow the reprogramming of firmware in order to change power factor, active/reactive power reference. Furthermore, it was of interest to conduct some of the tests in a harmonic-polluted grid. As the installation was not under isolated laboratory conditions, but directly grid-connected on the premises of an industrial facility, it would have been difficult, expensive and dangerous to perform such tests. To overcome all these issues, the field test validation was replaced with a hardware-in-the-loop (HIL) real-time simulation.

9.1 Real-time HIL modeling and simulation

The Typhoon HIL402 real-time simulator was selected for the HIL platform of this research for its advanced real-time capability (1 μs simulation step) and FPGA chip customization for power electronics systems. Figure 9.1 shows HIL402 device with a DSP docking board and a mounted controller card.

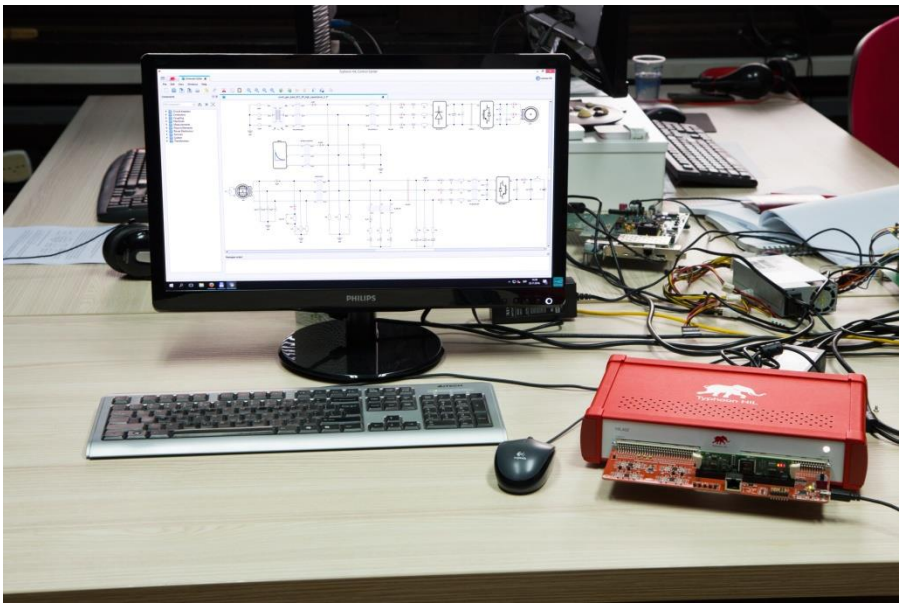

Figure 9.1: HIL402 real-time simulator with a DSP docking board.

To effectively replace a field test, the following components had to be modeled: PV module, micro-inverter and grid voltage source. These components are modeled in Typhoon HIL Control Center software and run on a FPGA core while the micro-inverter controller is implemented on a separate DSP processor.

9.1.1 PV model

The PV module is modeled as a voltage-controlled current source with capacitance connected in parallel, as shown in Figure 9.2. The current source represents a single PV cell which can be multiplied to a number contained in a module or entire array. Typhoon HIL software enables detailed and realistic PV model parameterization using manufacturer datasheet. The model is based on GS Power 255Wp mono Si, a PV module used in the actual test facility. Figure 9.2 shows a sample I-V and P-V curves during MPPT tracking for the given PV module.

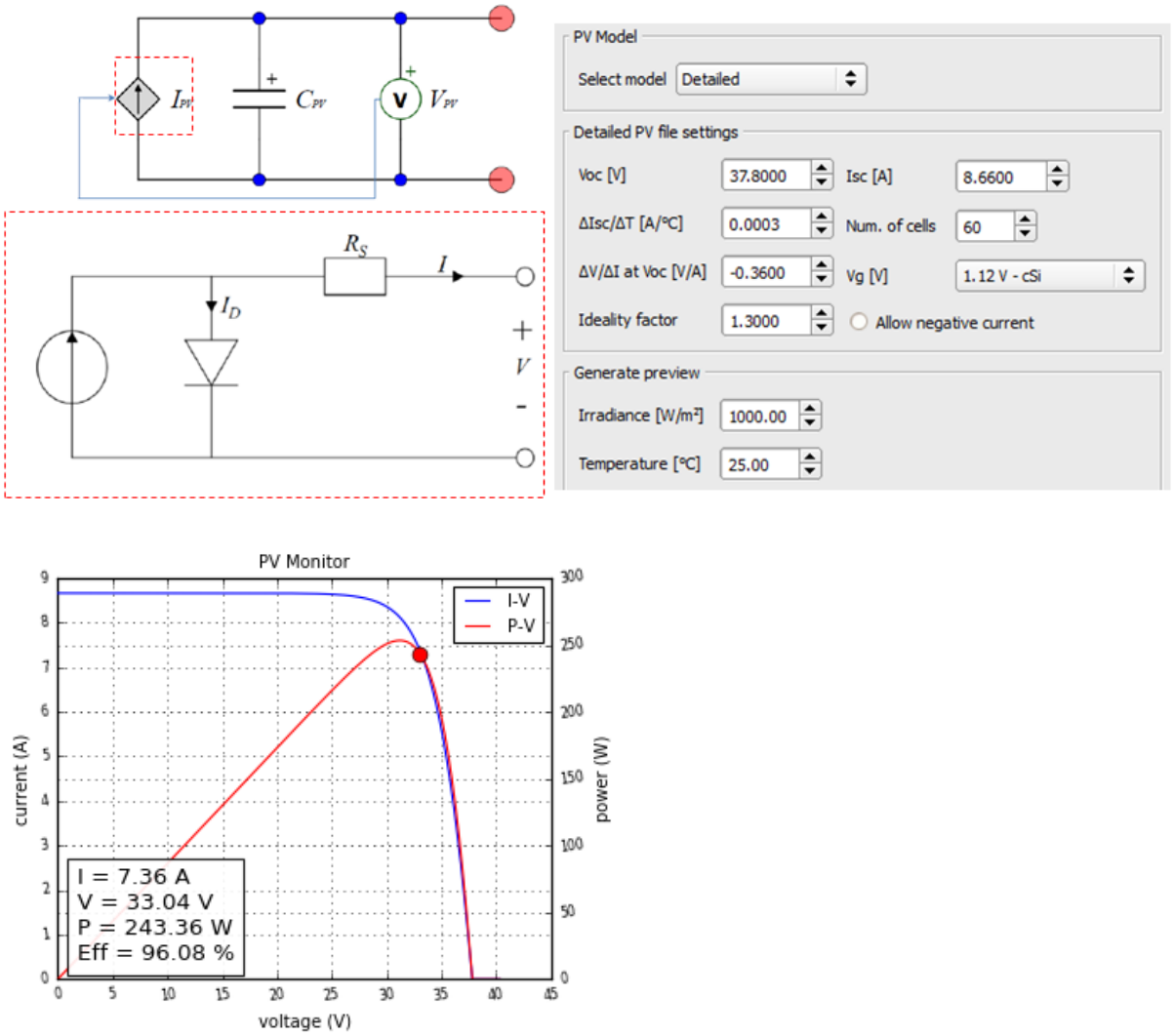

Figure 9.2: Detailed PV model and parametric setup.

9.1.2 Micro-inverter model

The single-phase micro-inverter is implemented as a two stage device consisting of boost converter and a full-bridge inverter coupled via DC link capacitance (Figure 9.3). Contactors are behind LCL filter which interfaces the inverter to the grid. Its main electrical specifications are presented in Table 9.1.

The MPPT is based on the perturb-and-observe algorithm. The output is a duty cycle reference that feeds into the boost converter. The boost converter is operating at 6 kHz switching frequency. Burst mode operation uses hysteresis control to protect the DC link from

overvoltage/undervoltage stress during inverter startup and low irradiance situation. The DC link consist of 96.4 µF capacitance rated at 450V.

Table 9.1: Micro-inverter electrical specifications.

Nominal input voltage	35.8V
Maximum input voltage	55V
Minimum input voltage	18V
MPPT range	20V to 40V
Nominal input current	7.6A
Maximum input current	11A
Maximum inrush current	8A (max 150ms)
DC-DC nominal output voltage	320V
DC-DC max. output voltage	450V
Nominal AC output voltage	230V
Nominal output current	1.1A
Power factor	0.98 at full load
Nominal output power	250W
DC-DC switching frequency	6kHz
DC-AC switching frequency	10kHz

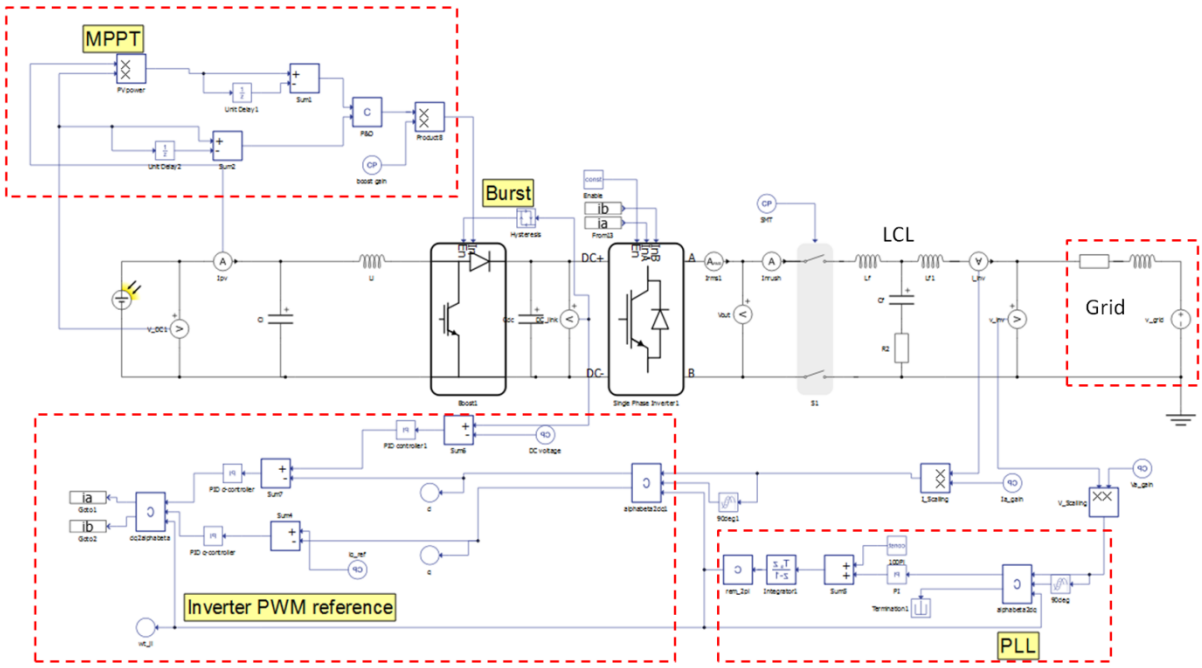

Figure 9.3: Micro-inverter model with control signals.

The inverter control is based on unipolar PWM modulation. Figure 9.4 shows 180° displacement between sinusoidal references for each inverter leg.

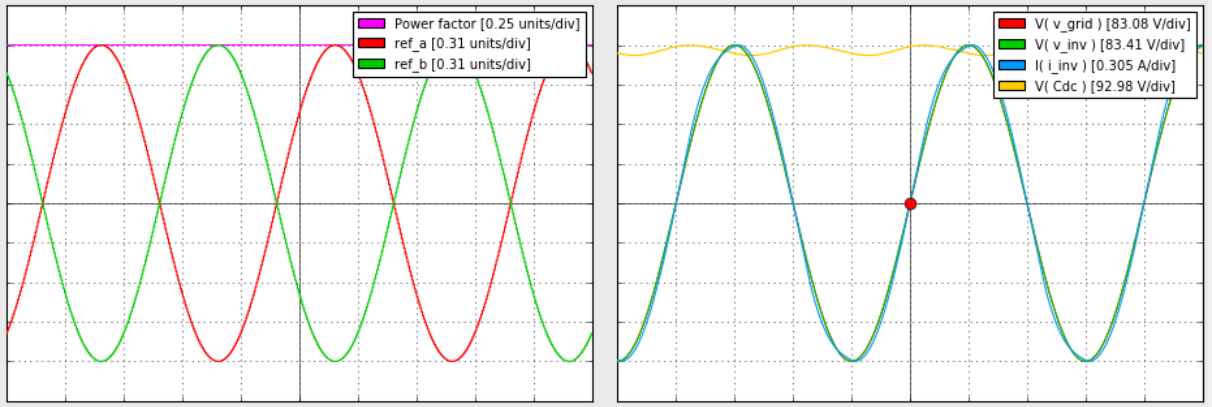

Figure 9.4: Reference control (left) and output voltage/current signals (right).

This inverter does not implement active power decoupling therefore DC link gets slight oscillations coming from AC side as shown by *V(Cdc)* signal. The switching frequency is 10kHz. Both PLL and current control are based on Park transformation from αβ rotating to dq stationary reference frame. The current's active and reactive components are regulated via PI controllers, then a reverse Park transformation is performed to obtain two sinusoidal signal references for the inverter. The LV grid impedance is modeled to represent the Polish average end-of-the-feeder supply impedance (R=1.03Ω, L=1.75mH) according to impedance survey performed in [119].

Thermal model

Typhoon HIL allows up to five inverter thermal models that can be simulated simultaneously with electrical model. Figure 9.5, on the left, shows the thermal modeling principle, which is the transmission line equivalent circuit model [126], where P_{AVG} is the average inverter power, T_A and T are the ambient temperature and internal temperatures and

R_{th} and C_{th} are thermal resistance and thermal capacitance, respectively. On the right is shown how these parameters can be obtained experimentally.

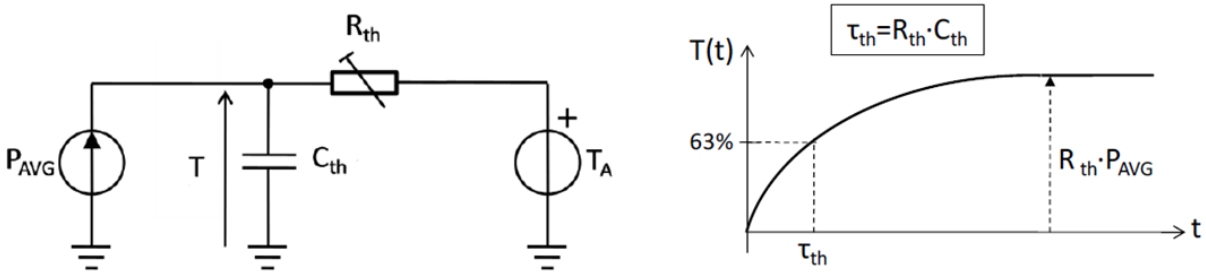

Figure 9.5: Thermal modeling of electrical components.

In this study 3 models are used (Figure 9.6) to demonstrate the effects of control method on internal temperature and validate conclusions from previous chapter (i.e. cool-down benefit of curtailment). The R_{th} is the same in all three models and is obtained from a field study on micro-inverter thermal performance [127] . There is no experimental data for C_{th}, nonetheless it is selected arbitrarily and varied in all three models to demonstrate different thermal transient behavior resulting from change in power output.

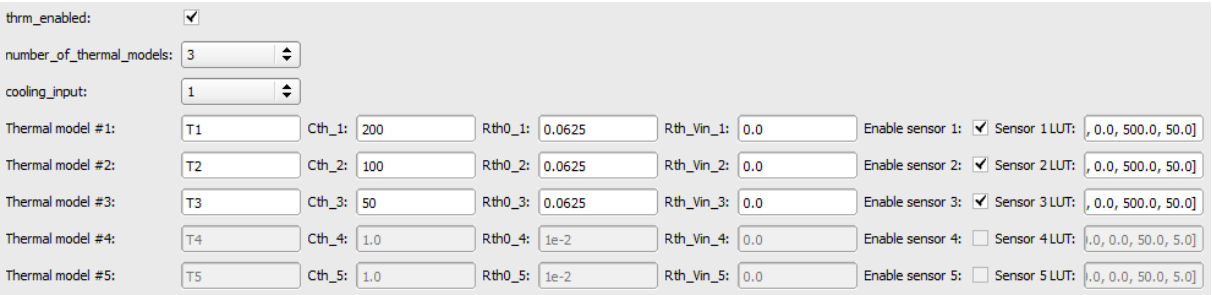

Figure 9.6: Three inverter thermal models with parameters.

The "Rth_Vin_1" refers to $\Delta R_{th}/\Delta V_{in}$, or the gradient of thermal resistance change with fan speed (in case of a DC fan, a DC voltage). Since micro-inverters rely only on passive cooling this term is set to zero.

Harmonic model

The inverter under test does not support active harmonic filtering and only relies on passive LCL output filter. To generate a current reference an external voltage reference is used, therefore if the voltage is polluted with harmonics, the injected current will also be polluted with harmonics. The harmonic model is based on a limit case of Polish power quality requirements [128]. Advantage was given to lower-order odd harmonics as they are more dangerous, because they carry more energy and are more difficult to filter. The first 10 odd harmonics at their allowed limit give a distorted sine wave as shown in Figure 9.7. This gives 11% total harmonic distortion (THD) for voltage.

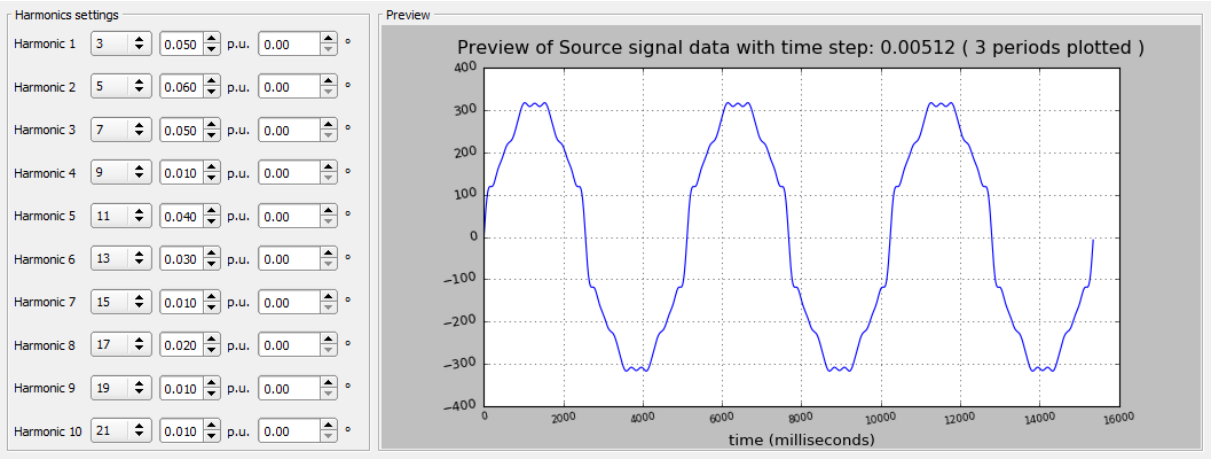

Figure 9.7: Harmonic model of voltage at PCC.

9.2 Effect of SMT control retrofit

On a single micro-inverter level the SMT is no different than regular connecting and disconnecting of the inverter from the grid. Figure 9.8 shows inverter operation during two trip events of different duration.

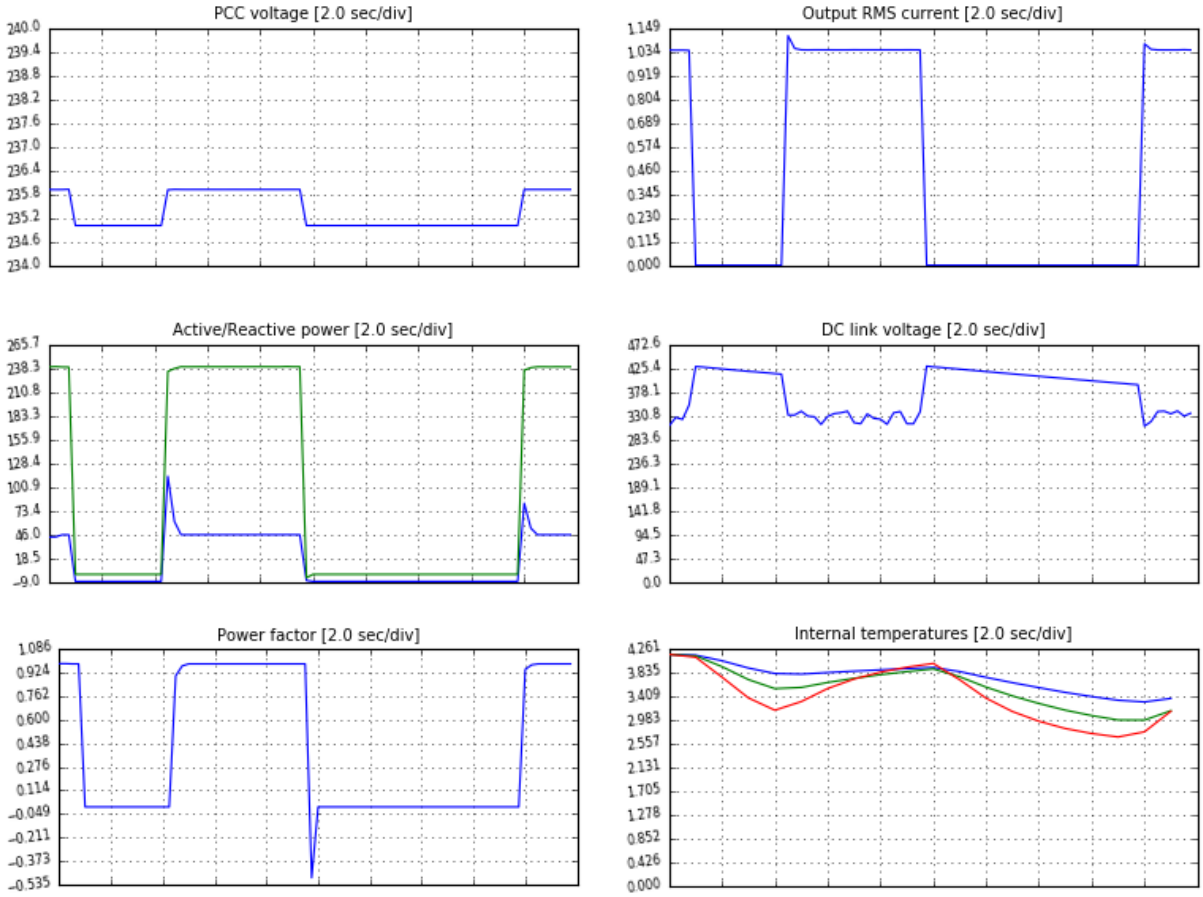

Figure 9.8: Effects of SMT on grid voltage and inverter electrical and thermal behaviour.

The switching off at maximum active power of 240W (green line) caused a voltage drop from 235.9V to 235V. A single micro-inverter unit is capable of delivering instant 0.9V reduction upon curtailment request. There is a visible increase in electrical stress on the DC capacitor during disconnected state, however the burst control is doing its task to prevent DC overvoltage.

The internal temperature is a scaled voltage signal (1V=10°C). The blue green and red lines respectively represent three inverters with different thermal capacitances. Inverter with highest thermal capacitance (blue temperature line) shows the greatest temperature inertia to changes in the electric power. Since thermal capacitance is physically dependent on system's mass and volume the physically smaller micro-inverters experience greater benefit of thermal

stress reduction than large size inverters. The greatest temperature reduction achieved goes up to 11°C.

The DC link voltage control is crucial in both regulating the DC voltage and eliminating high inrush currents. An example in Figure 9.9 shows a response with burst control disabled.

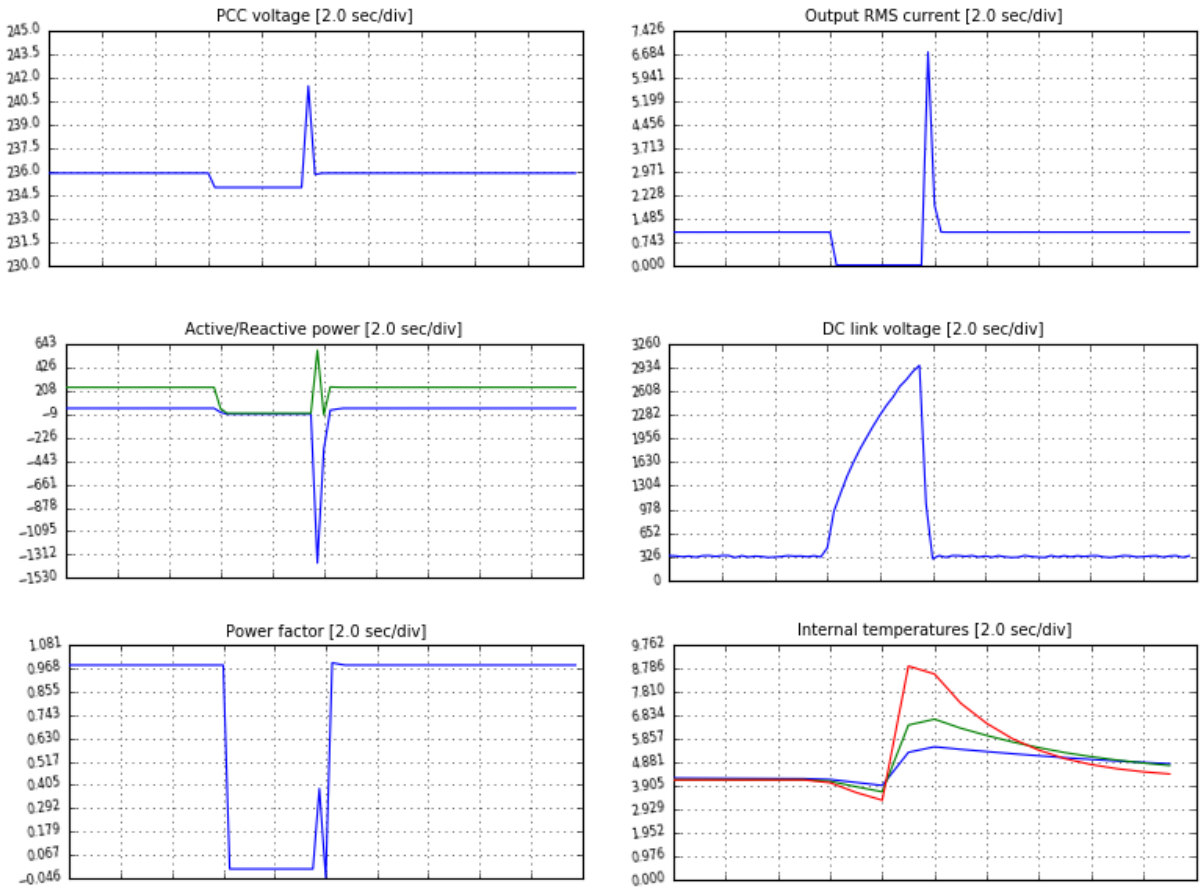

Figure 9.9: DC overvoltage upon reconnection of inverter with burst control disabled.

In worst case DC link capacitors would be destroyed. Potential for grid overvoltage is increased which is contrary to the objective of overvoltage prevention. The inrush current in this case is quite close to 8A maximum.

It was discovered that occasionally a DC link undervoltage happens despite the enabled burst control (Figure 9.10). The problem is known in other research works [129] and

it can occur at low irradiance conditions which was also demonstrated in low irradiance test where inverter active power would drop under 50%. (Figure 9.11).

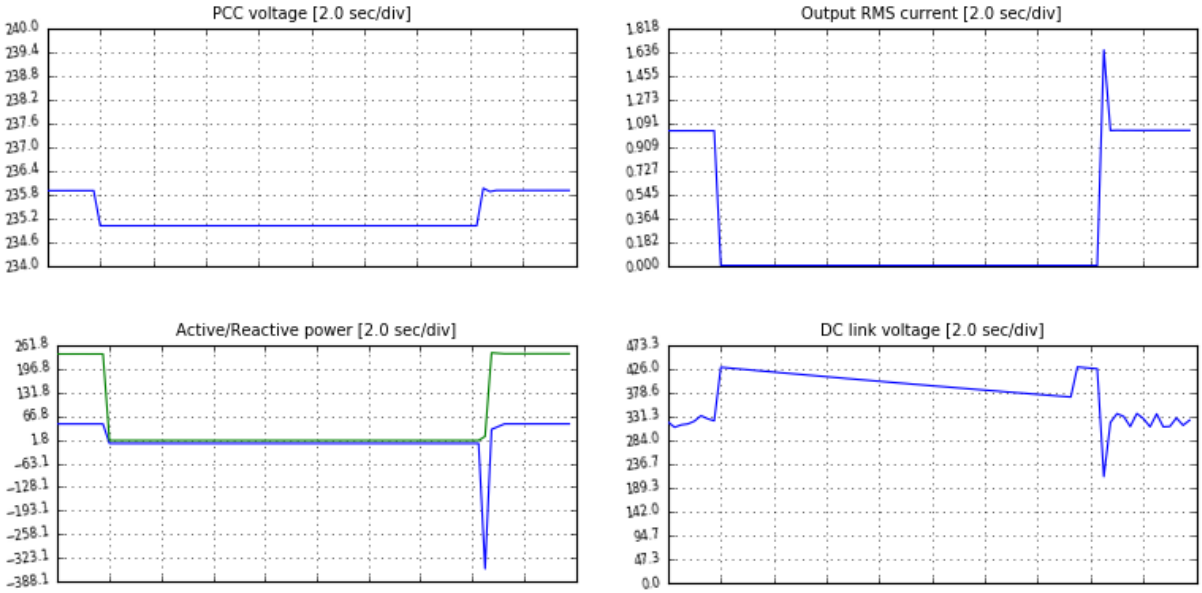

Figure 9.10: DC link undervoltage upon inverter reconnection at lower burst control threshold.

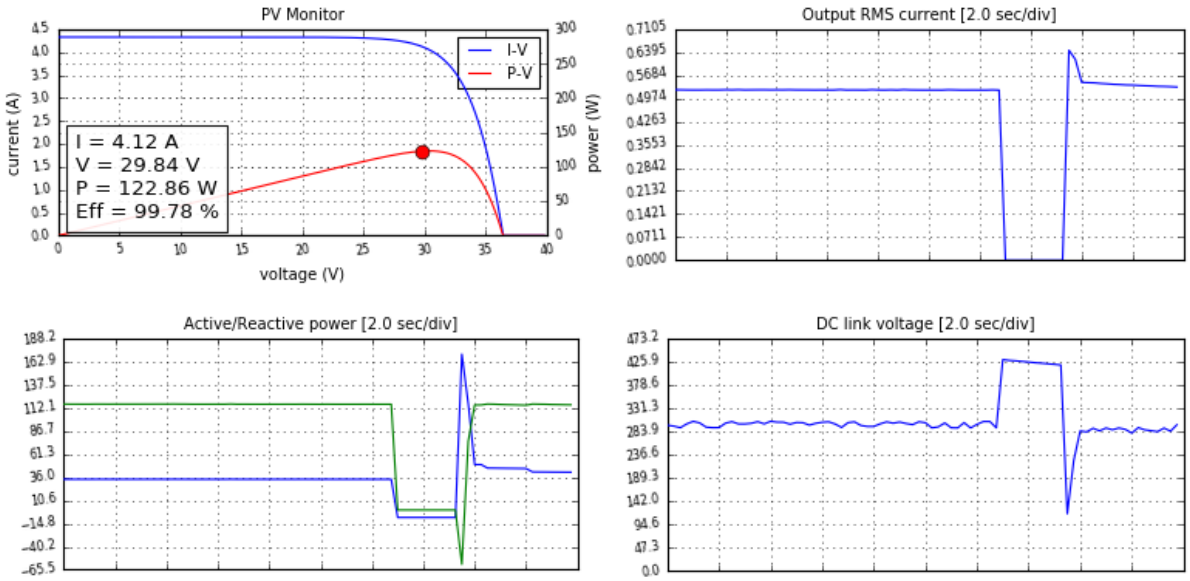

Figure 9.11 DC link undervoltage upon inverter reconnection under low irradiance conditions.

Under harmonic environment the grid voltage at which curtailment starts is about 1.4V higher due to harmonics. What works in favor of SMT over another (i.e. reactive power)

control approach is that the magnitude of injected harmonic current is greatly minimized. Figure 9.12 shows a current signal after the inverter shifts power factor (left) and disconnects (right) under high harmonics situation. Harmonic current magnitude is five times lower in disconnected state caused by SMT (0.16A) compared to reactive power control (0,852A). With reactive power control the current THD is 5% while with SMT it equals 94%. In the latter case, the cycling current contribution is coming only from capacitive reactance. This is a consequence of the evaluation board design – the LCL filter being positioned behind the relay.

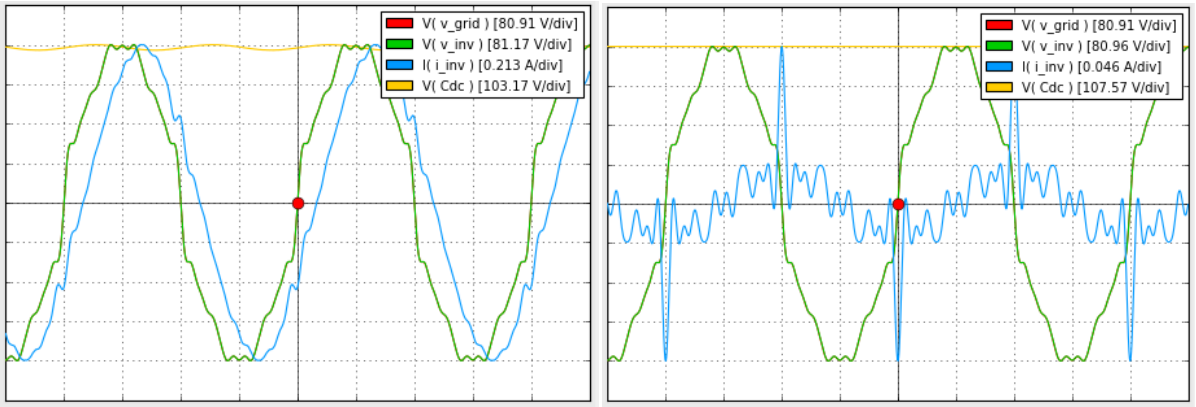

Figure 9.12: Harmonic current injection in connected and disconnected state.

9.3 Effects of reactive power control retrofit

In Chapter 5 it was mentioned that inverter manufacturers view reactive power control as unacceptable retrofit measure from reliability point of view. In Figure 9.13 a power factor variation test is shown.

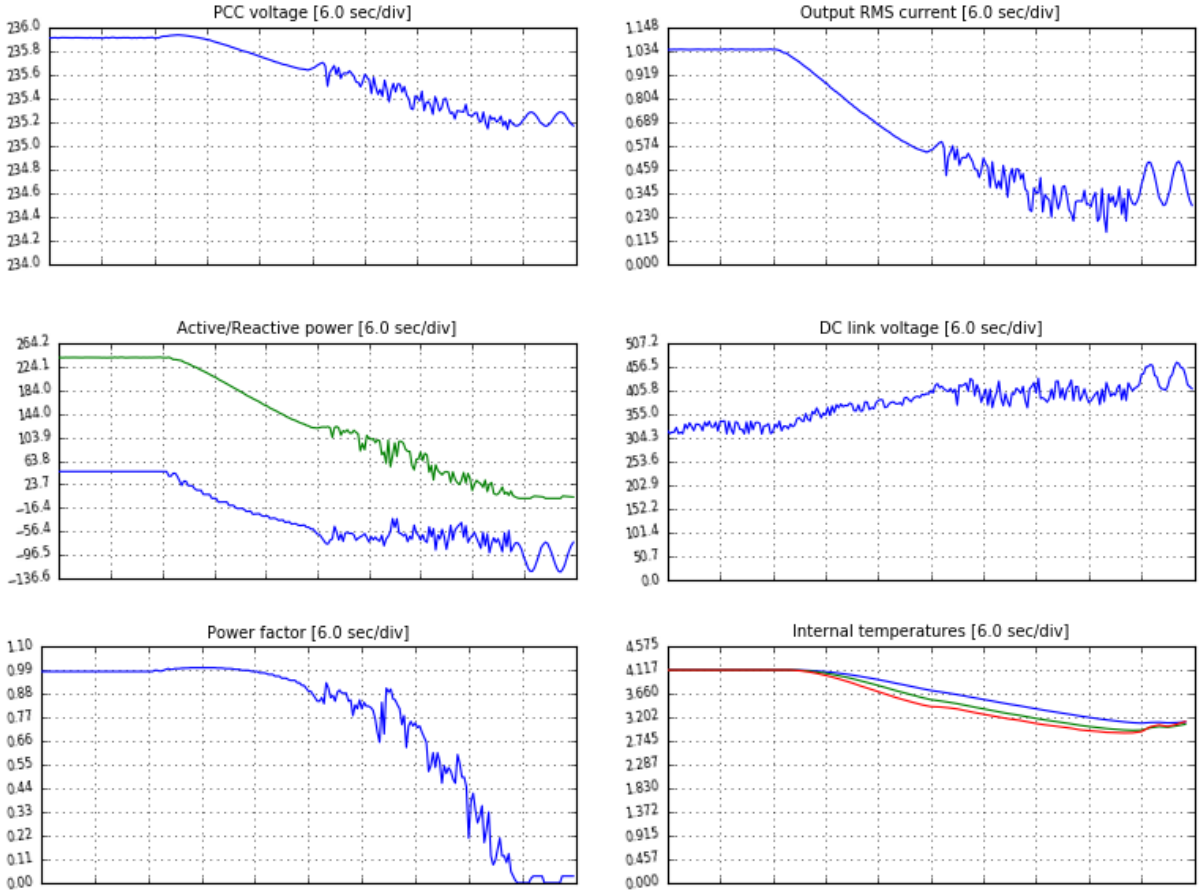

Figure 9.13: Attempt to control reactive power causes instability and DC link overvoltage.

Initially there is slight growth in voltage before it actually starts to drop. The inverter's power factor is starting at 0.98 capacitive range and must cross over unity which slightly increases voltage, then slides into inductive range and starts decreasing voltage. After 0.88 power factor, the current controller becomes unstable and eventually it ends up with DC link 450V limit being exceeded.

The contribution of 0.6V grid voltage reduction (from 235.9V to 235.3V) cannot be ascribed solely to reactive power. It is evident that active power is changing too. Since the inverter is not sized for extra reactive power capacity, the active and reactive power are strongly coupled in order to maintain a constant power factor at near-unity level. Controlling the reactive power will cause change in the active power and vice versa. It takes about 18

seconds until the control reference forces change in the power factor, but by that time power factor is 0.88, far lower than allowed under VDE (requirement for small power devices PF > 0.95). The Figure 9.14 shows results obtained from five times smaller reactive power reference gain so that active power is not significantly affected and power factor is maintained around unity.

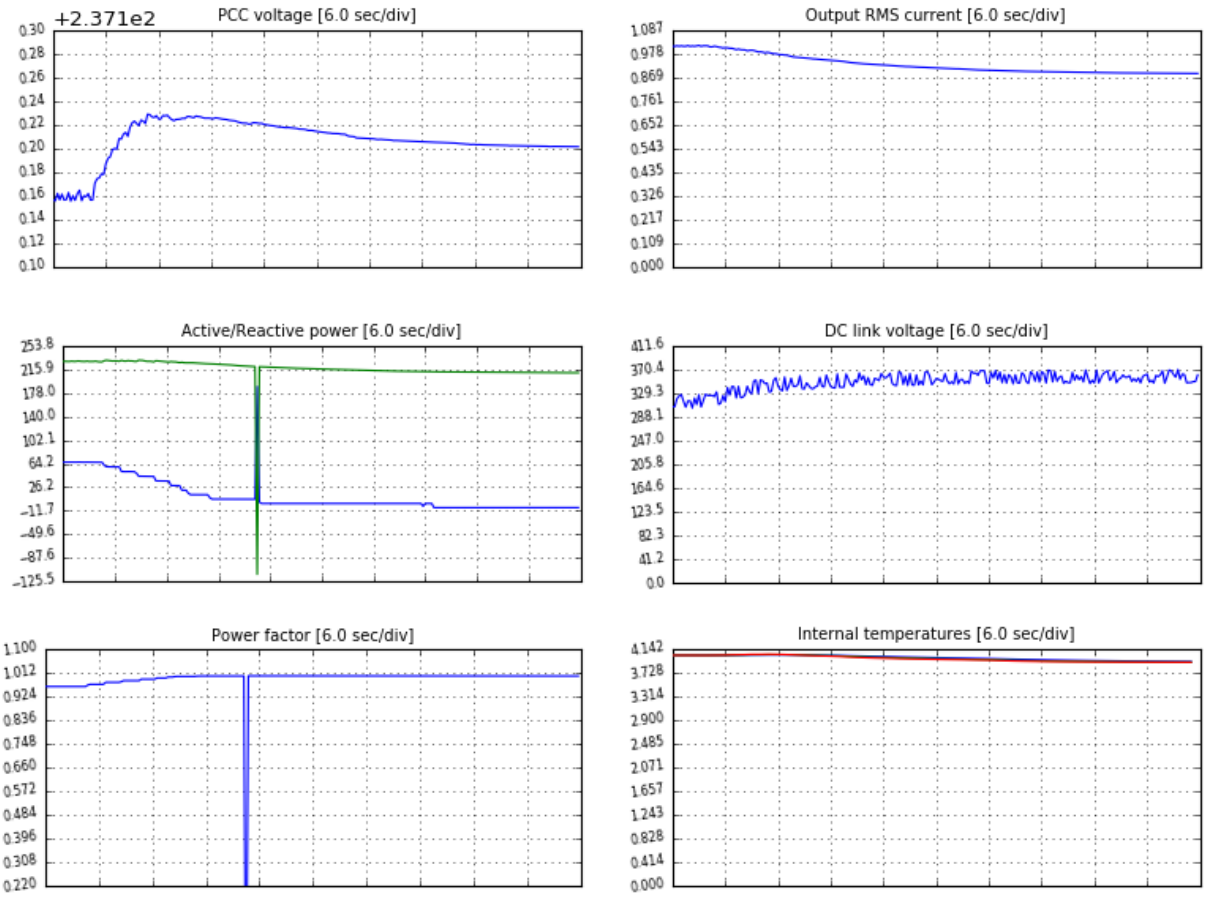

Figure 9.14: Reactive power without active power control has no practical effect on grid voltage reduction.

The almost pure reactive power contributes negatively by adding 0.04V to the grid voltage. This holds no meaningful significance for the grid support needs. Similarly there is no practical reduction of the internal temperature (not more than 2°C).

Concerning controller response, according to VDE a maximum transition period of 10 minutes from start to set control point is required. The transitions shown in these tests last no

more than 30s, so they would meet the requirements. However, manipulating the response speed is very limited as reactive power control retrofit directly targets the PI controller input. Changing proportional and integral terms and then testing the inverter while connected could hardly be performed remotely and the risk of inverter being damaged is considerable.

The effects of reactive power control in a high harmonic environment are displayed in Figure 9.15. Distorted voltage and current pairs are shown: 0.98 leading power factor (top) and 0.88 lagging (bottom). The power factor change from leading to lagging has distorted the current signal from 5%-7% THD.

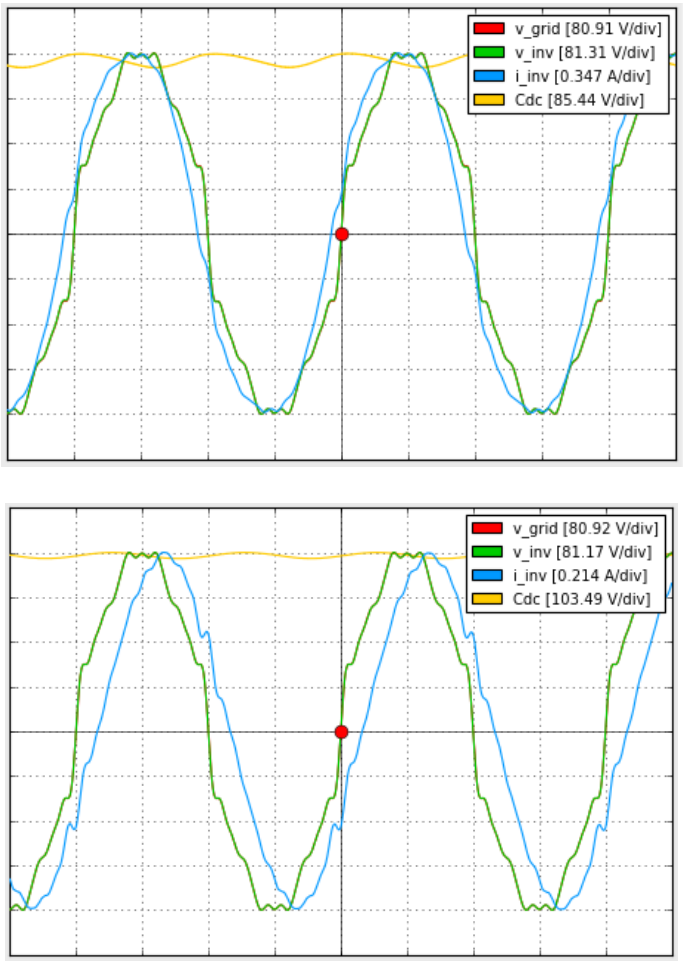

Figure 9.15: Change in power factor distorts the current signal.

9.4 Effects of droop APC retrofit

The droop APC implementation follows the idea from previous chapters that described it as a ramp control executed by varying the boost converter duty cycle. The ramp reference is given in Figure 9.16. The idea is to ramp-down the power to zero then raise it back to maximum, while watching the standard effect on grid voltage, power factor, thermal model etc. In Figure 9.17, the results of executing ramp APC are shown. The red marker demarcates the safe and unsafe operating zone.

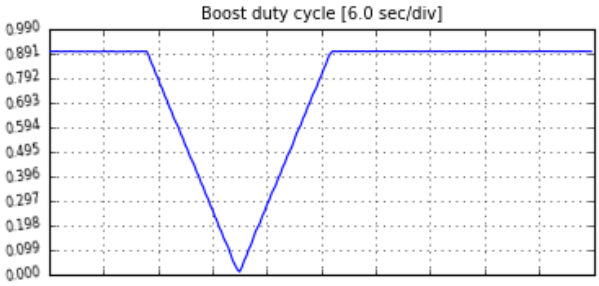

Figure 9.16: Active power ramp as control reference for boost converter duty cycle.

Curtailment starts while power factor is at 0.98 leading. The major limitation in utilizing full ramp reference is the DC link voltage that drops unacceptably low. Taking only DC link as limitation the grid voltage reduction per single micro-inverter unit is 0.6V (from 235.9V to 235.3V) which is smaller than 0.9V done by SMT.

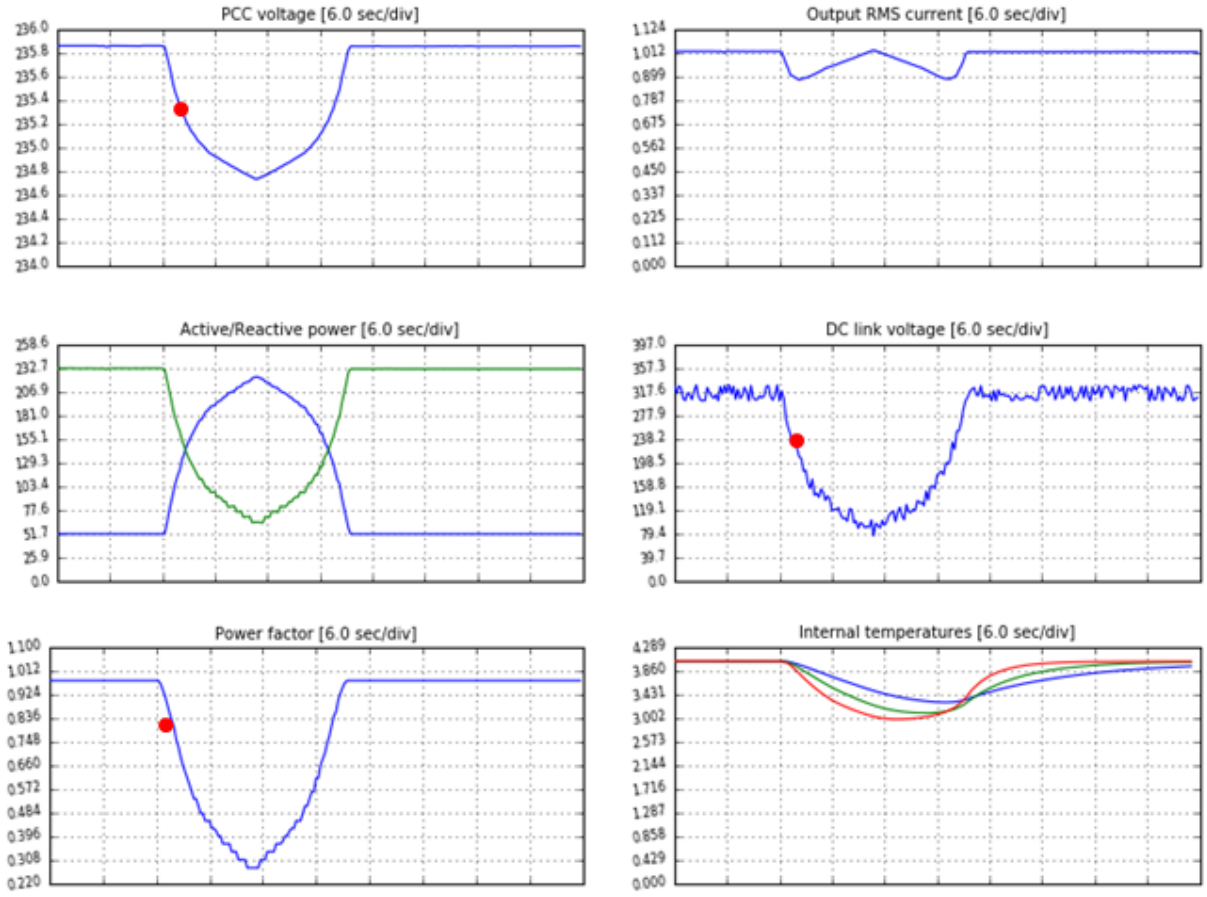

Figure 9.17: Active power control causes reactive power to change as well. Limitations imposed by DC link voltage and power factor.

However this voltage reduction comes with power factor out of permissible range (0.84). If power factor was to remain within tolerance (0.95) the voltage reduction is even smaller (<0.3V).

Figure 9.18 shows experiment repeated, this time starting with power factor at unity. While contribution to grid voltage and internal temperatures reduction is similar as in previous case, the current ramp-down behaves more according to reference. DC link is maintained at higher levels than in previous test, but it still limits the full utilization of active power for grid voltage reduction. It is recommended that power factor should be adjusted from 0.98 to 1 as a pre-curtailment action for a better controller response.

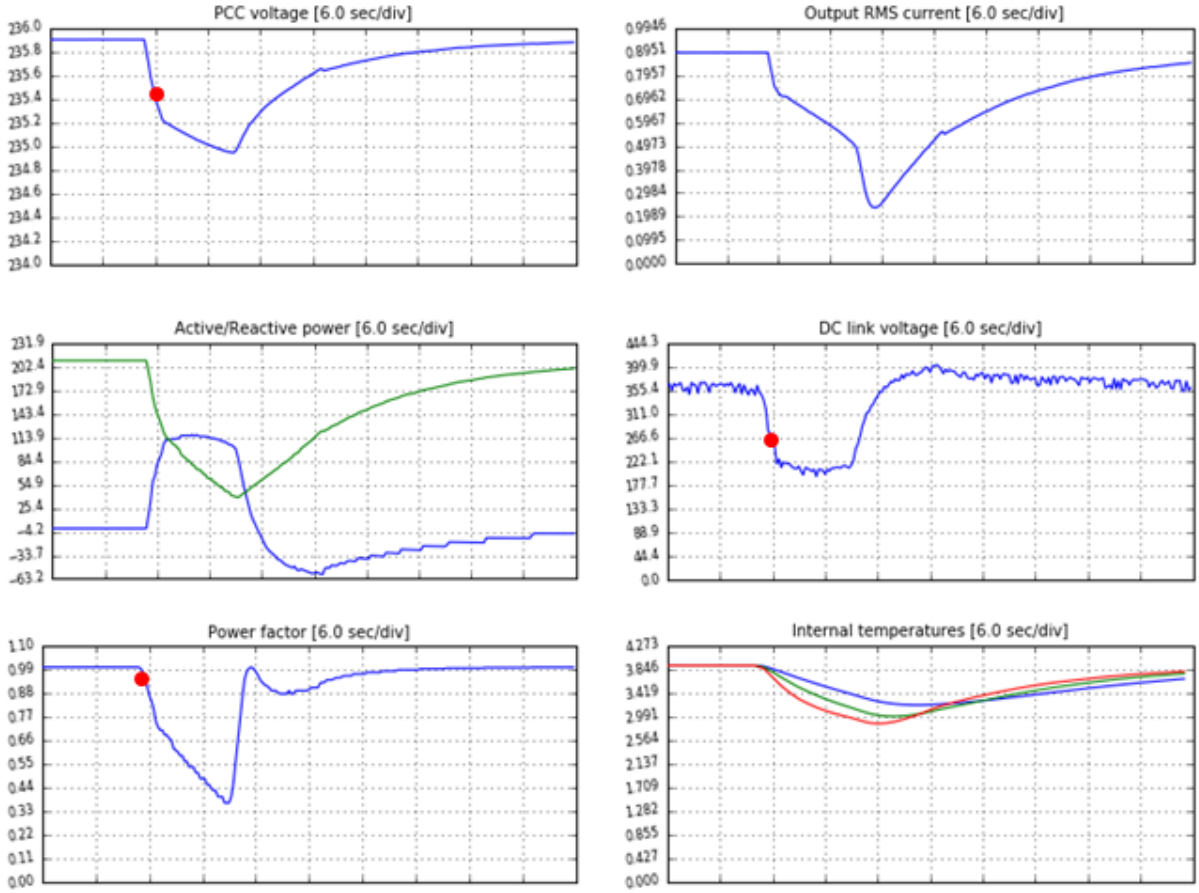

Figure 9.18: Better response to active power control with unity power factor.

9.5 Summary

In this chapter three different control strategies to reduce grid voltage were evaluated as a software retrofit possibility. The SMT implementation can provide the highest grid voltage reduction of 0.9V, and the highest internal temperature reduction of up to 11°C. The low irradiance and simulated failure of DC link control shows that, prior to SMT implementation, a proper DC link voltage control functionality is required. Such a fundamental control feature is expect to be thoroughly tested in currently deployed micro-inverter products. The SMT is a better option if inverter harmonic contribution needs to be reduced as distorted currents get eliminated by its disconnection from the grid.

Changing the reactive power reference while micro-inverter operates at a constant power factor cannot cause the reactive power to lower the voltage independently from active power. The effectiveness of lowering voltage is 34% compared to the SMT and can be attributed entirely to active power. It is the same effectiveness of droop APC showing that in both cases it is practically active power alone contributing in the voltage decrease. The almost pure reactive power contribution to grid voltage reduction is no more than 0.07V, which holds no practical significance for grid support needs. Since the reactive power control approach is acting directly on the PI controller of the inverter's current loop, its characteristics would have to be well known before retrofit otherwise large references could push it towards marginal stability/instability. It was demonstrated that the controller instability can backfire with oscillations and overvoltage at DC link. With respect to harmonics scenario, the reactive power retrofit would increase the THD of injected current from 5% to 7%.

The APC retrofit does not target the PI control directly but rather conditions the output at boost converter level. The duty cycle variation has more flexibility than reactive current reference variation. However, the range of variation is still limited by active-reactive power coupling (constant power factor operation). At some point the power factor deteriorates as the reactive power tries to compensate the drop in active power. In parallel with this condition, a large DC link undervoltage occurs. While APC with its 0.6V contribution can compete with SMT's of 0.9V, the software retrofit must ensure that the inverter under consideration has some form of active-reactive power decoupling implemented beforehand.

CHAPTER 10

Discussion and Conclusion

This thesis presented one of possible solutions to the problem of overvoltage at the PCC caused by the poor correlation between load and PV generator on one hand, and the limited grid hosting capacity on the other. This is a popular problem in the power systems community. There is a variety of centralized and decentralized solutions described and referenced in Chapter 3. Given that this thesis was a work package of a larger project focused on technical solutions for NPEB development, the scope was narrowed down to decentralized inverter-based solutions.

Through Chapters 4 and 5 the micro-inverters were evaluated as the most suitable PV inverter niche to carry out the solution implementation and meet the research objectives sustainably, especially due to possibility of remote software retrofit and increased system-level reliability. In fact, the known benefits of micro-inverter modularity inspired the design of the proposed SMT method presented in Chapter 6. The idea of reusing existing functionality conceived the SMT as a modified overvoltage protection at PV module level, while delivering a completely new APC functionality at system level. This provided the granularity of control, and opened up the potential for remote software retrofit without risking the reliability of micro-inverter operation.

The first half of this research is mainly in the domain of power distribution system study, focusing on validating the SMT method through its ability to effectively handle voltage rise situations and prevent overvoltage. First a high-level 14 bus power system analysis with integrated SMT control was performed in Chapter 7. It was shown that overvoltage could be eliminated in a high PV penetration scenario without major losses. Both local and multi bus wide-area voltage control was investigated. These analysis did not consider the complexity of

an individual micro-inverter unit but rather treated it atomically as an asset to manage voltage/active power flexibly. The economic analysis of overvoltage losses in Chapter 8 leans on results obtained in Chapter 7.

The simple, “on-off” approach of SMT method, implemented in a highly modular inverter topology, was promising to remove the complexity of continuous power control, promoting a software retrofit-friendly and reliability-oriented approach. Towards the second half of the research project it become more pressing to validate these claims, especially given the expectations of research contribution to the industry. It is in second part of Chapter 8 (the reliability study) where the research went from system-oriented to component-oriented, and consequently moved from power systems to power electronics study. The reliability study showed that curtailing power can have a positive impact on thermal and electrical stress of the inverter components, but it also warned of the possibility for conflicting ideas from design-for-reliability point of view.

Before the practical realization of research a question was raised: why only focus on active power control retrofit through SMT method? Its value should be better understood if compared with other retrofit scenarios like ramp control of active and reactive power. These software retrofit scenarios were investigated in a real-time HIL simulation study. The HIL study provided a better insight into constraints of each control method considered. The active power control proved to have a dominant effect on PCC voltage drop contribution. There was a minor overlooking (DC link issues) involving SMT retrofit, to practical impossibility facing reactive power control retrofit (virtually no voltage drop contribution and controller instability). In terms of thermal performance and harmonic current magnitude reduction, the SMT proved to be the most beneficial retrofit option.

10.1 Future research

While SMT performed successfully in almost 100% of overvoltage prevention cases, some negative things were noticed: some micro-inverters missed their scheduled trip sequence causing overvoltage; unfair distribution of feed-in losses. More work on the parametrization schemes that involved different V_{START}/V_{STOP} as well as new wide area trip delay schemes could account better for these problems.

In addition to overvoltage prevention a voltage unbalance monitoring solution utilizing micro-inverter gateway infrastructure was proposed in Chapter 7. As these gateways are not advanced enough to provide a better real-time performance due to one minute aggregate sample limit, the SMT version with unbalance control was not considered. It would be worthwhile revisiting this idea using higher aggregate sample gateways, as for single-phase devices unbalance is difficult to assess and control. Since unbalance can be a precursor to overvoltage a hybrid control would offer a more complete overvoltage prevention solution.

The micro-inverter systems utilize both local and remote communication layers which certainly affect the implementation and the system dynamic response to SMT. This research was mainly concerned with electrical aspects, but for a more comprehensive smart grid approach and practical significance for integration with DSO remote control, it would be interesting to involve communication layer and investigate the effects on system dynamics.

The reliability prediction study is based on 217Plus method. This method is good for design-for-reliability and test development, but being purely statistical with failure rate models that do not include the physics of failure it would not be the most appropriate prediction method for micro-inverters already deployed in the field. Failure mode analysis would augment this study, but it would require, difficult-to-obtain, field data from

manufacturers. The proposed approach with time fraction weighting factors was a step towards physics of failure-type of analysis.

The HIL study unraveled the compatibility problems associated with trying to update the software of inverters operating at constant power factor, especially in case of reactive power retrofit. Considering that the thesis advocates software retrofit, a software reliability analysis could help understand the true risks associated with field update of already deployed micro-inverters relative to selected power control method.

BIBLIOGRAPHY

[1] W. Schröppel, “Electrical power vision 2040 for Europe - A EUREL study,” *Elektrotechnik und Informationstechnik*, vol. 130, no. 3, pp. 93–96, 2013.

[2] S. Niu, Y. Jia, W. Wang, R. He, L. Hu, and Y. Liu, “Electricity consumption and human development level: A comparative analysis based on panel data for 50 countries,” *Int. J. Electr. Power Energy Syst.*, vol. 53, pp. 338–347, 2013.

[3] J. G. (Han) Slootweg, “Central and Decentral Power Generation - lecture 2,” 2014.

[4] D. Ackermann T, Andersson G, SOden L, “Distributed generation: a definition,” *Electr. Power Syst. Res.*, vol. 57, p. ;57(3):195–204., 2001.

[5] B. Owens, “The Rise of Distributed Power,” 2014.

[6] H. Piggott, “Wind speed measurement in the city,” 2007. [Online]. Available: http://www.scoraigwind.com/citywinds/. [Accessed: 27-Jun-2016].

[7] M. Boxwell, “Solar Electricity Handbook,” 2016. [Online]. Available: http://solarelectricityhandbook.com/Solar-Articles/wind-turbines.html. [Accessed: 27-Jun-2016].

[8] T. Hoium, “Renewable Energy Battle: Wind vs. Solar,” *The Motley Fool*, 2012. [Online]. Available: http://www.fool.com/investing/general/2012/02/14/renewable-energy-battle-wind-vs-solar.aspx. [Accessed: 27-Jun-2016].

[9] A. J. Marszal, P. Heiselberg, J. S. Bourrelle, E. Musall, K. Voss, I. Sartori, and A. Napolitano, “Zero Energy Building - A review of definitions and calculation methodologies,” *Energy Build.*, vol. 43, no. 4, pp. 971–979, 2011.

[10] J. (Irec) Salom, J. Widén, J. a Candanedo, I. Sartori, K. Voss, and A. J. Marszal, “Understanding Net Zero Energy Buildings: Evaluation of load matching and grid interaction indicators,” in *Proc. Build. Simul. 2011*, 2011, vol. 6, pp. 14–16.

[11] M. Bojić, N. Nikolić, D. Nikolić, J. Skerlić, and I. Miletić, “Toward a positive-net-energy residential building in Serbian conditions,” *Appl. Energy*, vol. 88, no. 7, pp. 2407–2419, Jul. 2011.

[12] “Shifting from net-zero to net-positive energy buildings.” [Online]. Available: http://www.tandfonline.com/doi/pdf/10.1080/09613218.2014.950452. [Accessed: 30-Dec-2015].

[13] P. Schavemaker and L. Van der Sluis, *Electrical power system essentials*. Wiley, 2008.

[14] Kundur, *Power System Stability And Control*. EPRI, 1994.

[15] K. Kauhaniemi and L. Kumpulainen, “Impact of distributed generation on the protection of distribution networks,” in *Eighth IEE International Conference on Developments in Power System Protection*, 2004, vol. 2004, no. Mv, pp. 315–318.

[16] S. C. Sciacca and W. R. Block, “Advanced SCADA concepts,” *IEEE Comput. Appl. Power*, vol. 8, no. 1, pp. 23–28, 1995.

[17] A. Bernardo, N. Silva, A. Carrapatoso, P. Rodrigues, and F. Melo, “Monitor BT pilot project: Combined voltage regulation approach for LV grids with PV penetration,” in *23rd International Conference on Electricity Distribution*, 2015, no. June, pp. 15–18.

[18] J. G. Slootweg, S. W. H. de Haan, H. Polinder, and W. L. Kling, “Voltage Control Methods with Grid Connected WindTurbines: a tutorial review,” *Wind Eng.*, vol. 25, no. 6, pp. 353–365, 2001.

[19] Y. Yang, F. Blaabjerg, H. Wang, Y. Yongheng, F. Blaabjerg, and W. Huai, “Low voltage ride-through of single-phase transformerless photovoltaic inverters,” in *Energy Conversion Congress and Exposition (ECCE), 2013 IEEE*, 2013, vol. 50, no. 3, pp. 4762–4769.

[20] J. C. Boemer, K. Burges, P. Zolotarev, J. Lehner, P. Wajant, M. Fürst, R. Brohm, and T. Kumm, “Overview of German Grid Issues and Retrofit of Photovoltaic Power Plants in Germany for the Prevention of Frequency Stability Problems in Abnormal System Conditions of the ENTSO-E Region Continental Europe,” *1st Int. Work. Integr. Sol. Power into Power Syst.*, no. October, p. 6, 2011.

[21] E. Coster, J. Myrzik, and W. Kling, “Effect of DG on distribution grid protection,” in *Distributed Generation*, D. N. Gaonkar, Ed. InTechOpen, 2010, pp. 93–118.

[22] J. F. G. Cobben, “Power quality: Implications at the point of connection,” Technische Universiteit Eindhoven, 2007.

[23] A. F. Abdul Kadir, A. Mohamed, and H. Shareef, “Harmonic impact of different distributed generation units on low voltage distribution system,” in *2011 IEEE International Electric Machines & Drives Conference (IEMDC)*, 2011, pp. 1201–1206.

[24] H. Akagi, “New trends in active filters for power conditioning,” *IEEE Trans. Ind. Appl.*, vol. 32, no. 6, pp. 1312–1322, 1996.

[25] J. G. Slootweg and W. L. Kling, “Is the Answer Blowing in the Wind?,” *IEEE Power Energy Mag.*, vol. 1, no. 6, pp. 26–33, 2003.

[26] B. X. B. Xiao-min, M. J. M. Jun-xia, and Z. N. Z. Ning-hui, “Functional analysis of advanced metering infrastructure in smart grid,” *Power Syst. Technol. POWERCON 2010 Int. Conf.*, pp. 1–4, 2010.

[27] N. H. Phương, “Multi-Agent System based Active Distribution Networks,” Eindhoven University of Technology, 2010.

[28] K.-H. Mak and B. L. Holland, “Migrating electrical power network SCADA systems to TCP/IP and Ethernet networking,” *Power Eng. J.*, vol. 16, no. 6, pp. 305–311, 2002.

[29] N. Bui, A. P. Castellani, P. Casari, and M. Zorzi, “The internet of energy: A web-enabled smart grid system,” *IEEE Netw.*, vol. 26, no. 4, pp. 39–45, 2012.

[30] Gungor, V.C, Sahin, D, Kocak, T. ; Ergut, S, “Smart Grid Technologies: Communication Technologies and Standards,” *Ind. Informatics*, vol. 7, no. 4, pp. 529–539, 2011.

[31] R. Y. R. Yan and T. K. Saha, “Power ramp rate control for grid connected photovoltaic system,” *IPEC, 2010 Conf. Proc.*, pp. 83–88, 2010.

[32] B. Verhelst, C. Debruyne, J. Vanalme, J. Desmet, J. Capelle, and L. Vandevelde, “Economic evaluation of the influence of overvoltages and the integration of small storage capacity in residential PV-installations,” in *IEEE PES Innovative Smart Grid Technologies Conference Europe*, 2011, pp. 1–6.

[33] C. Debruyne, J. Desmet, J. Vanalme, B. Verhelst, G. Vanalme, and L. Vandevelde, “Maximum power injection acceptance in a residential area,” in *International Conference on Renewable Energies and Power Quality*.

[34] J. Widén, E. Wäckelgård, and P. D. Lund, “Options for improving the load matching capability of distributed photovoltaics: Methodology and application to high-latitude data,” *Sol. Energy*, vol. 83, no. 11, pp. 1953–1966, 2009.

[35] R. Tonkoski, D. Turcotte, and T. H. M. El-Fouly, “Impact of High PV Penetration on Voltage Profiles in Residential Neighborhoods,” *IEEE Trans. Sustain. Energy*, vol. 3, no. 3, pp. 518–527, Jul. 2012.

[36] J. Widén, E. Wäckelgård, J. Paatero, and P. Lund, “Impacts of distributed photovoltaics on network voltages: Stochastic simulations of three Swedish low-voltage distribution grids,” *Electr. Power Syst. Res.*, vol. 80, no. 12, pp. 1562–1571, 2010.

[37] C. Bergerland, J. Johansson, J. Widén, and T. Walla, “Determining and Increasing the Hosting Capacity for Photovoltaics in Swedish Distribution Grids,” *27th Eur. Photovolt. Sol. Energy Conf. Exhib.*, pp. 4414–4420, Oct. 2012.

[38] J. V. Paatero and P. D. Lund, “Effects of large-scale photovoltaic power integration on electricity distribution networks,” *Renew. Energy*, vol. 32, no. 2, pp. 216–234, 2007.

[39] M. Thomson and D. G. Infield, “Impact of widespread photovoltaics generation on distribution systems,” *IET Renew. Power Gener.*, vol. 1, no. 1, p. 33, 2007.

[40] P. Pillay and M. Manyage, “Definitions of Voltage Unbalance,” *IEEE Power Eng. Rev.*, no. May, pp. 50–51, 2001.

[41] D. Johan and T. Van Craenenbroeck, “Voltage Disturbances 5.1.3,” 5.1.3, 2002.

[42] S. C. Vegunta, P. Twomey, and D. Randles, “Impact of PV and load penetration on LV network voltages and unbalance and potential solutions,” in *22 nd International Conference on Electricity Distribution*, 2013, no. 1481, pp. 10–13.

[43] F. Shahnia, A. Ghosh, G. Ledwich, and F. Zare, “Voltage unbalance improvement in low voltage residential feeders with rooftop PVs using custom power devices,” *Int. J. Electr. Power Energy Syst.*, vol. 55, pp. 362–377, 2014.

[44] P. D. F. Ferreira, P. M. S. Carvalho, L. a F. M. Ferreira, and M. D. Ilic, “Distributed energy resources integration challenges in low-voltage networks: Voltage control limitations and risk of cascading,” *IEEE Trans. Sustain. Energy*, vol. 4, no. 1, pp. 82–88, 2013.

[45] T. Stetz, F. Marten, and M. Braun, “Improved low voltage grid-integration of photovoltaic systems in Germany,” *IEEE Trans. Sustain. Energy*, vol. 4, no. 2, pp. 534–542, 2013.

[46] C. Gao and M. a. Redfern, “A review of voltage control techniques of networks with distributed generations using On-Load Tap Changer transformers,” *Univ. Power Eng. Conf. (UPEC), 2010 45th Int.*, pp. 3–8, 2010.

[47] D. E. Mawarni, P. H. Nguyen, and W. L. Kling, “A Case Study of Using OLTC to Mitigate Overvoltage in a Rural European Low Voltage Network,” no. 608998, 2015.

[48] DNV GL, “Future Grids Webcast.” [Online]. Available: https://www.dnvgl.com/energy/video/watch/future-grids-noindex.html. [Accessed: 29-Jan-2016].

[49] R. Yan, B. Marais, and T. K. Saha, “Impacts of residential photovoltaic power fluctuation on on-load tap changer operation and a solution using DSTATCOM,” *Electr. Power Syst. Res.*, vol. 111, pp. 185–193, 2014.

[50] E. Alegria, T. Brown, E. Minear, and R. H. Lasseter, “CERTS Microgrid Demonstration with Large- Scale Energy Storage and Renewable Generation,” *IEEE Trans. Smart Grid*, vol. 5, no. 2, pp. 1–7, 2013.

[51] B. B. McKeon, J. Furukawa, and S. Fenstermacher, “Advanced Lead–Acid Batteries and the Development of Grid-Scale Energy Storage Systems,” *Proc. IEEE*, vol. 102, no. 6, pp. 951–963, Jun. 2014.

[52] R. Tonkoski and L. A. C. Lopes, “Impact of active power curtailment on overvoltage prevention and energy production of PV inverters connected to low voltage residential feeders,” *Renew. Energy*, vol. 36, no. 12, pp. 3566–3574, 2011.

[53] S. Conti, A. Greco, N. Messina, and S. Raiti, “Local voltage regulation in LV distribution networks with PV distributed generation,” *Power Electronics, Electrical Drives, Automation and Motion, 2006. SPEEDAM 2006. International Symposium on*. pp. 519–524, 2006.

[54] Q. Z. and J. W. Bialek, “Generation curtailment to manage voltage constraints in distribution networks,” *Gener. Transm. Distrib. IET*, vol. 1, no. 2, pp. 492–498, 2007.

[55] E. Demirok, P. C. González, K. H. B. Frederiksen, D. Sera, P. Rodriguez, and R. Teodorescu, “Local reactive power control methods for overvoltage prevention of distributed solar inverters in low-voltage grids,” *IEEE J. Photovoltaics*, vol. 1, no. 2, pp. 174–182, 2011.

[56] K. Turitsyn, P. Šulc, S. Backhaus, and M. Chertkov, “Distributed control of reactive power flow in a radial distribution circuit with high photovoltaic penetration,” in *IEEE PES General Meeting*, 2010, pp. 1–6.

[57] T. Beach, A. Kozinda, and V. Rao, “Advanced inverters for distributed PV: Latent Opportunities for Loaclized Reactive Power Compensation,” 2013.

[58] K. Lemkens, F. Geth, P. Vingerhoets, and G. Deconinck, “Reducing overvoltage problems with active power curtailment - Simulation results,” *2013 4th IEEE/PES Innov. Smart Grid Technol. Eur. ISGT Eur. 2013*, pp. 4–8, 2013.

[59] Y. Ueda, K. Kurokawa, and T. Tanabe, “Study on the over voltage problem and battery operation for grid-connected residential PV systems,” *22nd Eur. Photovolt. Sol. Energy Conf.*, no. September, pp. 3094–3097, 2007.

[60] F. Marra, Y. T. Fawzy, T. Bulo, and B. Blažič, “Energy storage options for voltage support in low-voltage grids with high penetration of photovoltaic,” *IEEE PES Innov. Smart Grid Technol. Conf. Eur.*, pp. 1–7, 2012.

[61] P. H. Nguyen, J. M. A. Myrzik, and W. L. Kling, “Coordination of voltage regulation in active networks,” *Transm. Distrib. Expo. Conf. 2008 IEEE PES Powering Towar. Futur. PIMS 2008*, pp. 1–6, 2008.

[62] S. Hsieh, “Economic Evaluation of the Hybrid Enhancing Scheme With DSTATCOM and Active Power Curtailment for PV Penetration in Taipower Distribution Systems,” vol. 51, no. 3, pp. 1953–1961, 2015.

[63] M. N. Kabir, Y. Mishra, G. Ledwich, S. Member, Z. Y. Dong, and K. P. Wong, “Coordinated Control of Grid-Connected Photovoltaic Reactive Power and Battery Energy Storage Systems to Improve the Voltage Profile of a Residential Distribution Feeder,” *IEEE Trans. Ind. Informatics*, vol. 10, no. 2, pp. 967–977, 2014.

[64] R. Tonkoski, L. A. C. Lopes, and T. H. M. El-Fouly, “Coordinated active power curtailment of grid connected PV inverters for overvoltage prevention,” *IEEE Trans. Sustain. Energy*, vol. 2, no. 2, pp. 139–147, 2011.

[65] K. H. Chua, Y. S. Lim, J. Wong, P. Taylor, E. Morris, and S. Morris, “Voltage Unbalance Mitigation in Low Voltage Distribution Networks with Photovoltaic Systems,” *J. Electron. Sci. Technol.*, vol. 10, no. 1, pp. 1–6, 2012.

[66] R. Turri, R. Caldon, and M. Coppo, “A network voltage control strategy for LV inverter interfaced users,” *8th Mediterr. Conf. Power Gener. Transm. Distrib. Energy Convers. (MEDPOWER 2012)*, no. 1, pp. 41–41, 2012.

[67] F. Wang, J. L. Duarte, and M. A. M. Hendrix, “Control of grid-interfacing inverters with integrated voltage unbalance correction,” in *2008 IEEE Power Electronics Specialists Conference*, 2008, pp. 310–316.

[68] S. Weckx, C. Gonzalez, and J. Driesen, “Reducing grid losses and voltage unbalance with PV inverters,” *IEEE Power Energy Soc. Gen. Meet.*, vol. 2014–Octob, no. October, 2014.

[69] IEA-PVPS, “Community-Scale Solar Photovoltaics: Housing and Public Development Examples,” 2008.

[70] Y. Ueda, K. Kurokawa, T. Tanabe, K. Kitamura, and H. Sugihara, “Analysis Results of Output Power Loss Due to the Grid Voltage Rise in Grid-Connected Photovoltaic Power Generation Systems,” *IEEE Trans. Ind. Electron.*, vol. 55, no. 7, pp. 2744–2751, 2008.

[71] E. Caamaño, D. Suna, J. Thornycroft, S. Cobben, M. Elswijk, B. Gaiddon, T. Erge, and H. Laukamp, “Utilities Experience and Perception of PV Distributed Generation,” 2007.

[72] J. St. John, “How HECO is Using Enphase’s Data to Open its Grid to More Solar,” *Greentech Media*. [Online]. Available: http://www.greentechmedia.com/articles/read/how-heco-is-using-enphase-data-to-open-its-grid-to-more-solar. [Accessed: 09-Feb-2016].

[73] Annabel Hepworth, “Rooftop solar panels overloading electricity grid,” *The Australian*. [Online]. Available: http://www.theaustralian.com.au/news/rooftop-solar-panels-overloading-electricity-grid/story-e6frg6n6-1226165360822. [Accessed: 09-Feb-2016].

[74] S. Vorrath, “Ergon confirms rule changes to take rooftop solar boom off-grid,” *Renew Economy*. [Online]. Available: http://reneweconomy.com.au/2014/ergon-confirms-rule-changes-to-take-rooftop-solar-boom-off-grid-27210. [Accessed: 09-Feb-2016].

[75] D. P. Hohm and M. E. Ropp, “Comparative study of maximum power point tracking algorithms,” *Prog. Photovoltaics Res. Appl.*, vol. 11, no. 1, pp. 47–62, 2003.

[76] M. Alonso-Garcia, J. Ruiz, and F. Chenlo, “Experimental study of mismatch and shading effects in the – characteristic of a photovoltaic module,” *Sol. Energy Mater. Sol. Cells*, vol. 90, no. 3, pp. 329–340, Feb. 2006.

[77] C. Deline, B. Marion, J. Granata, and S. Gonzalez, “A Performance and Economic Analysis of Distributed Power Electronics in Photovoltaic Systems,” *Contract*, no. January, 2011.

[78] J. M. A. Myrzik and M. Calais, “String and module integrated inverters for single-phase grid connected photovoltaic systems - a review,” vol. 2, p. 8 pp. Vol.2-pp., 2003.

[79] C. Deline, “Partially shaded operation of multi-string photovoltaic systems,” *Conf. Rec. IEEE Photovolt. Spec. Conf.*, pp. 394–399, 2010.

[80] S. Rogalla, B. Burger, B. Goeldi, and H. Schmidt, “Light and shadow-When is MPP-Tracking at the module level worthwhile?,” *25th Eur. Photovolt. Sol. Energy Conf. Exhib.*, no. September, pp. 6–10, 2010.

[81] M. A. Gross, S. O. Martin, and N. M. Pearsall, “Estimation of output enhancement of a partially shaded BIPV array by the use of AC modules,” in *Conference Record of the Twenty Sixth IEEE Photovoltaic Specialists Conference - 1997*, 1997, pp. 1381–1384.

[82] A. D. Briggs, M. Manager, and M. Baldassari, “Performance of Enphase Microinverter Systems v . PVWatts Estimates,” 2011.

[83] I. de Jong and H. Oldenkamp, “The Return of the AC-Module Inverter,” *24th Eur. Photovolt. Sol. Energy Conf. 21-25 Sept. 2009, Hamburg, Ger.*, pp. 3101–3104, Nov. 2009.

[84] S. W. H. De Haan, “TEST RESULTS OF A 130W AC MODULE ; a modular solar ac power station,” pp. 925–928, 1994.

[85] R. H. Wills, F. E. Hall, S. J. Strong, and J. H. Wohlgemuth, “The AC photovoltaic module,” in *Conference Record of the Twenty Fifth IEEE Photovoltaic Specialists Conference - 1996*, 1996, pp. 1231–1234.

[86] C. Prapanavarat, M. Barnes, and N. Jenkins, “Investigation of the performance of a photovoltaic AC module,” *IEE Proc.*, vol. 149, no. 4, pp. 472–478, 2002.

[87] Y. Chen and C. Liao, “Three-Port Flyback-Type Single-Phase Micro- Inverter With Active Power Decoupling Circuit,” vol. 2, pp. 501–506, 2011.

[88] S. Harb, H. Hu, and N. Kutkut, “A three-port Photovoltaic (PV) micro-inverter with power decoupling capability,” in *Applied Power Electronics Conference and Exposition (APEC)*, 2011, no. 2, pp. 203–208.

[89] A. K. S. Bhat and S. D. Dewan, “Resonant inverters for photovoltaic array to utility interface.,” *IEEE Trans. Aerosp. Electron. Syst.*, vol. 24, no. 4, pp. 377–386, 1988.

[90] X. Yuan, Y. Zhang, Z. High, and T. Park, “Status and Opportunities of Photovoltaic Inverters in Grid-Tied and Micro-Grid Systems,” pp. 0–3, 2006.

[91] Attanasio Rosario, “250 W grid connected microinverter,” 2012.

[92] Y. Huang, M. Shen, S. Member, F. Z. Peng, and J. Wang, “Z -Source Inverter for Residential Photovoltaic Systems,” vol. 21, no. 6, pp. 1776–1782, 2006.

[93] E. Engineering and Q. I. Circuit, “Quasi-Z-Source Inverter for Photovoltaic Power Generation Systems,” pp. 918–924, 2009.

[94] Y. Zhou, L. Liu, and H. Li, “A High-Performance Photovoltaic Module-Integrated Converter (MIC) Based on Cascaded Quasi-Z-Source,” vol. 28, no. 6, pp. 2727–2738, 2013.

[95] M. Dargatz, “‘Utility-Interactive’: What it Means , What Protection it Ensures,” 2010.

[96] Bower W and R. M., “Evaluation of islanding detection methods for photovoltaic utility-interactive power systems,” Albuquerque, 2002.

[97] D. S.-M. Luke Schwartfeger, “Review of Distributed Generation Interconnection Standards,” p. 13, 2014.

[98] VDE, “VDE-AR-N 4105:2011-08 Power generation systems connected to the low-voltage distribution network Technical minimum requirements for the connection to and parallel operation with low-voltage distribution networks,” 2011.

[99] P. Fairley, “800,000 Microinverters Remotely Retrofitted on Oahu - in One Day,” *IEEE Spectrum*, 2015. [Online]. Available: http://spectrum.ieee.org/energywise/green-tech/solar/in-one-day-800000-microinverters-remotely-retrofitted-on-oahu. [Accessed: 09-Feb-2016].

[100] O. Gagrica, T. Uhl, P. H. Nguyen, and W. L. Kling, “Sustainable transition to high PV penetration : Curtailment retrofit for the already deployed micro-inverters,” *ECOS2015*, 2015.

[101] R. Tonkoski, I. S. Member, L. A. C. Lopes, and I. S. Member, “Voltage Regulation in Radial Distribution Feeders with High Penetration of Photovoltaic,” in *IEEE Energy2030*, 2008, no. Lv.

[102] F. Provoost, “Intelligent Distribution Network Design,” Technische Universiteit Eindhoven, 2009.

[103] S. Yang, A. Bryant, P. Mawby, S. Member, D. Xiang, L. Ran, S. Member, P. Tavner, and S. Member, “An Industry-Based Survey of Reliability in Power Electronic Converters,” *IEEE Trans. Ind. Appl.*, vol. 47, no. 3, pp. 1441–1451, 2011.

[104] C. J. Muray, A. Davoudi, and P. L. Chapman, “Reliability Analysis for Single-Phase Photovoltaic Inverters with Reactive Power Support,” in *IEEE Power and Energy Conference at Illinois (PECI)*, 2011, no. 3, pp. 1–6.

[105] A. Engler, “Applicability of droops in low voltage grids,” *Int. J. Distrib. Energy Resour. Smart Grids*, no. 1, pp. 1–5, 2005.

[106] Vishay Siliconix, “Current Rating of Power Semiconductors,” 2010.

[107] O. Gagrica, W. Kling, and T. Uhl, “Control of micro-inverters as an overvoltage prevention method under high PV penetration,” *Mech. Control*, vol. 32, no. 2, p. 52, 2013.

[108] O. Gagrica, P. H. Nguyen, W. L. Kling, and T. Uhl, “Microinverter Curtailment Strategy for Increasing Photovoltaic Penetration in Low-Voltage Networks,” *IEEE Trans. Sustain. Energy*, vol. 6, no. 2, pp. 369–379, 2015.

[109] Enphase Inc, “Envoy Communications Gateway,” 2015. [Online]. Available: https://enphase.com/sites/default/files/Envoy_DS_EN_60Hz.pdf. [Accessed: 01-Jun-2015].

[110] ABB, “Product manual CDD (concentrator data device),” 2014. [Online]. Available: http://www05.abb.com/global/scot/scot232.nsf/veritydisplay/4777de35bd05a22b85257cd30002f0fb/$file/CDD Product manual.pdf. [Accessed: 03-Nov-2015].

[111] C. L. Masters, “Voltage rise: the big issue when connecting embedded generation to long 11 kV overhead lines,” *Power Eng. J.*, vol. 16, no. 1, pp. 5–12, 2002.

[112] S. Bhattacharyya, *Power Quality Requirements and Responsibilities at the Point of Connection*. 2011.

[113] EDSN, “Profielen elektriciteit 2012,” Baarn, 2012.

[114] UT-CEM, “Simulink Smartgrid Simulation 1: The Basics.” [Online]. Available: https://www.youtube.com/watch?v=UvOJh534cok. [Accessed: 31-May-2016].

[115] P. Salmeron and A. Perez, “Evaluation of the Distortion and Unbalance Emission Levels in Electric Networks,” in *Power Quality Issues*, InTech, 2013.

[116] N. Tangsunantham and C. Pirak, “Voltage unbalance measurement in three-phase smart meter applied to AMI systems,” in *2013 10th International Conference on*

Electrical Engineering/Electronics, Computer, Telecommunications and Information Technology, ECTI-CON 2013, 2013, pp. 1–5.

[117] F. Shahnia, R. Majumder, A. Ghosh, G. Ledwich, and F. Zare, "Voltage imbalance analysis in residential low voltage distribution networks with rooftop PVs," *Electr. Power Syst. Res.*, vol. 81, no. 9, pp. 1805–1814, 2011.

[118] W. Li, *Risk assessment of power systems : models, methods, and applications*, 2nd ed. IEEE Wiley, 2005.

[119] IEC, "Consideration of reference impedances and public supply network impedances for use in determining the disturbance characteristics of electrical equipment having a rated current ≤75 A per phase," Geneva, 2012.

[120] H. Wang and F. Blaabjerg, "Reliability of capacitors for DC-link applications in power electronic converters—an overview," *IEEE Trans. Ind. Appl.*, vol. 50, no. 5, pp. 3569–3578, 2014.

[121] S. J. Castillo, R. S. Balog, and P. Enjeti, "Predicting capacitor reliability in a module-integrated photovoltaic inverter using stress factors from an environmental usage model," in *North American Power Symposium 2010, NAPS 2010*, 2010.

[122] D. Nicholls, "What is 217Plus and Where Did It Come From?," in *2007 Annual Reliability and Maintainability Symposium*, 2007, no. June 2005, pp. 22–27.

[123] W. Denson, "Handbook of 217Plus Reliability Prediction Models," 2006.

[124] "STEVAL-ISV003V1 Bill of Materials." [Online]. Available: http://www.bdtic.com/DownLoad/ST/STEVAL-ISV003V1_bom.pdf. [Accessed: 13-Jun-2016].

[125] O. Gagrica, M. Marzec, and T. Uhl, “Comparison of reliability impacts of two active power curtailment methods for PV micro-inverters,” *Microelectron. Reliab.*, vol. 58, pp. 133–140, Dec. 2016.

[126] Freescale Semiconductor, “Thermal Analysis of Semiconductor Systems,” *White Pap.*, 2008.

[127] R. H. F. M. Hossain, Y. Xu, T. J. Peshek, L. Ji, A. R. Abramson, “Microinverter Thermal Performance in the Real-World: Measurements and Modeling,” *PLoS One*, vol. 10, no. 7, p. e0131279, Jul. 2015.

[128] *Rozporządzenie Ministra Gospodarki i Pracy z dnia 20 grudnia 2004 r. w sprawie szczegółowych warunków przyłączenia podmiotów do sieci elektroenergetycznych, ruchu i eksploatacji tych sieci*.

[129] Y. Du, W. Xiao, Y. Hu, and D. D. C. Lu, “Control approach to achieve burst mode operation with DC-link voltage protection in single-phase two-stage PV inverters,” in *2014 IEEE Energy Conversion Congress and Exposition, ECCE 2014*, 2014, vol. 1, pp. 47–52.

ISBN: 978-90-386-5195-8